Ceramides as therapeutic targets in bronchopulmonary dysplasia

Ali Hamraghani

A thesis submitted in partial fulfillment of the requirements for the
Master's degree in Cellular and Molecular Medicine

Department of Cellular and Molecular Medicine
Faculty of Medicine
University of Ottawa

Abstract

Bronchopulmonary dysplasia (BPD) is a chronic lung disorder associated with extremely premature birth, resulting from arrested development of the microvasculature and consequently disrupted alveologenesis. Premature infants are dependent on respiratory support, including oxygen supplementation and mechanical ventilation (MV), that are considered the main modifiable contributors to BPD. The mechanistic link between the injurious stimulus (e.g., hyperoxia) and disrupted lung development has been less clear. Recent works suggest the up regulation of ceramides in the injured lung as a potentially key factor. Ceramides regulate tissue growth pathways, by increasing autophagy and apoptosis. Ceramides are increased in tracheal aspirates of preterm infants receiving MV. Moreover, attenuation of ceramide synthesis by Sphingomyelin Phosphodiesterase 1 (SMPD1) inhibition prevented MV induced cell death in experimental animals. Whether ceramides may play a role in hyperoxia-induced lung injury remains less studied. To examine this issue, I employed an experimental rat model of BPD caused by exposure to hyperoxia for 14 days (85% O_2 postnatal days [PND] 1-7 and 60% O_2 PND 7-14) followed by intermittent hypoxia from PND 14-21 (termed the HIH BPD-like lung injury model). Lung injury in this model was characterized by hypoplastic pulmonary vasculature, pulmonary hypertension, and "emphysematous" lung structure due to inhibited alveologenesis. My findings demonstrated that exposure to severe hyperoxia (PND 1-7) lead to a rapid increase in the lung of pro-apoptotic ceramides, commencing on PND 1 and persisting to PND 7. Lung autophagy markers were up-regulated concurrent with increased ceramides, which was followed by increased apoptosis on PND 7, predominantly in distal lung epithelial cells. Treatment of HIH-exposed rat pups with daily S.C Desipramine 10 mg/kg/d (an SMPD1 inhibitor) prevented up-regulated lung ceramide content, autophagy, and apoptosis. Desipramine also prevented HIH-induced lung

inflammation, vascular hypoplasia and pulmonary hypertension and partially improved markers of distal alveolar development. I also examined contents of four key ceramide pathway proteins in human autopsy-derived lung sections from infants with and without BPD, which revealed a significant increase in ceramide pathway proteins in BPD lungs when compared to controls. Coupled with earlier work, my findings support a key role for up-regulated ceramides in both human and experimental chronic neonatal lung injury. Inhibition of injurious ceramide production with Desipramine represents a promising strategy for the prevention of BPD.

Table of Contents

List of Figures

Chapter 1: Introduction

Chapter 3: Results

Chapter 4: Discussion

List of Tables

Chapter 2: Materials and Methods

List of Abbreviations

Abbreviation	Definition
ANOVA	Analysis of variance
ASM	Acid sphingomyelinase
AT2	Alveolar type 2
ATG	Autophagy-related
BALF	Bronchoalveolar lavage fluid
BCA	Bicinchoninic acid
BPD	Bronchopulmonary dysplasia
Casp 3	Caspase 3
Caspases	Cysteine aspartate-specific proteases
CDH1	E-cadherin
CE	Coefficients of error
CerS2	Ceramide synthase 2
CF	Cystic fibrosis
CHEO	Children's Hospital of Eastern Ontario
Cl.Casp 3	Cleaved caspase 3
Cl.PARP	Cleaved PARP
Co-IF	Co-immunofluorescence
COPD	Chronic obstructive pulmonary disease
cPH	Chronic pulmonary hypertension
CV	Coefficients of variation
CYP	Cytochrome P450
DAB	3,3-diaminobenzidine
DAPI	4',6-diamidino-2-phenylindole
DI water	Deionized water
ECL	Enhanced chemiluminescence
EDTA	Ethylenediaminetetraacetic acid
ER 1	Epitope retrieval 1
ER 2	Epitope retrieval 2

FADD	Fas associated death domain
FDA	Food and Drug Administration
FI	Fulton's index
FiO_2	Fraction of inspired oxygen
GA	Gestational age
GMA	Glycol methacrylate
H_2O_2	Hydrogen peroxide
HIH	Hyperoxia-intermittent hypoxia
HPLC	High-performance liquid chromatography
HRP	Horseradish peroxidase
I.P	Intraperitoneal
IF	Immunofluorescence
IHC	Immunohistochemistry
IUGR	Intrauterine growth restriction
Lass 1	Ceramide synthase 1
LC-MS/MS	Liquid chromatography tandem mass spectrometry
LV	Left ventricle
Lv	Length density
MAP1LC3B	Microtubule-associated protein 1 light chain 3 B
MLI	Mean linear intercept
MRM	Multiple reaction monitoring
mTOR	Mammalian target of rapamycin
MV	Mechanical ventilation
MWA	Medial wall area
NO	Nitric oxide
NP-40	Nonyl phenoxypolyethoxylethanol
Nv	Numerical density
PAP	Pulmonary arterial pressure
PARP	Poly (ADP-ribose) polymerase
PBS	Phosphate-buffered saline

PKC	Protein kinase C
PND	Postnatal day
PVDF	Polyvinylidene fluoride
PVR	Pulmonary vascular resistance
RDS	Respiratory distress syndrome
RIPA	Radioimmunoprecipitation
RNS	Reactive nitrogen species
ROS	Reactive oxygen species
RPM	Revolutions per minute
RV	Right ventricle
S	Septum
S.C	Subcutaneous
S1P	Sphingosine-1 phosphate
SD	Sprague-Dawley
SDS	Sodium dodecyl sulfate
SDS-PAGE	Sodium dodecyl-sulfate polyacrylamide gel electrophoresis
SGMS1	Sphingomyelin synthase 1
SMPD1	Sphingomyelin phosphodiesterase 1
SPT	Serine palmitoyl transferase
SURS	Serial uniform random sectioning
Sv	Surface density
TBS	Tris-buffered saline
TGF-β1	Transforming growth factor-β1
TNF	Tumor necrosis factor
TSP-1	Thrombospondin-1
TUNEL	Terminal deoxynucleotidyl transferase dUTP nick end labeling
Vv	Volume density
WB	Western blot

Acknowledgement

Over the past two years, I have had the privilege of working with a group of highly experienced and knowledgeable scientists, whose contributions have greatly enriched my experience as a graduate student. Firstly, I would like to express my sincere gratitude to Dr. Robert Jankov for his unwavering support, guidance, and remarkable mentorship, which has been instrumental in my professional and personal growth.

Secondly, I extend my thanks to Dr. Behzad Yeganeh for his exceptional support and guidance during my time at CHEO RI. His passion, dedication, and work ethic serve as an inspiration and I deeply value our discussions, collaborations, and his continual encouragements.

I am also grateful to Drs Bernard Thébaud and Tommy Alain, members of my Thesis Advisory Committee, for their invaluable input and guidance throughout my master's degree, which have not only enriched my research but also fostered my development as a researcher.

Furthermore, I extend my appreciation to Dr. Bernard Thébaud and Dr. Zakia Djaoud for their willingness to evaluate my thesis and defense exam, and for their valuable contributions to my learning and growth during my master's training.

Special recognition is also extended to the outstanding the members of the laboratory of Dr. Jankov, including Mrs. Kate Daniel and Mrs. Chantal Gaudet, whose unwavering support and assistance in daily laboratory tasks and answering my inquiries have been invaluable.

The supportive and nurturing work environment at CHEO RI has made me feel truly at home, and for this, I am immensely thankful to the entire community, particularly Mrs. Lynn Kate, Mrs. Martine St-Jean, Ms. Nathalie Earl, Mr. Allan Humphrey, Mr. Keith Wilson, and Mrs. Joycelyn Mmrah. I am deeply appreciative of the collective efforts of everyone mentioned above, without whom this journey would not have been possible.

Chapter 1: Introduction

1.1 Preterm Birth:

Preterm birth, defined as birth prior to 37 completed weeks' gestation, is the leading cause of early childhood mortality, impacting children worldwide [1]. During the third trimester of pregnancy, many vital organs in the human body, including the brain [2], lungs [3], and liver [4], are still in the process of development. Delivery before term gestation is therefore associated with a higher risk of severe disabilities or even mortality [5, 6]. Extremely premature birth, defined as birth occurring before 29 completed weeks of gestation, presents a particular challenge [7]. In Canada and other developed countries, it contributes excessively to infant mortality rates and increased risks of morbidity throughout an individual's life. This, in turn, imposes a substantial financial burden on the healthcare system [8]. Despite accounting for only a small fraction of live births in Canada (~0.5% or 1,870 cases in 2018 according to the Canadian Neonatal Network), extreme prematurity is responsible for more than 75% of neonatal deaths and the vast majority of cases of chronic respiratory and neurological morbidity in children [5, 9]. These statistics underscore the critical importance of understanding the root causes of chronic respiratory and neurological morbidity in premature infants.

1.2 Human Lung Development:

Mammalian lung development progresses through a series of five overlapping phases, as illustrated in Figure 1 [10]. These five stereotypical stages are crucial for the formation and maturation of the respiratory system [11]:

1. Embryonic Stage (weeks 3-6): Emergence of the lung buds.

2. Pseudoglandular Stage (weeks 6-16): Lung buds undergo rapid proliferation and transform into the primary airways. Additionally, peripheral acinar buds begin to form, contributing to the branching structure of the developing lung.

3. Canalicular Stage (weeks 16-26): Characterized by the completion of proximal airway branching.

4. Saccular Stage (weeks 26-36): Terminal saccules budding out from the proximal airspaces are formed, which greatly increases the surface area of the distal lung airspaces. This expansion is facilitated by the presence of type 1 and 2 pneumocytes and expansion of septal capillaries, which together provide a degree of efficiency in gas exchange capable of supporting life. It is also in this stage that the production of pulmonary surfactant begins.

5. Alveolar Stage (from weeks 36 until adolescence): This phase leads to a marked increase in both the number and surface area of distal airspaces, known as alveoli. This growth is crucial for achieving the highest possible level of gas exchange efficiency in the respiratory system.

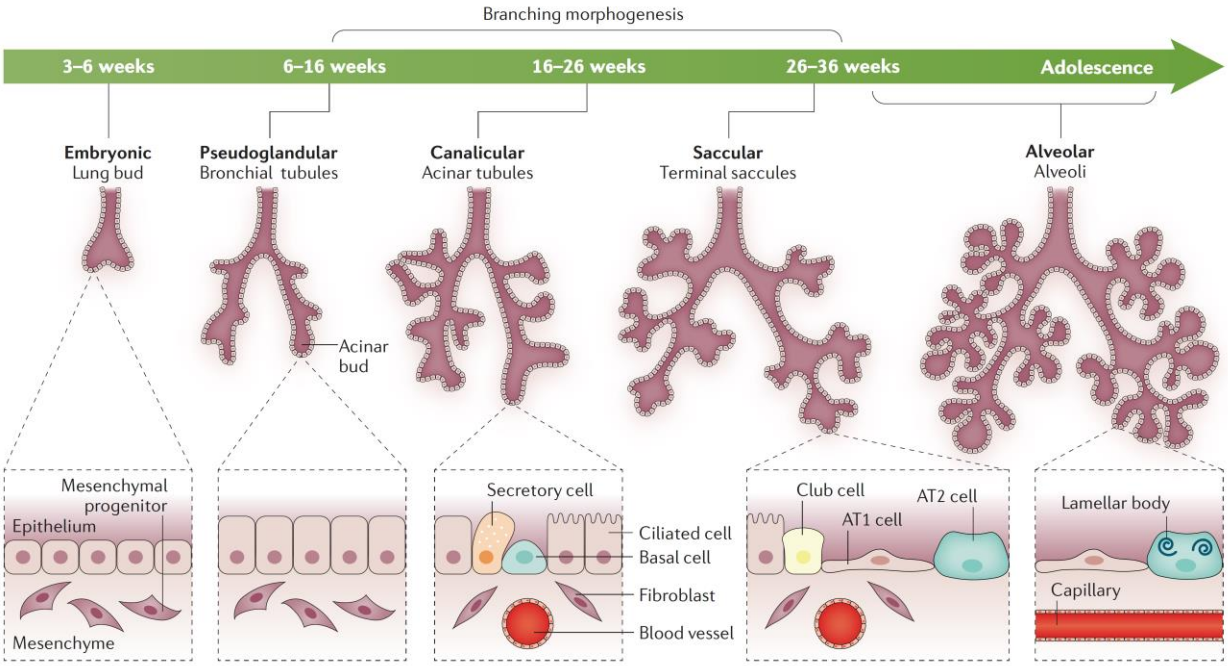

Figure 1: Stages of normal human lung development. Human lung development progresses through distinct stages, commencing with lung bud formation in the embryonic phase and extending to alveolar maturation during advancing gestation until adolescence. Within the pseudoglandular and canalicular phases, the lung buds undergo proliferation to establish the airways. During the saccular stage, epithelial cells lining the conducting airways differentiate, leading to the formation of saccules that enable the gas exchange. Subsequently, alveolar type 2 (AT2) cells initiate the production of surfactant lipid and proteins crucial for preventing lung collapse (atelectasis) and ensuring proper respiratory function. In the alveolar phase, maturation and alveolar septal growth persist, ultimately reaching the highest surface area in the lung. *Bernard Thébaud et al., Nat Rev Dis Primers, (2019)*

1.3 Bronchopulmonary Dysplasia (BPD):

BPD is a chronic lung disorder associated with extremely premature birth [12], resulting from the disruption of alveologenesis [13]. Clinically, it is defined by the requirement for supplemental oxygen and/or mechanical ventilation at 36 weeks corrected gestational age (GA) [14]. Pathologically, it is characterized by a decrease in the number of alveoli, an increase in the dimensions of distal airspaces, thickening of the capillary-gas interface [9, 15] and hypoplasia of the lung microvasculature [16]. In addition, varying degrees of inflammation [17], and fibrosis within lung tissue are observed [18]. Premature infants experience compromised alveolar gas exchange requiring the use of respiratory support, including oxygen supplementation and mechanical ventilation (MV) [12], which are major contributors to BPD [19].

Despite advances in current prenatal and postnatal treatments, such as antenatal steroids, surfactant replacement therapy, and "gentler" ventilation approaches, the prevalence of BPD among premature infants born before 29 weeks GA remains at approximately 40% [20]. Avoidance of excessive oxygen concentrations and increased use of non-invasive ventilation have decreased the overall severity of BPD, but have not impacted its incidence [21].

Survivors of BPD experience a range of morbidities [22], as indicated by frequent hospital admission and high rates of medical visits due to recurrent respiratory exacerbation [23], respiratory infections [24], and pulmonary hypertension [25]. In these cases, sustained lung function abnormalities may persist into childhood and even into adulthood, manifesting as poor exercise tolerance and reliance on chronic respiratory medications [26]. Moreover, there is increased risk of non-pulmonary comorbidities, such as neurocognitive impairment and retinopathy of prematurity, a major cause of visual impairment and blindness [27, 28]. Considering the increasing survival rates of preterm infants at the limits of viability, the incidence and impact

of BPD are likely to continue rising [10]. Currently, there are no safe or effective therapies to reverse or prevent BPD [9]. Recognizing this critical gap, the U.S. Food and Drug Administration (FDA) has identified BPD as an urgent priority for the development of new treatments [29].

1.4 Hyperoxia, BPD and Cell Death:

In previous studies, it has been demonstrated that hyperoxia and MV are the main modifiable contributors to BPD [30]. Prolonged oxygen therapy can induce the generation of reactive oxygen species (ROS) in the lung tissue of premature neonates [31], contributing to the pathogenesis of BPD when antioxidant defense is inadequate [32]. The incidence and severity of BPD exhibits a direct relationship with the amount and duration of respiratory support (Figure 2) [33]. These insults interact with genetic predisposition [34, 35], antenatal factors (e.g., chorioamnionitis) [36] and postnatal factors (e.g., sepsis, fluid overload, patent ductus arteriosus) [37, 38], leading to varying degrees of inflammation and oxidative stress in the lung. Previous research conducted in Dr. Jankov's laboratory has highlighted "nitroxidative" stress as critical to neonatal lung injury, particularly due to nitric oxide-derived reactive nitrogen species, such as peroxynitrite, causing both oxidation and highly damaging protein nitration [9, 39]. Downstream of nitroxidative stress, the pathophysiology of BPD is characterized by an imbalance between cell growth and cell death signaling pathways, including autophagy [40] and apoptosis [41], resulting in cell death in some cell types (distal airway epithelium) [42] and increased proliferation in others (airway and vascular smooth muscle) [43]. The mechanistic link between the injurious stimuli (hyperoxia, MV) and (nitr)oxidative stress has been less clear. *Recent work suggests the up regulation of ceramides as a potentially key factor [44-46].*

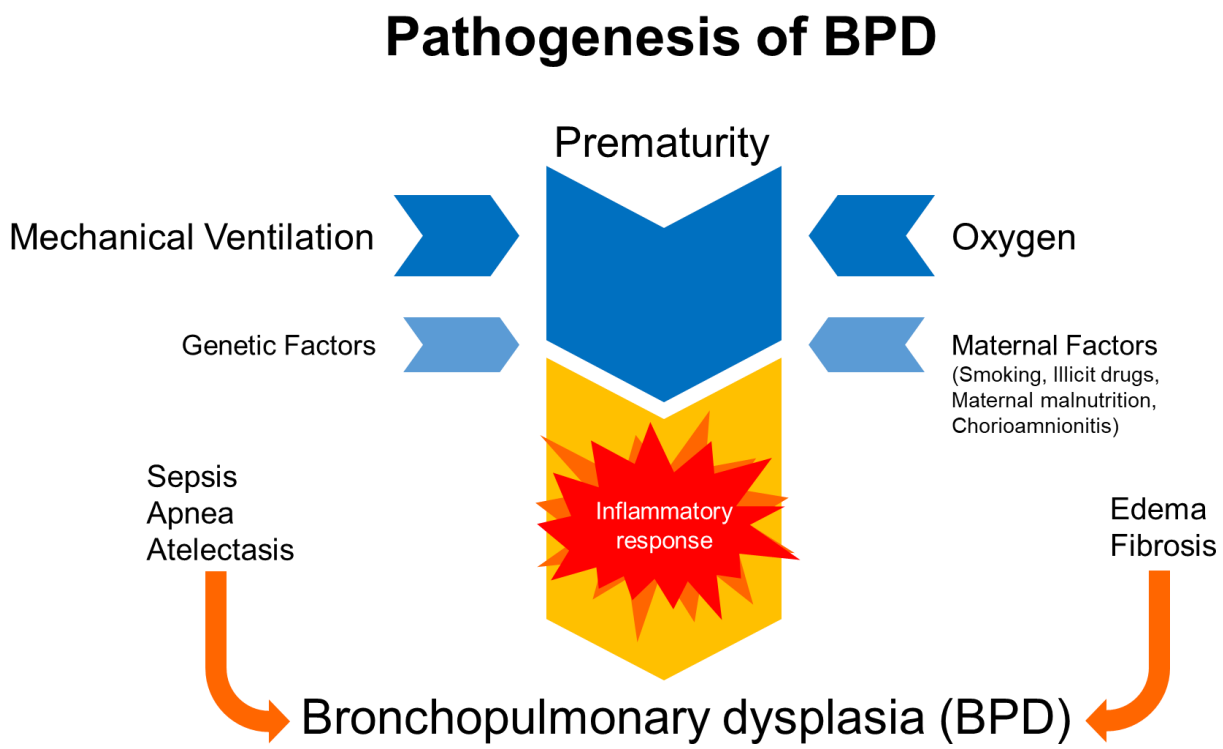

Figure 2: Overview of the pathogenesis of BPD, illustrating the various factors contributing to the inflammatory response. The primary causes of BPD include prematurity, MV, and hyperoxia. Prematurity stands out as the most significant risk factor, requiring higher respiratory support and increases the vulnerability of immature lungs. Additional maternal risk factors, such as intrauterine growth restriction (IUGR), smoking, and chorioamnionitis, along with genetic risk factors, may also contribute substantially to the onset of BPD. Furthermore, postnatal factors such as sepsis, edema, and fibrosis have been identified to be associated with an elevated risk of BPD.

1.5 Apoptosis:

Apoptosis, derived from the Greek word meaning the natural process of leaves falling from trees, represent programmed cell death characterized by complex molecular signaling systems that trigger an orderly, energy-dependent enzymatic breakdown of DNA, lipids, and other macromolecules [47]. Cells undergoing apoptosis exhibit rapid morphological changes, including cell rounding, pseudopod shrinkage, decreased cellular volume, chromatin condensation (pyknosis), and nuclear fragmentation (karyorrhexis), followed by plasma membrane blebbing and eventual ingestion by phagocytes [47]. Apoptosis plays a key role in maintaining the homeostatic balance between cell formation and cell death [48]. It is a tightly regulated and highly synchronized phenomenon coordinated by an extensive group of proteases known as cysteine aspartate-specific proteases (caspases) [49]. Caspases are widely expressed in the cell in an inactive form (procaspases), which, once triggered (by cleavage), activate other procaspases, initiating a protease cascade that irreversibly commits the cell to death [50].

In mammals, two major pathways are involved in the initiation of apoptosis: extrinsic and intrinsic. The extrinsic pathway is triggered by external signals, such as the binding of ligands to cell surface death receptors, which are typically members of the tumor necrosis factor (TNF) receptor gene family [48, 51]. Conversely, the intrinsic pathway is triggered by internal stimuli, such as oxidative stress, DNA damage and lack of growth factors [48]. Despite differences in their induction and regulation, these pathways are linked and intersect at various stages, where molecules in one pathway can influence the other [41]. Mitochondria play a central role in the crosstalk connecting these two pathways. The initiation of either pathway results in a caspase activation cascade leading to the mitochondrial release of cytochrome c and the formation of the apoptosome complex, ultimately committing the cell to apoptosis (Figure 3) [41, 48].

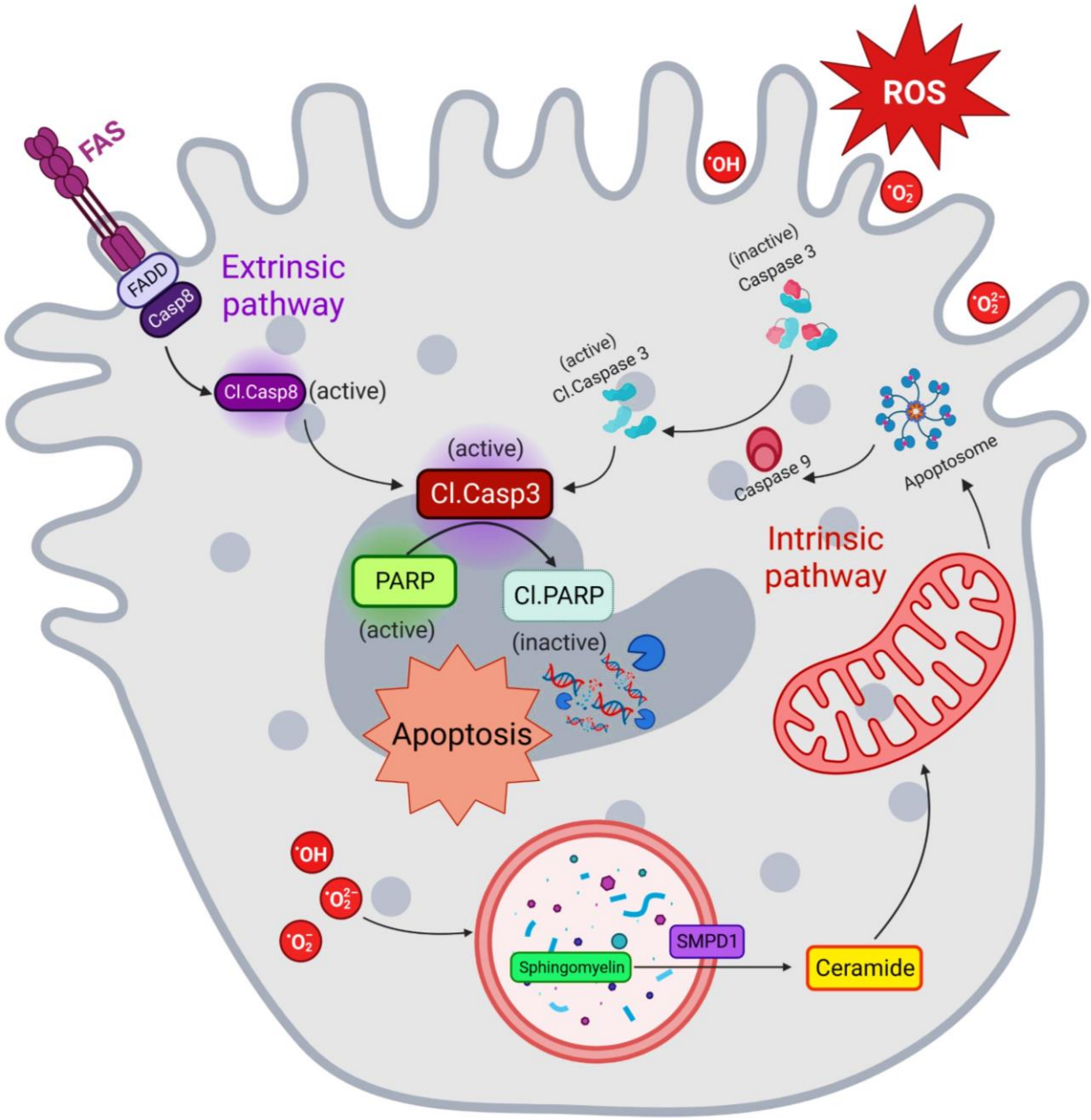

Figure 3: A schematic representation of apoptosis, emphasizing the two primary pathways, the "Extrinsic" and "Intrinsic" pathways, each activated by specific triggering signals. The extrinsic pathway initiates from outside of the cell through receptor-mediated stimuli, leading to the activation of caspase 8 (cleaved caspase 8) as an initiator. This activation subsequently triggers the executioner caspase 3 (Casp 3), a key participant in the core apoptosis pathway. Conversely, the intrinsic route commences with an injury inside the cell, resulting in the release of proapoptotic proteins from the mitochondrial membrane. This leads to apoptosome formation and activation of the initiator caspase 9, which then triggers Casp 3 as an executioner. These events culminate in nuclear fragmentation and chromatin condensation. Fas associated death domain (FADD), Reactive oxygen species (ROS), Sphingomyelin phosphodiesterase 1 (SMPD1).

1.6 Autophagy:

Autophagy, which literally translates to "self-eating", is a lysosome-dependent intracellular degradation program responsible for the turnover of cellular organelles and long-lived proteins [52]. The main sequential steps in autophagy include induction, autophagosome formation, autophagosome-lysosome fusion, and degradation [53]. Autophagy plays a pivotal role in cellular homeostasis and adaptation to adverse environments, contributing to both physiological and pathological outcomes [54]. More than 30 autophagy-related (*ATG*) genes and their products have been identified, with some of the most investigated ones including *ATG5*, *Beclin-1*, *ATG12*, and the microtubule-associated protein 1 light chain 3 B (*MAP1LC3B or LC3B*) genes [55].

In mammals, the conversion of LC3B protein from LC3BI (free form) to LC3BII (phosphatidylethanolamine–conjugated form) is considered a critical step in autophagosome formation and is commonly employed to detect autophagy [54]. Although autophagy and apoptosis are distinct processes regulated by different signaling elements, they can cooperate, being interconnected via numerous regulatory molecules including Bcl-2/Beclin1, LC3BII/Fas, caspases, mitochondria and sphingolipids [46, 56, 57]. This interaction explains how changes in autophagy activation can lead to cell death through apoptosis [58, 59]. Indeed, inhibitors of mammalian target of rapamycin (mTOR), a checkpoint pathway that suppresses autophagy [60], prevents hyperoxia-induced lung injury in neonatal mice [40] and rats [61].

1.7 Sphingolipids and Ceramides:

Sphingolipids constitute a major class of lipid components in all eukaryotic cells [62]. Prominent subclasses of sphingolipids include Ceramide, Sphingomyelin, and Glycosphingolipids [63]. In addition to their structural features, these lipids play crucial roles in various cellular

functions. Ceramide, in particular, serve as the foundational structural entity within this group and can undergo conversion into various sphingolipids [64].

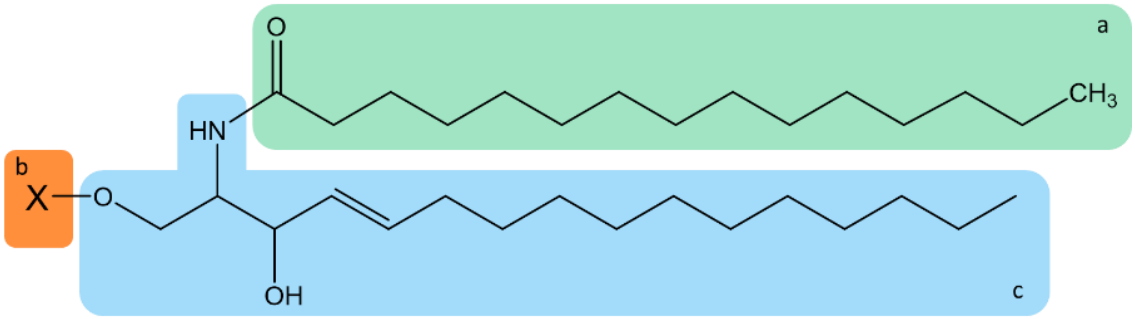

Figure 4: The image illustrates sphingolipid structure, consisting of three major groups: a) Fatty acid (Acyl group) in green, b) Head group (X), and c) Sphingosine (the backbone) in blue.

In all ceramides (Figure 4) the sphingosine component is fixed, and the head group consists of hydrogen. However, the fatty acid acyl group exhibits variability in chain length and saturation, thereby determining different ceramide classes and functions. According to acyl chain length, three categories can be identified:

1. Medium chain (14 carbon fatty acids).

2. Long chain (16, 18 and 20 carbon fatty acids).

3. Very long chain (22, 24 and 26 carbon fatty acids).

While long (C16–20) and very long (C22–24) acyl chains are the most common, even longer acyl chains (C26–36) are also found in special cells during their differentiation and maturation [65]. As depicted in Figure 5, ceramides are produced through three main metabolic pathways: 1) *de novo* synthesis, 2) sphingomyelin hydrolysis and 3) the salvage pathway [66]. Ceramides play a key role in regulating tissue growth pathways, autophagy, apoptosis, and cell proliferation [62]. Previous studies on the MV-induced lung injury revealed the crucial role of C16-ceramide in the autophagy activation and apoptotic cell death [45, 46]. Koybasi and

colleagues demonstrated that increase of C18-ceramide generation in human head and neck squamous cell carcinoma restrained cell growth by modulation of telomerase activity and induction of apoptotic cell death [67]. In contrast, it has been identified that increase of very long chain ceramide (C24:0- and C24:1-Ceramide) promotes proliferation in breast and colon cancer cells [68].

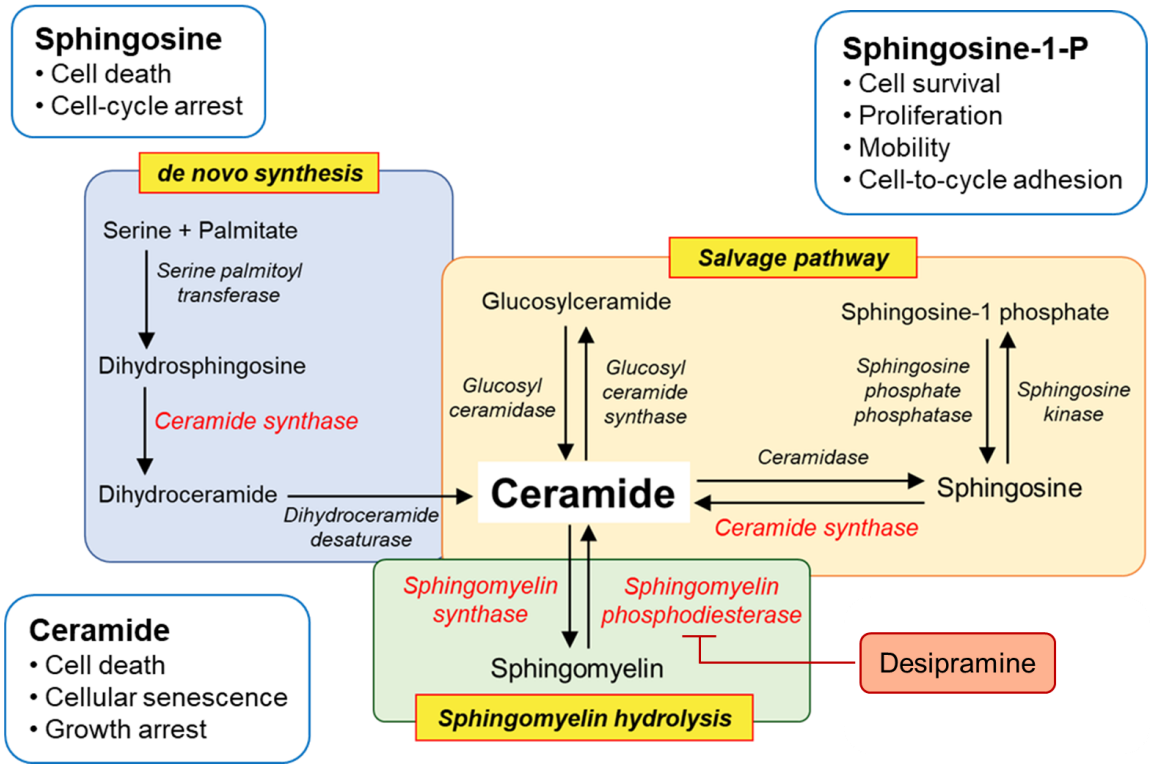

Figure 5: Overview of sphingolipid metabolism and its major functions. The three main pathways of ceramide synthesis are the *de novo* pathway, sphingomyelin hydrolysis (mediated by Sphingomyelin phosphodiesterase), and the salvage pathway. In the *de novo* pathway, the condensation between serine and palmitate represents the rate-limiting step, catalyzed by serine palmitoyl transferase (SPT). Sphingomyelinase enzymes utilize sphingomyelin as a substrate for ceramide production. In the recycling or salvage pathway, ceramide can be reversibly degraded to sphingosine by ceramidase or produced from sphingosine through ceramide synthase activity. Ceramide and sphingosine-1 phosphate (S1P) exhibit opposing signaling characteristics, contributing to the maintenance of homeostatic balance. Ceramide is considered as a pro-apoptotic molecule that induces cell death, while S1P can promote cell survival and proliferation. Desipramine is a functional SMPD1 inhibitor, acting on the sphingomyelin hydrolysis pathway of ceramide synthesis. (Lee, Yeganeh et al., *Apoptosis*2015)

Recent studies have revealed the potential involvement of sphingolipids in the pathogenesis of BPD [69]. In lung diseases, dysregulation in sphingolipid metabolism is associated with elevated levels of ceramide and its synthetic enzymes [45]. Altered sphingolipid and ceramide levels have also been implicated in the pathology of various adult respiratory diseases including asthma [70], cystic fibrosis (CF), chronic obstructive pulmonary disease (COPD) [71], and cigarette-smoke induced lung injury [72]. Neonatal rodents exposed to hyperoxia exhibit increased total ceramides in bronchoalveolar lavage fluid [44]. In addition, van Mastrigt et al [45] reported a significant increase in ceramide concentration (both long chain and very long chain) in tracheal aspirates from 122 preterm Dutch newborns mechanically ventilated during the first 7 days of life. In a subsequent mechanistic study, the relationship between ceramide production, autophagy, and apoptosis during acute experimental MV-induced lung injury was examined in newborn rats [46]. Attenuation of ceramide synthesis by SMPD1 inhibition with Desipramine (and to a lesser extent, Fluoxetine, also an SMPD1 inhibitor), prevented autophagy-mediated cell death [46].

Several SMPD1 inhibitors with diverse therapeutic indications are currently accessible [73]. Table 1 illustrates the current repertoire of potential SMPD1 inhibitors alongside their corresponding pharmacologic characteristics. Notably, Desipramine emerges as an FDA-approved drug, offering superior efficacy [46] and safety profiles, particularly in neonatal cohorts [74].

Drugs	**Main indication**	**Main known mechanism of action**
Desipramine	Depressive disorder	Norepinephrine reuptake inhibitor
Fluoxetine	Depressive disorder	Selective serotonin reuptake inhibitor
Benztropine	Parkinson’s disease	Anti cholinergic
Amlodipine	Hypertension	Calcium channel blocker

Table 1: Potential SMPD1 inhibitors and their pharmacologic characteristics.

1.8 Desipramine:

Desipramine hydrochloride *(Norpramin®)* is a dibenzazepine compound (two benzene rings fused to an azepine ring = tricyclic) (Figure 6), first approved for clinical use in 1964 as a close analogue of Imipramine *(Tofranil®)*, the first tricyclic antidepressant. This class of drugs has also been used for treatment of depressive disorders, anxiety, and nocturnal enuresis. However, their overall use has declined since the 1990s with the introduction of selective serotonin reuptake inhibitors, such as Fluoxetine. The pharmacokinetics and cellular distribution of dibenzazepines have been extensively studied [75]. Following administration, Desipramine is primarily metabolized by CYP2D6 to its 2-hydroxy metabolite, which is renally excreted and by CYP1A2 and CYP2C19 to its *N*-demethylated (primary amine) metabolite [75]. Daily dosing is sufficient to reach steady-state levels (adult dose 100-200 mg/day). Desipramine is a functional inhibitor of SMPD1 (also known as acid sphingomyelinase or ASM), a key hydrolase found in lysosomes, (a central organelle involved in the autophagy pathway with over 60 luminal hydrolases), which regulates the production of ceramides from sphingomyelin. Intracellularly, Desipramine accumulates in lysosomes, where SMPD1 resides, and attaches to the lysosomal inner membrane leaflet by electrostatic forces [76]. Its inhibitory activity on SMPD1 has been postulated as the primary mechanism of antidepressant effect [77].

For my thesis work, I aimed to conduct a comprehensive investigation into the impact of hyperoxia exposure on ceramide levels in the lung tissue of newborn rats, with a focus on evaluating ceramides as a novel therapeutic target for prevention of hyperoxic lung injury. I explored strategies to limit ceramide production through SMPD1 inhibition, with a goal to further bolstering evidence for this approach as a promising therapeutic avenue for the prevention of BPD.

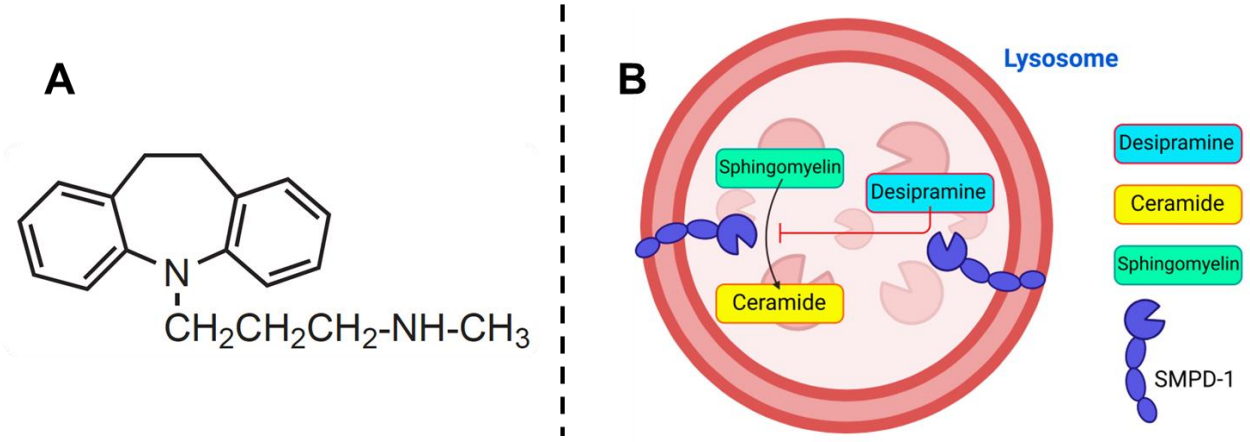

Figure 6: Desipramine structure and inhibitory function on SMPD1. (A) illustrates the structure of Desipramine molecule, a tricyclic antidepressant that exerts its action through the inhibition of norepinephrine reuptake in the synaptic clefts. In (B), it is demonstrated that Desipramine functions as an inhibitor of SMPD1, effectively preventing the production of ceramide from sphingomyelin.

1.9 Description of Rat BPD-like Lung Injury Model:

The majority of our understanding about the pathogenesis of BPD is derived from animal models [78]. Rodents are suitable models for studying human preterm lung injury due to the delayed timing of alveolar development, which commences in the postnatal period [79, 80]. Another advantage of rodents is the maturity of their surfactant system, which is biochemically more advanced compared to preterm humans at a comparable stage of lung development. Consequently, defective surfactant maturation can be eliminated as a contributing factor, allowing for a focused investigation into other contributors, such as oxidative stress [80].

Rats are the most commonly employed rodent species, as pulmonary vascular injury can be more easily induced than in mice [81, 82], and their larger size more easily facilitates instrumentation and imaging [80]. Recognizing the need for a permanent lung injury model in rats, resembling that observed in humans, Dr. Jankov's group published a novel rat model [39]

involving continuous exposure to 60% O_2 from postnatal days (PND) 1-14, followed by intermittent hypoxia (10% O_2 for 10 min every 4 hours) for an additional 14 days until PND 28. The inclusion of intermittent hypoxia was designed to replicate the severe desaturation "spells" observed in neonates with evolving BPD. This addition prevented spontaneous recovery of arrested alveolarization that occurred following recovery from exposure to moderate hyperoxia alone, producing a structural and functional phenotype more closely resembling that of young adult survivors of BPD [39]. We have since further refined this model in two ways. Firstly, by exposing animals to 85% O_2 from PND 1-7 (and 60% O_2 from PND 7-14), resulting in a more pronounced disruption of airway development. Continuation of 85% O_2 exposure beyond 7 days ultimately leads to growth restriction and often death, which is avoided by reverting to 60% O_2 during the second week of exposure [80]. Secondly, we now employ only one week of intermittent hypoxia (10% O_2 for 10 min every 4 hours, from PND 14-21; 21-day model), which has an equivalent effect to 2 weeks (28-day model, as previously published [39]) in preventing the recovery of arrested alveolarization. We term this new model the hyperoxia-intermittent hypoxia (HIH) model (see illustration in Figure 18 in the Results section).

1.10 Rationale:

The exact mechanisms linking hyperoxia exposure, cell death and lung injury are not yet completely understood. Previous studies have demonstrated the role of ceramide in MV-induced lung injury and epithelial cell death through activation of autophagy and apoptosis [46, 69, 83]. These studies also demonstrated that the inhibition of ceramide production through SMPD1 attenuates cell death induced by MV [46]. However, it is important to note that the MV model is brief by necessity (rodents cannot survive MV for more than a few days) and therefore does not produce a lung injury resembling BPD, which requires time to develop and to which hyperoxia is

also an important contributing factor. Therefore, we sought to test the effects of ceramide inhibition in the HIH BPD model described above.

1.11 Objectives and hypotheses:

The objectives of my master's thesis project are as follows:

1. To demonstrate the impact of hyperoxia on ceramide levels in the lungs of newborn rats.
2. To establish the chronological sequence of events involving elevated ceramides, autophagy, and apoptosis in the lungs of newborn rats exposed to hyperoxia.
3. To assess the effectiveness of Desipramine in preventing experimental BPD-like lung injury in newborn rats.
4. Additionally, I aimed to investigate the presence and contents of key ceramide pathway proteins in archived lung tissue sections from extremely premature infants (autopsy specimens) who died, either with or without BPD.

In accordance with my research objectives, I posit the following hypotheses: First, hyperoxia will elevate ceramide levels, subsequently inducing activation of autophagy and apoptosis (cell death pathways) in the distal airspace epithelium. Second, inhibition of SMPD1 will reduce ceramide production in the lungs, thereby preventing the activation of cell death pathways and preventing BPD-like lung injury. Third, it is expected that the contents of ceramide pathway proteins will be increased in the lungs of human infants with BPD in comparison to control subjects without BPD.

Chapter 2: Materials and Methods

2.1 Materials:

2.1.1 Animals:

Timed-pregnant Sprague-Dawley (SD) rats were purchased from Taconic Farms (Germantown, New York, USA).

2.1.2 Reagents and Chemicals:

Desipramine hydrochloride (powder) was purchased from Selleck Chemicals (Batch no. S548502, cat no. S5485, Houston, TX, USA). The Pierce™ BCA assay kit (cat no. A55864) and phosphatase inhibitors (cat no. A32957) were purchased from Pierce™ - ThermoFisher. Protease inhibitors were from MilliporeSigma™ (cat no. 539131-10VL). Pre-cast Tris-glycine 4-20% gradient gels (mini-PROTEAN® TGX Stain-Free™) were from Bio-Rad. The transfer membrane used was polyvinylidene fluoride (PVDF) with low background fluorescence and a pore size of 0.45 µm sourced from MilliporeSigma™ (Immobilon®, cat no. IPFL00010). Chemiluminescent reagent (Clarity™ and Clarity Max™ Western ECL substrate, Bio-Rad), imaging system (ChemiDoc Touch) were from Bio-Rad. The fluorescent mounting medium used was the TrueVIEW® autofluorescence quenching kit containing 4',6-diamidino-2-phenylindole (DAPI) (cat no. SP-8500-15) sourced from Vector Laboratories. Acids, alcohols, organic solvents, paraformaldehyde from ThermoFisher, Permount (cat no. SP15-100) and Superfrost/Plus microscope slides (cat no. 12-550-15) were purchased from ThermoFisher.

2.1.3 Antibodies:

Antibodies used for Western blot (WB), immunofluorescence (IF) and immunohistochemistry (IHC) to detect autophagy included anti LC3B Rabbit polyclonal (cat no. 3868, Cell Signaling, Danvers, MA, USA) and anti ATG5-12 (D5F5U) Rabbit monoclonal (cat no.

12994, Cell Signaling, Danvers, MA, USA). Apoptosis markers included anti cleaved caspase 3 (Cl.Casp 3) Rabbit polyclonal (cat no. 9661, Cell Signaling, Danvers, MA, USA), anti cleaved PARP (Cl.PARP) Rabbit monoclonal (cat no. 94885, Cell signaling, Danvers, MA, USA), anti Cl.PARP Rabbit monoclonal (cat no. ab32064, Abcam, Cambridge, MA, USA). Epithelial cell marker antibody: Anti E-cadherin (CDH1) Mouse monoclonal (cat no. 14472, Cell Signaling, Danvers, MA, USA). The housekeeping protein antibody used was anti β-actin Mouse monoclonal (cat no. 3700, Cell Signaling, Danvers, MA, USA). The following primary antibodies were used for IHC staining in this study: anti SMPD1 Rabbit polyclonal (cat no. 14609-1-AP, Proteintech, Rosemont, USA), anti Sphingomyelin synthase 1 (SGMS1) Rabbit polyclonal (cat no. PA5-83764, Invitrogen, Waltham, MA, USA), anti Ceramide synthase 1 (Lass 1) Rabbit polyclonal (cat no. PA5-112596, Invitrogen, Waltham, MA, USA), anti Ceramide synthase 2 (CerS2) Mouse monoclonal (cat no. TA809918, OriGene, Rockville, MD 20850, USA). Further details for each antibody are provided in Table 2.

The following horseradish peroxidase (HRP)-conjugated secondary antibodies for WB were used in this study: Goat anti Rabbit HRP-linked (cat no. 7074, Cell Signaling, Danvers, MA, USA), Horse anti Mouse HRP-linked (cat no. 7076, Cell signaling, Danvers, MA, USA). For secondary fluorescence conjugated antibodies Cy5-conjugated Goat anti Rabbit (cat no. 111-175-144, Jackson ImmunoResearch, PA, USA) and Alexa Flour 488-conjugated Goat anti Mouse (cat no. A-11001 Invitrogen, Waltham, MA, USA) were employed. Further details for each antibody are provided in Table 3.

2.1.4 Terminal Deoxynucleotidyl Transferase dUTP Nick End Labeling (TUNEL) Assay:

Apoptotic cells were visualized using the HRP-DAB TUNEL Assay Kit (ab206386, Abcam) in accordance with the manufacturer's instructions.

2.2 Methods:

2.2.1 *In Vivo* Experiments:

All procedures involving animals were approved by the Animal Care Committee at the University of Ottawa and conformed to the guidelines of the Canadian Council on Animal Care. Food and water were available *ad libitum*, and room lighting was programmed for 12h:12h light/dark cycles. Pups and dams were housed in programmable O_2 exposure chambers (Biospherix) and exposed to either HIH or room air (21% O_2; normoxia control) after birth. Each litter was maintained at a size of 10-12 pups to control for nutritional effects, and dams were exchanged daily between paired normoxia and hyperoxia chambers to prevent maternal oxygen toxicity. From PND 1, pups received daily subcutaneous (S.C) injections of Desipramine or vehicle (sterile water for injection). Injection volumes (5 µl per gram of body weight) were identical for both the vehicle and Desipramine. Initial dose-response studies (10 and 20 mg/kg) were conducted to determine the more effective dose of Desipramine in lowering ceramide concentration in the lungs tissue of newborn rats exposed to hyperoxia. My animal study involved tissue collection at three different time points to measure the specified parameters in the lungs of newborn and juvenile rats: PND 1, PND 7 and PND 21.

For the PND 1 time point, pups from all litters received one dose of Desipramine or vehicle immediately after birth and were then exposed to either hyperoxia (85% O_2) or room air (21% O_2). After 24 hours, the lung tissues were collected. The left lung was fixed in 10% formalin for 48

hours, dehydrated, and paraffin-embedded for immunohistochemistry, while the right lung was rapidly frozen in liquid nitrogen and stored in -80°C for ceramide measurement and WB analysis. For the PND 7 time point, newborn pups were exposed to severe hyperoxia (85% O_2) or room air (21% O_2) and received Desipramine or vehicle injections once daily; after which pups were euthanized, and the lung tissues were harvested in the same manner as described for PND 1.

The PND 21 study was conducted with pups derived from 8 litters (approximately 100 pups in total, distributed across 4 groups, with each group comprising a minimum of two litters). During the first week, pups were exposed to either severe hyperoxia (85% O_2) or room air (21% O_2). In the second week, the hyperoxic conditions for the exposed pups transitioned from severe hyperoxia to moderate hyperoxia (60% O_2), while there was no alteration for the room air group. In the last week, the hyperoxia-exposed pups underwent intermittent hypoxia (10% O_2 every 4 hours for 10 minutes), whereas there was no modification for the room air group. On PND 21, the pups were euthanized, and the lung tissues were either collected and immediately frozen in liquid nitrogen or inflation-fixed for design-based stereology, described in the next section.

2.2.2 Preparation of Rat Lungs for Structural-Morphological Studies:

Tissue preparation proceeded according to the comprehensive official research policy statement by American Thoracic Society/European Respiratory Society [84] and latest primer published by Matthias Ochs and Julia Schipke [85] for accurate quantitative assessment of lung structure. Animals were anesthetized with 5% isoflurane followed by intraperitoneal (I.P) ketamine (80 mg/kg) and Xylazine (20 mg/kg). The thoracic cavity was opened, the trachea was cannulated, and the lungs were air-inflated at 25 cmH_2O pressure to recruit the lungs, and subsequently decreased to a constant 20 cmH_2O pressure, ensuring that the lungs were on the descending limb of the pressure-volume curve. The pulmonary veins were divided, and a fine

needle was inserted into the right ventricle (RV). Subsequently, the pulmonary circulation was flushed with 1X phosphate-buffered saline (PBS) containing 1 U/ml heparin until the lungs appeared white. The lungs were then perfusion-fixed at 100 cmH_2O pressure with a fresh, ice-cold solution of 4% (w/v) paraformaldehyde and 0.1% (v/v) glutaraldehyde in 1X PBS via the RV needle, while being continuously air-inflated.

Following perfusion fixation, the trachea was ligated distal to the cannula, and the lungs and heart were removed *en bloc*. After a 24-hour incubation in fixative, the left main stem bronchus was ligated, the left lung separated, and its volume was measured by the weight of displaced water (Archimedes method) and recorded. Right lung lobes (reserved for histological staining) and left lungs (for morphometry by design-based stereology) were dehydrated by incubation in a series of ethanol solutions and cleared in xylene. Left lung lobes, separated in two parts, were embedded in paraffin or glycol methacrylate (GMA). Following paraffin embedding, 5-µm sections were cut and placed on Superfrost/Plus slides, dried overnight at 37°C and baked at 60°C for 1 hour. Following GMA embedding, semi-thin (1-µm) sections were cut and placed upon a drop of distilled water on Superfrost/Plus slides and air-dried overnight.

2.2.3 Design-based Stereology:

Measurements were conducted on left lung sections. Paraffin-embedded tissue blocks were sectioned following established principles for serial uniform random sectioning (SURS) [86-89], ensuring a minimum of 8 sections per tissue block, spaced 350 µm apart (each 70 sections). The first level was obtained at a randomly determined number of sections, ranging between 1-70, utilizing a software-based random number generator (Stereo Investigator® Pulmonary Edition version 2020, MBF Bioscience, Williston, VT, USA) from when lung tissue first appeared. For GMA-embedded sections, a minimum of 5 sections per tissue block were obtained, spaced 690

μm apart. The first section in the series was acquired at a randomly assigned number of sections from the first appearance of tissue, ranging between 1-690 sections.

For paraffin sections, two contiguous sections were immunostained for a macrophage marker, CD68 (for macrophage counts; performed at the Louise Pelletier Histology Core, University of Ottawa), or stained with Hart's elastin (alveolar number, small vessel length, arterial medial wall area). For GMA sections, one section per level was stained with toluidine blue for quantification of distal airspace dimensions and surface area. All lung sections were digitally scanned using the BLiSS® brightfield scanner (MBF Bioscience) and imported into stereology software for analysis while adhering to SURS principles (Serial Section Manager, Stereo Investigator®).

Volume density (Vv) for distal lung parenchyma (excluding proximal airways and vessels), alveolar septum, and distal airspaces were measured using the Area Fraction Fractionator point-counting probe. Alveolar (alveolar surface area/lung parenchyma volume) surface density (Sv) was measured using the Weibel linear probe. Sv and Vv measurements were also employed to calculate the mean linear intercept (MLI = [4/Sv] × Vv airspaces/parenchyma).

Alveoli were counted using the Physical Fractionator probe (dissector height 5 μm) on contiguous Hart's elastin-stained sections to obtain numerical density (Nv) and total left lung alveolar counts (Nv × Vv parenchyma/lung) for which septal bridges were counted, following the methodology described by Ochs et al [90]. Total macrophages (characterized by rounded CD68-positive cells with a diameter exceeding 10 μm) were counted using the Physical Fractionator probe (dissector height 5 μm) to obtain numerical density, from which total left lung counts were extrapolated. The length of small blood vessels (with an external diameter ranging from 20-60 μm) was measured using the two-dimensional Fractionator plane probe to determine length density (Lv

= [2 × vessels counted]/[number of sites examined × site area]) and total left lung small vessels length (Lv × Vv parenchyma/lung). A comprehensive sampling approach (a minimum of 200 probe-feature interaction counts from at least 4 sections per lung) was employed for all probes to achieve coefficients of error (CE; Gundersen m=1 method) < 0.1 and CE^2/coefficients of variation $(CV)^2$ ratios < 0.5.

For the measurement of Arterial Medial Wall Area (MWA), 4-6 digitally scanned elastin-stained sections, obtained through SURS were utilized. These sections were employed to identify intra-acinar pulmonary arteries (with a mean external diameter of 20-120 μm; a minimum of 100/lung) associated with respiratory bronchioles, where the complete circumference and both inner and outer elastic laminae were visible. The mean external diameter was determined from measurements in two perpendicular planes to account for any irregularities in vessel shape, excluding vessels cut tangentially (with a > 3-fold difference between perpendicular planes). The Area Fraction Fractionator probe was employed to measure area fractions of the medial wall and its associated lumen. The MWA-percentage was then calculated using the formula: area fraction medial wall × 100.

2.2.4 Immunohistochemistry (IHC) Staining (on human samples):

Five-micrometer sections from formalin-fixed, paraffin-embedded lung tissues underwent automated IHC staining using the Leica Bond™-III system (Leica Biosystems, Buffalo Grove, IL, USA). The staining protocol employed was a modification of routine IHC protocol, with the elimination of the post-primary step. Details regarding antibodies, dilutions and antigen retrieval methods are provided in Table 3. Optimal antibody dilution and antigen retrieval methods was predetermined for each antibody using serial dilutions tittered on random lung sections from patients with BPD, with samples from the same patient used for each antibody. Sections underwent

heat-mediated antigen retrieval (utilizing BOND epitope retrieval (ER) solution 1 or 2 from Leica Biosystems) for 20 minutes, followed by incubation at room temperature with primary antibody for 30 minutes and detection using an HRP-conjugated compact polymer system (PowerVision^{+}, Leica Biosystems). Subsequently, slides were then stained with DAB as the chromogen, counterstained with Hematoxylin, mounted, and cover slipped.

Target	Samples	Host/Class	Dilution	Method
Lass1 (Cers1)	Human neonate lung	Rabbit/Poly	1:800	ER 1 (PH 6.0)
CerS2	Human neonate lung	Mouse/Mono	1:6000	ER 2 (PH 9.0)
SMPD1	Human neonate lung	Rabbit/Poly	1:300	ER 2 (PH 9.0)
SGMS1	Human neonate lung	Rabbit/Poly	1:100	ER 2 (PH 9.0)

Table 2: Antibodies, dilutions, antigen retrieval methods used for IHC of human tissues.

2.2.5 Western Blot (WB) Analyses:

Fresh frozen right lung tissues from PND 1 and PND 7 animals were individually homogenized and sonicated in RIPA-SDS lysis buffer (10mM Tris pH 7.4, 150mM NaCl, 10mM KCl, 1mM EDTA 0.5% deoxycholic acid, 0.5% Tween® 20, 0.5% NP-40, 0.1% SDS) containing protease and phosphatase inhibitors, with the procedure conducted under ice-cooled conditions. The lysates were incubated on ice for 30 minutes, then sonicated at 20% amplitude for 15 seconds following 30 second rest, this cycle repeated for 8 times. The sonicated lysates were centrifuged at 15,000 RPM for 20 minutes under 4°C, and the resulting supernatants were gently transferred to fresh tubes and stored at -80°C. The protein concentrations of the tissue lysates were quantified using the Pierce™ BCA protein assay kit from ThermoFisher scientific (cat no. A55864).

Lysate proteins were separated under reducing conditions by Sodium dodecyl-sulfate polyacrylamide gel electrophoresis (SDS-PAGE). Following electrophoresis, the proteins were

transferred to PVDF membranes using the Trans-Blot® Turbo™ Transfer System from Bio-Rad. All membranes were blocked with EveryBlot Blocking buffer from Bio-Rad (cat no. 12010020) for 15 minutes at room temperature, followed by overnight incubation with the primary antibody of interest at 4°C. On the following day, blots were washed with Tris-buffered saline (TBS) with 0.1% Tween® 20 and incubated with a proper secondary antibody for 1 hour at room temperature. The dilutions were 1:1000 for all primary antibodies, except for β-actin (1:20000), and 1:5000 for all secondary antibodies. Bands were quantified by digital densitometry of non-saturated images with background density removed and normalized to corresponding pan-protein content, each corrected for total protein/lane quantified by housekeeping proteins (β-actin).

2.2.6 Immunofluorescence (IF) Staining:

Paraffin-embedded sections of left lungs were deparaffinized in xylene, cleared, and subsequently rehydrated through a graded series of ethanol solutions. Heat-mediated antigen retrieval was performed using an EMS Retriever 2100 pressure cooker from Electron Microscopy Sciences (cat no. R2100-US, Hatfield, PA, USA) immersed in IHC-Tek™ epitope retrieval solution provided from IHC World (cat no. IW-1100, MD, USA). Following antigen retrieval, slides in the container were cooled down for 30 minutes at room temperature. Slides were then removed from the epitope retrieval solution and quickly dipped in deionized water (DI water) to wash out excess salts. The tissue sections were then circled with a hydrophobic ImmEdge pen from Vector Laboratories (cat no. H-4000, CA, USA) and briefly washed three times for 5 minutes each with 1X PBS.

The blocking solution containing permeabilization buffer was applied to the section and incubated for 30 minutes at room temperature. Subsequently, the sections were washed three times for 5 minutes each with and incubated overnight at 4°C with desired primary antibody. The next

day, appropriate fluorescent-conjugated secondary antibody was selected and incubated at room temperature in the dark for 1 hour. Sections were washed with 1X PBS three times for 5 minutes before autofluorescence quenching and counterstaining with DAPI. Images were digitally captured using a Zeiss epifluorescent microscope (Zeiss Axioimager M2 with Apotome 2, Carl Zeiss Microscopy GmbH, Göttingen, Germany) with appropriate filter sets. Identical images acquired with different filter sets were merged using ZEN Pro software (version 2.6, Carl Zeiss Microscopy GmbH).

2.2.7 Mass Spectral Analysis of Sphingolipids:

Liquid chromatography tandem mass spectrometry (LC-MS/MS) was performed on an Agilent 1290 Series binary pump (Agilent Technologies Inc, CA, USA) coupled to an AB5500 triple-quadrupole mass spectrometer (Sciex, ON, Canada) situated at the Analytical Facility for Bioactive Molecules, SickKids Research Institute, Toronto. Reverse-phase high-performance liquid chromatography (HPLC) was performed using a Kinetex C18 column (2.6 µm, 100×2.1 mm Phenomenex, CA, USA). Multiple Reaction Monitoring (MRM) mass transition parameters were optimized using a combination of pure standards (5 µl/min of 1 µg/ml). The sample injection volume was 1-5 µl. The mobile phase was consisted of (A) water/acetonitrile/methanol (2/1/1, v/v/v) and (B) tetrahydrofuran/acetonitrile/methanol (2/1/1, v/v/v). MRM Mass Transitions and Chromatographic Retention Times parameters have been previously published [83]. A separate standard curve was generated for each analyte measured using MRM area ratios for quantitative analysis (Analyte Peak Area/IS Peak Area). The results were then calculated by plotting the sample area ratios against their respective analyte specific standard curve. Data integration and quantitation was performed using AB Sciex Analyst 1.6 software.

2.3 Statistics:

Statistical analyses were performed using GraphPad Prism 8.0 software. All graphical data are presented as box and whisker plots. An unpaired, two-tailed Student's t-test was employed to compare two groups, while one-way ANOVA with post hoc Tukey test was utilized for comparisons among multiple groups. Mann-Whitney U test was used to compare differences between two independent groups when the variable was not normally distributed. Statistical significance was considered as $P < 0.05$. Detailed statistical information for all experiments can be found in the figure legends.

Target	Host/Class	Dilution for WB	Dilution for IF	Dilution for IHC	Company	Catalogue number
Primary Antibodies						
LC3B	Rabbit/Poly	-	1:150	-	Cell signaling	3868
ATG5-12 (D5F5U)	Rabbit/Mono	1:1000	-	-	Cell signaling	12994
Cl.Casp 3	Rabbit/Poly	-	1:150	-	Cell signaling	9661
Cl.PARP	Rabbit/Mono	1:1000	-	-	Cell signaling	94885
Cl.PARP	Rabbit/Mono	-	1:50	-	Abcam	ab32064
E-Cadherin	Mouse/Mono	-	1:100	-	Cell signaling	14472
β-actin	Mouse/Mono	1:20000	-	-	Cell signaling	3700
SMPD1	Rabbit/Poly	-	1:150	1:300	Proteintech	14609-1-AP
SGMS1	Rabbit/Poly	-	-	1:100	Invitrogen	PA5-83764
Lass1	Rabbit/Poly	-	-	1:800	Invitrogen	PA5-112596
CerS2	Mouse/Mono	-	-	1:6000	OriGene	TA809918
Secondary Antibodies						
Rabbit IgG (HRP-linked)	Goat	1:5000	-	-	Cell signaling	7074
Mouse IgG (HRP-linked)	Horse	1:5000	-	-	Cell signaling	7076
Rabbit IgG (Cy5-conjugated)	Goat	-	1:100	-	Jackson Research	111-175-144
Mouse IgG (Alexa Flour 488-conjugated)	Goat	-	1:150	-	Invitrogen	A-11001

Table 3: Details of Antibodies used for WB, IF and IHC. Including host, class, dilutions, vendor, and catalogue number.

Chapter 3: Results

3.1 Objective One: To demonstrate the impact of hyperoxia on ceramide levels in the lungs of newborn rats and effects of Desipramine treatment, an SMPD1 inhibitor.

3.1.1 Effects of Hyperoxia on Lung Ceramides:

Newborn rats were exposed to hyperoxia (85% O_2) or room air (21% O_2; control) from birth for up to 7 days. Animals were euthanized on PND 1 or PND 7, and the lung tissues harvested. Fresh-frozen samples of the right lung tissue were subjected to ceramide quantification using LC-MS/MS. The results from PND 1 samples revealed a significant and rapid upregulation of known and potentially pro-apoptotic ceramides (Figure 7). Examination of lung tissue from PND 7 further revealed that continuous exposure to hyperoxia for 7 days resulted in the sustained elevation of specific ceramide species when compared to the control group (Figure 8).

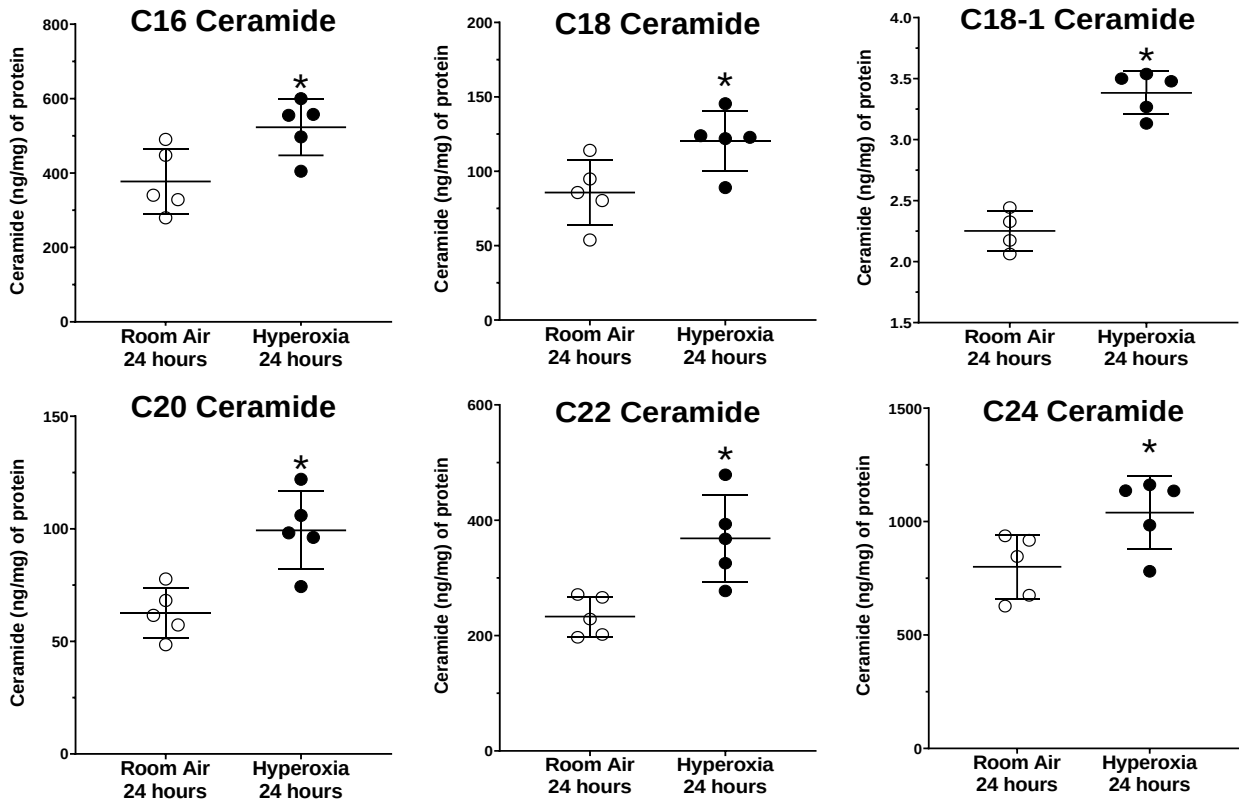

Figure 7: Ceramide levels after 24 hours of exposure to either room air or hyperoxia. 24 hours of hyperoxia exposure led to a significant elevation of pro-apoptotic ceramides in the lung tissue of newborn rats compared to the control animals housed room air. (* compared with room air control group; $P < 0.05$, by t test, $n = 5$ samples per group)

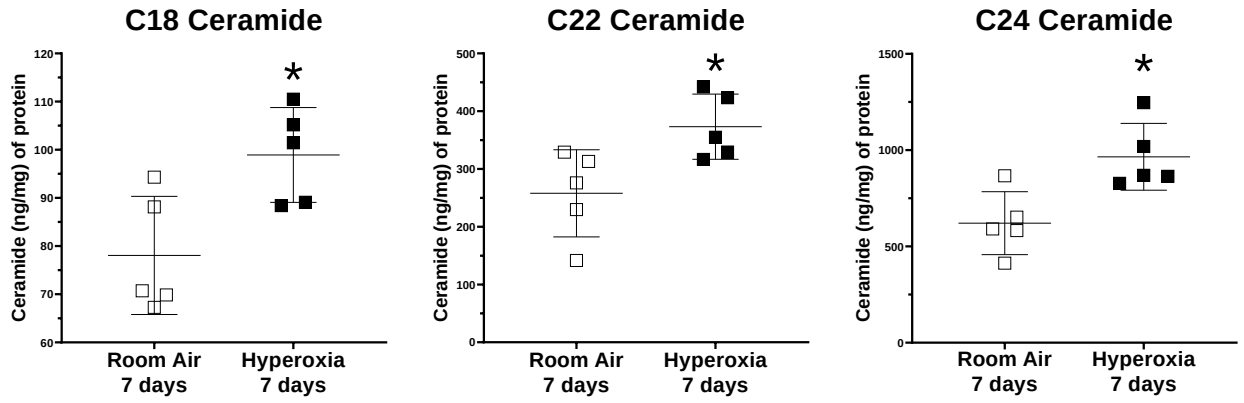

Figure 8: Ceramide levels after 7 days of exposure to either room air or hyperoxia. Continuous exposure to hyperoxia for 7 days resulted in a sustained and significant upregulation of certain species of pro-apoptotic ceramides in the lung tissue of newborn rats. (* compared with room air control group; $P < 0.05$, by t test, $n = 5$ samples per group)

3.1.2 Determining the optimal dose of Desipramine for Prevention of Ceramide Up-regulation in the Hyperoxia-exposed Lung:

Desipramine hydrochloride (diluted in sterile water for injection) was administered via S.C injection once daily to newborn rats. Despite Desipramine being orally available, daily gavage is impracticable in neonatal rats, and S.C administration is both less traumatic and more reliable for drug delivery. Previous rodent studies have utilized daily Desipramine dosages ranging from 10 to 20 mg/kg [46, 91]. To determine the most effective dose of Desipramine in preventing ceramide production, I performed a dose response experiment (10mg/kg and 20mg/kg) and measured the effects on lung ceramides levels after 24 hours (PND 1) and 7 days (PND 7) of hyperoxia exposure. For PND 1 lung samples, the increase in ceramides levels in vehicle-treated controls was notably reduced by a single dose of Desipramine, with 20mg/kg generally having a greater effect (Figure 9).

Consistent with PND 1 findings, ceramide measurement in the lung tissues on PND 7 revealed that daily Desipramine injections significantly reduced ceramide levels in hyperoxia-exposed rat pups compared to vehicle-treated group. However, in contrast to findings on PND 1, only Desipramine at 10mg/kg demonstrated a significant effect (Figure 10).

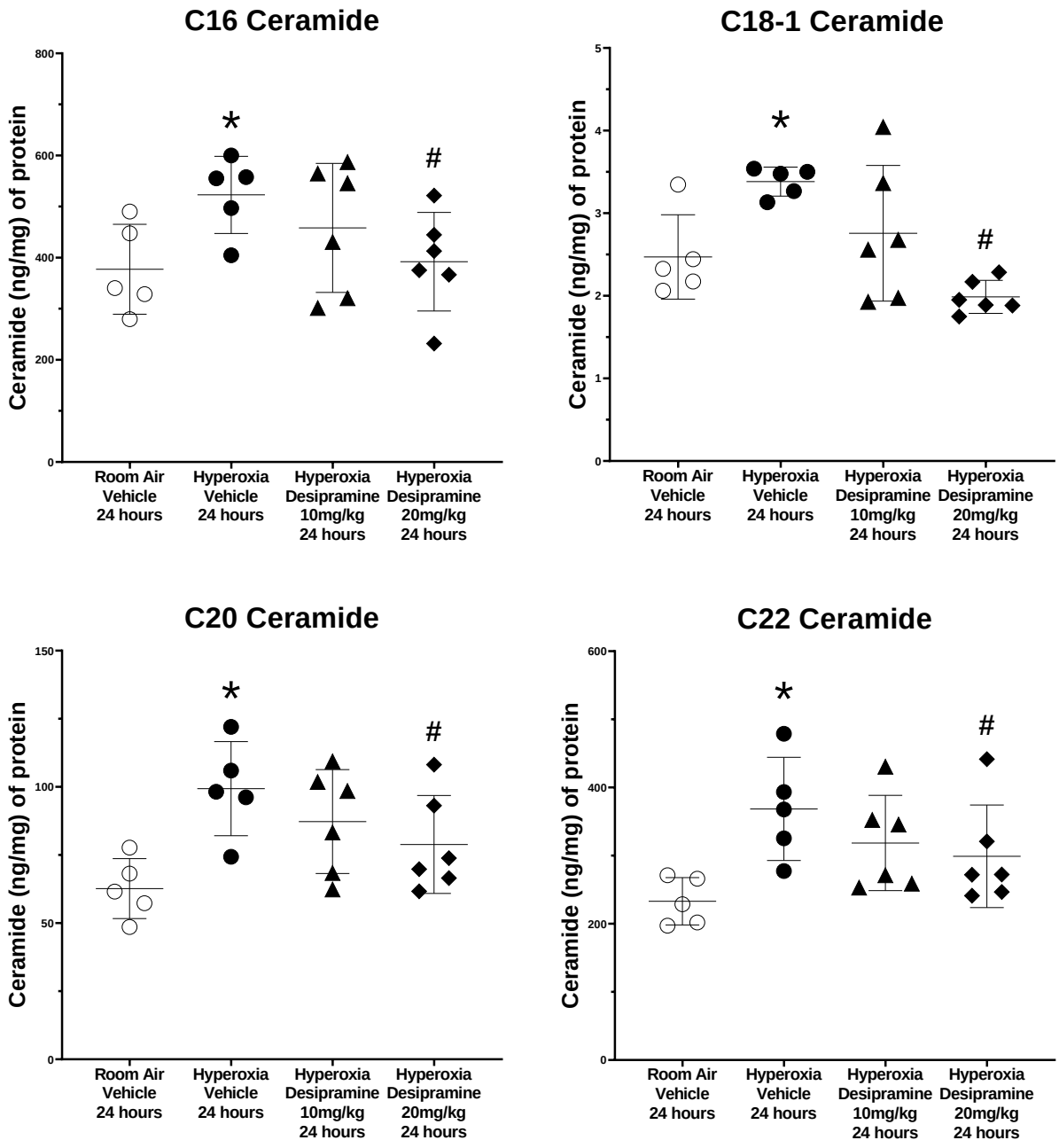

Figure 9: Ceramide levels after 24 hours of exposure to either room air or hyperoxia, with treatment groups receiving either vehicle, Desipramine at 10mg/kg, or 20mg/kg. Desipramine at 20mg/kg emerged as the more effective dose, significantly reducing pro-apoptotic ceramide levels in the lung tissue of newborn rat pups exposed to hyperoxia. (* compared to room air control group, # compared to hyperoxia vehicle group; $P < 0.05$, by one-way ANOVA, n = 5-6 samples per group)

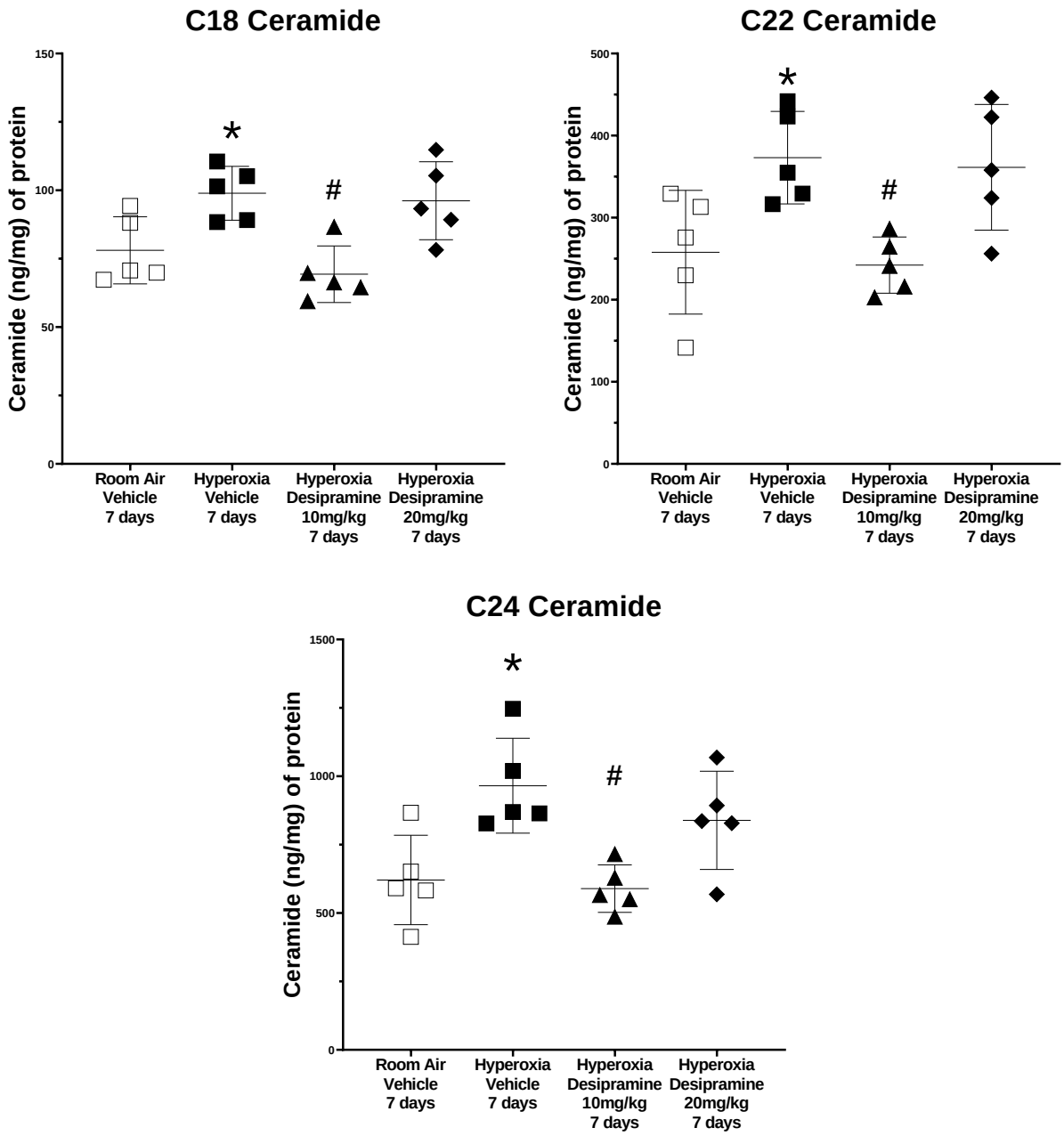

Figure 10: Ceramide levels after 7 days of continuous exposure to either room air or hyperoxia with treatment group receiving either vehicle, Desipramine at 10mg/kg, or 20mg/kg. Desipramine at 10mg/kg proved to be the more effective dose, significantly reducing pro-apoptotic ceramide levels in the lung tissue of hyperoxia-exposed newborn rat pups. (* compared to room air control group, # compared to hyperoxia vehicle group; $P < 0.05$, by one-way ANOVA, n = 5-6 samples per group)

3.2 Objective Two: To establish the chronological sequence of events involving elevated ceramides, autophagy, and apoptosis in the lungs of newborn rats exposed to hyperoxia.

3.2.1 Effects of Hyperoxia and Desipramine on Lung Markers of Autophagy:

Exposure to hyperoxia led to an elevation of ceramide, consistent with findings from a previous study in a MV model that demonstrated ceramide upregulation promoting autophagy-mediated cell death [46]. Therefore, I investigated autophagy markers in the lungs of newborn rats exposed to room air or hyperoxia using WB and IF staining techniques.

I conducted WB analysis for autophagy protein ATG5-12 on the PND 1 and PND 7 lung samples. The WB analysis of PND 1 lung samples revealed a significant increase in ATG5-12 level of the lungs of newborn rats exposed to hyperoxia compared to the room air control. However, it is noteworthy that immunoblotting of PND 7 samples showed no significant difference in autophagy marker ATG5-12 between air- and hyperoxia-exposed groups. Interestingly, in PND 1 samples, treatment with Desipramine (S.C daily injection, 10mg/kg) in the hyperoxia group significantly reduced the levels of the autophagy marker ATG5-12, compared to hyperoxia vehicle-treated animals (Figure 11). To corroborate these findings, I utilized IF staining on lung section of newborn rats using an antibody targeting the autophagy marker LC3B, confirming the results obtained through WB analysis, i.e., increased autophagy secondary to hyperoxia at PND 1, but not PND 7. In addition, I demonstrated the colocalization of LC3B with an epithelial cell marker, E-cadherin (CDH1), in the distal airspace epithelium of newborn rat lungs exposed to hyperoxia for 24 hours (Figure 12).

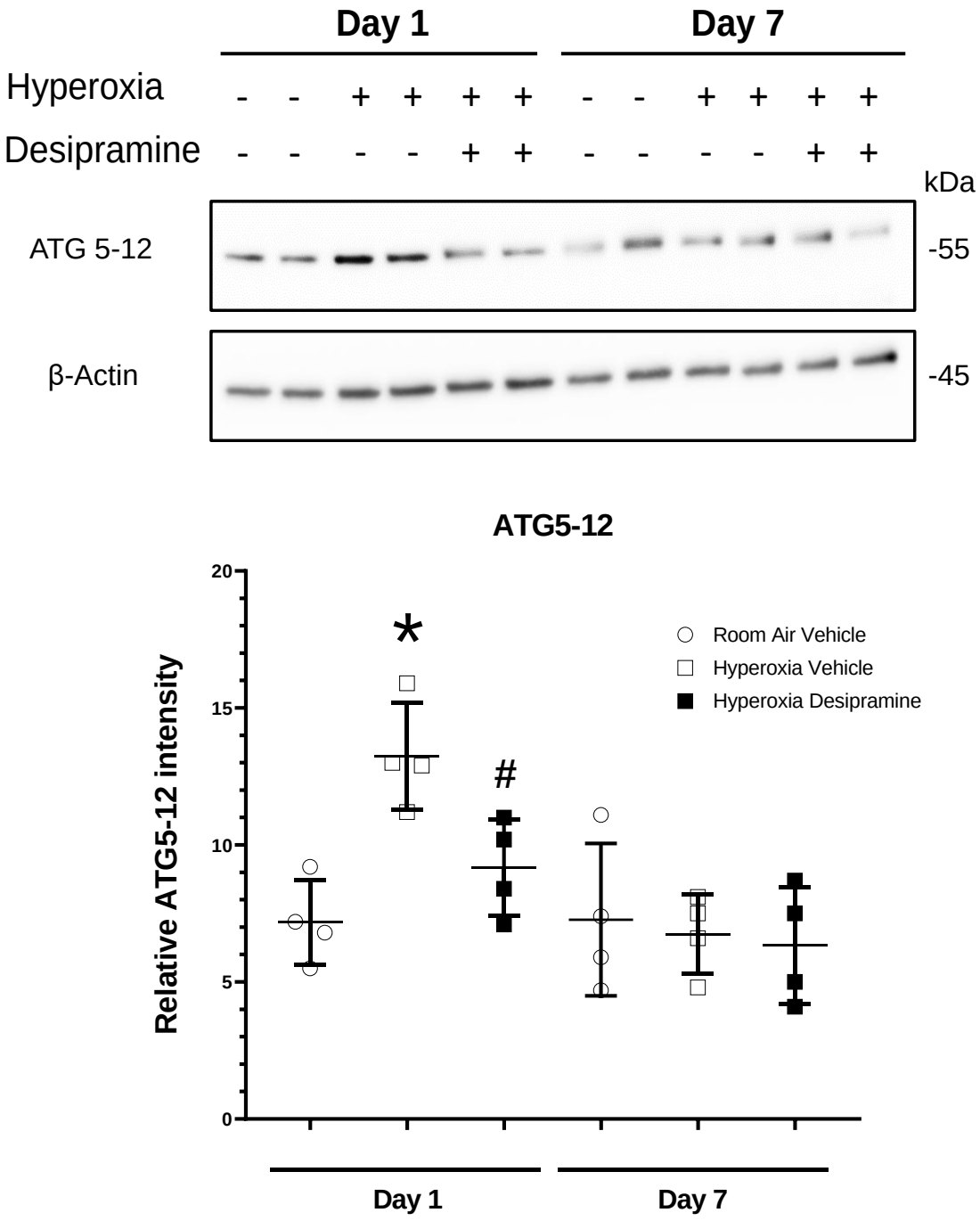

Figure 11: A representative WB image, illustrating the expression levels of the autophagy marker ATG5-12 in the lung tissues of PND 1 and PND 7 newborn rat pups. A significant increase in lung content of ATG5-12 was observed on PND 1 lung samples from hyperoxia-exposed rat pups. Notably, daily S.C injection of Desipramine at 10mg/kg resulted in a significant reduction in ATG5-12 levels. However, no significant difference was observed between the hyperoxia-exposed and room air control groups on PND 7. (* compared to Day-1 room air vehicle group, # compared to Day-1 hyperoxia vehicle group; $P < 0.05$, by one-way ANOVA, $n = 4$ samples per group)

PND 1 Room air Vehicle

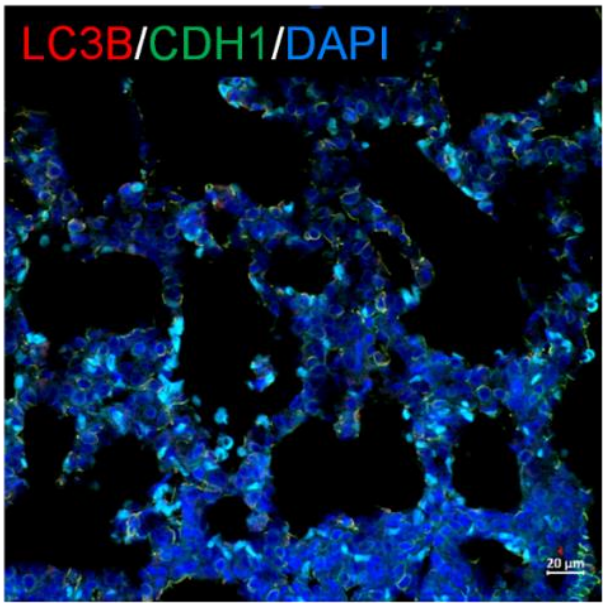

PND 1 Hyperoxia Vehicle

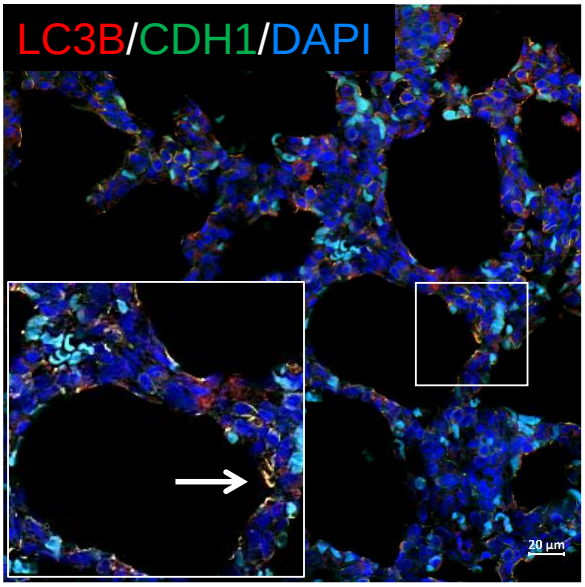

PND 1 Hyperoxia Desipramine

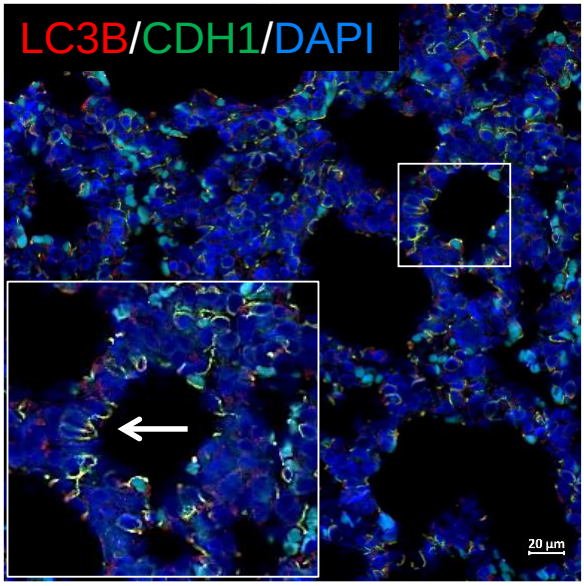

Figure 12: Co-immunofluorescence (Co-IF) staining of autophagy marker LC3B (red) and epithelial cell marker CDH1 (green) on PND 1 lung section of newborn rat pups exposed to room air with vehicle treatment, hyperoxia with vehicle treatment, or hyperoxia treated with Desipramine. Higher immunoreactivity of LC3B, indicative of increased autophagy, was observed in response to hyperoxia exposure, which was attenuated by Desipramine treatment. Additionally, colocalization analysis revealed the presence of LC3B with the CDH1 in the distal airspaces of newborn rat lungs exposed to hyperoxia.

3.2.2 Effects of Hyperoxia and Desipramine on Lung Markers of Apoptosis:

Based on the results obtained from hyperoxia exposure in the lung of newborn rats, which resulted in upregulation of pro-apoptotic ceramides, I aimed to investigate apoptosis activity on PND 1, and PND 7 lung tissues of rat pups exposed to either room air or hyperoxia. Initially, I employed WB to assess the apoptosis marker cleaved poly (ADP-ribose) polymerase (Cl.PARP). The results from PND 1 revealed no significant difference in the apoptosis marker Cl.PARP between the room air and hyperoxia exposure groups. Interestingly, immunoblotting analysis on PND 7 indicated a substantial increase in the levels of apoptosis marker Cl.PARP in the hyperoxia-exposed group compared to room air-exposed group. Consistent with the ceramide data, treatment with Desipramine (S.C daily injection, 10mg/kg) in the hyperoxia group significantly reduced lung content of the apoptosis marker Cl.PARP compared to hyperoxia vehicle-treated animals (Figure 13).

Furthermore, as a complimentary test, I performed co-IF staining on PND 7 lung sections using specific antibody against apoptosis proteins Cl.Casp 3 (Figure 14) and Cl.PARP (Figure 15), along with the epithelial cell marker CDH1. Co-IF staining results confirmed the WB data regarding increased apoptosis markers due to hyperoxia exposure in the lung of newborn rats and demonstrated the co-localization of apoptosis proteins with CDH1 (Figures 14 and 15). To visualize apoptotic cells in the PND 7 lung sections of rat pups, I also conducted *in situ* terminal deoxynucleotidyl transferase dUTP nick end labeling staining (TUNEL) assay on lung sections. The quantification of TUNEL-positive nuclei confirmed a significant overall increase in apoptosis in the hyperoxia-exposed group compared to room air on PND 7 (Figure 16). Both co-IF and TUNEL assay confirmed a reduction in apoptosis in the lung tissue of hyperoxia-exposed animals that received daily Desipramine treatment compared to the vehicle-treated control group.

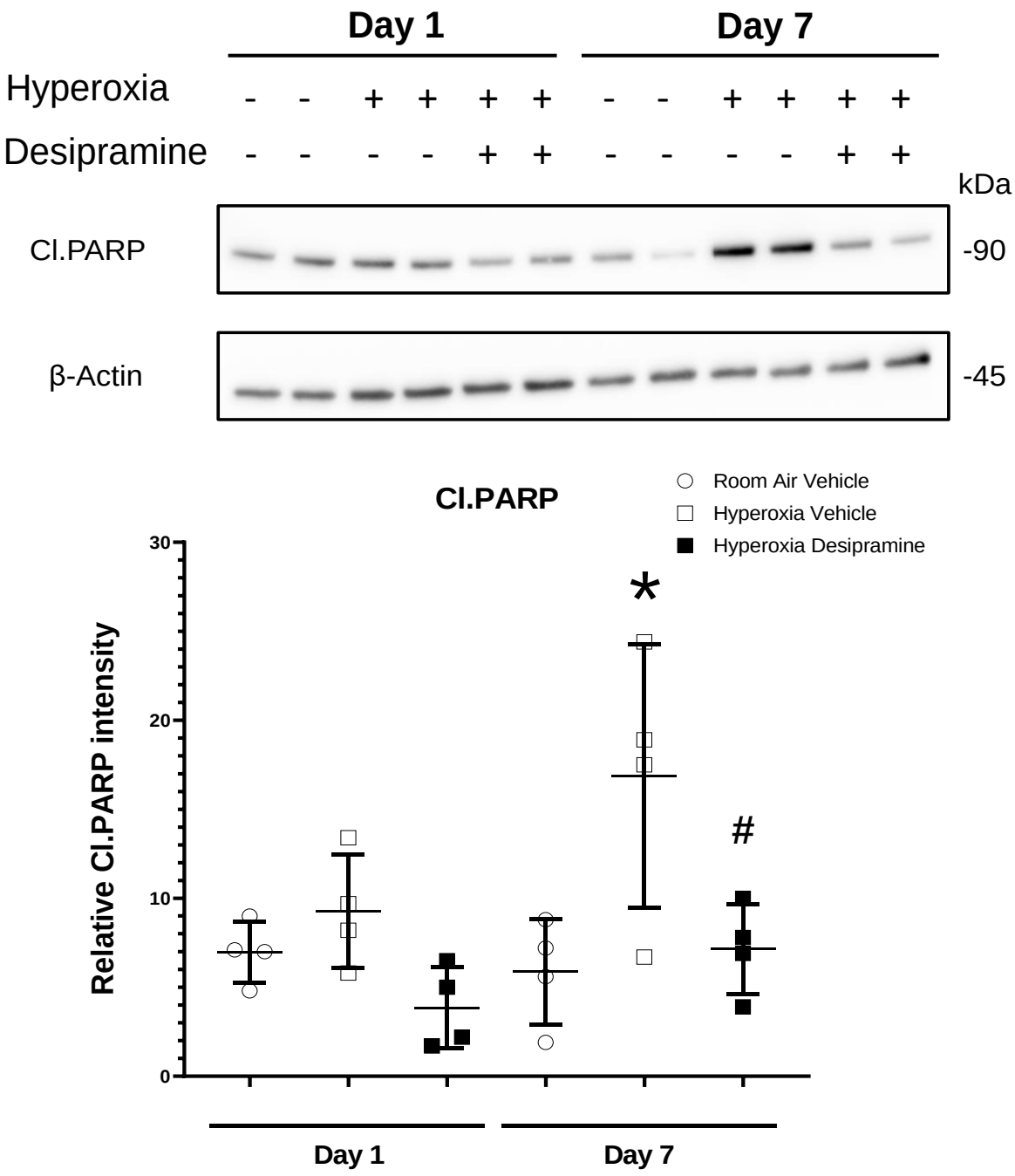

Figure 13: Representative WB images depicting the apoptosis marker Cl.PARP in the lung tissues of PND 1 and PND 7 newborn rat pups. The WB analysis of Cl.PARP on PND 1 revealed no significant difference observed between the hyperoxia-exposed group and the room air control. Conversely, on PND 7, there was a significant increase in Cl.PARP levels in the hyperoxia-exposed rat pups, with a significant reduction observed in the group treated with Desipramine (S.C daily injection, 10mg/kg). (* compared to Day-7 room air vehicle group, # compared to Day-7 hyperoxia vehicle group; $P < 0.05$, by one-way ANOVA, $n = 4$ samples per group)

PND 7 Room air Vehicle

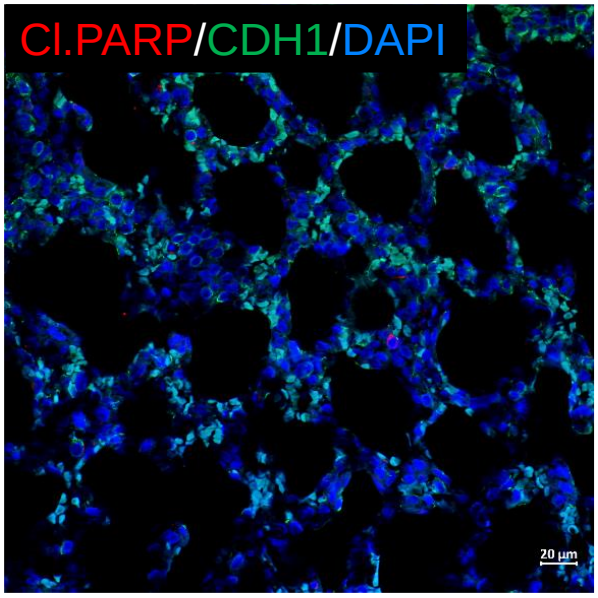

PND 7 Hyperoxia Vehicle

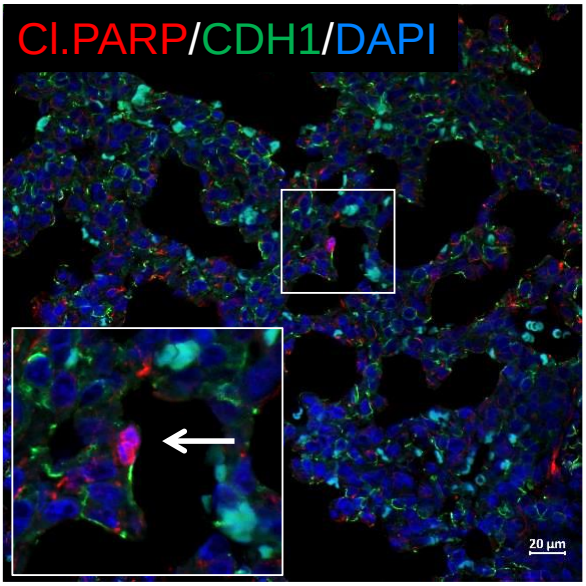

PND 7 Hyperoxia Desipramine

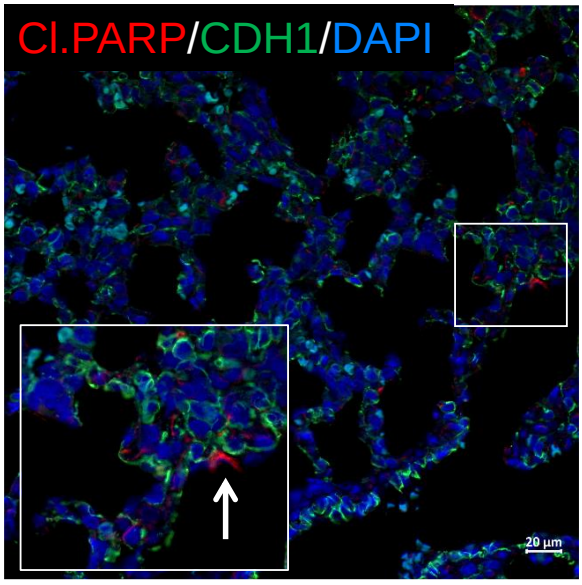

Figure 14: Co-IF staining of the apoptosis marker Cl.PARP (red) and epithelial cell marker CDH1 (green) on PND 7 lung sections of newborn rat pups exposed to either room air vehicle or hyperoxia and treated with either vehicle or Desipramine. Representative photomicrographs illustrate a higher immunoreactivity of Cl.PARP due to hyperoxia exposure, with a noticeable reduction observed with Desipramine treatment. Furthermore, colocalization of Cl.PARP with CDH1 is evident in the alveolar epithelium of newborn rat lungs exposed to hyperoxia.

PND 7 Room air Vehicle

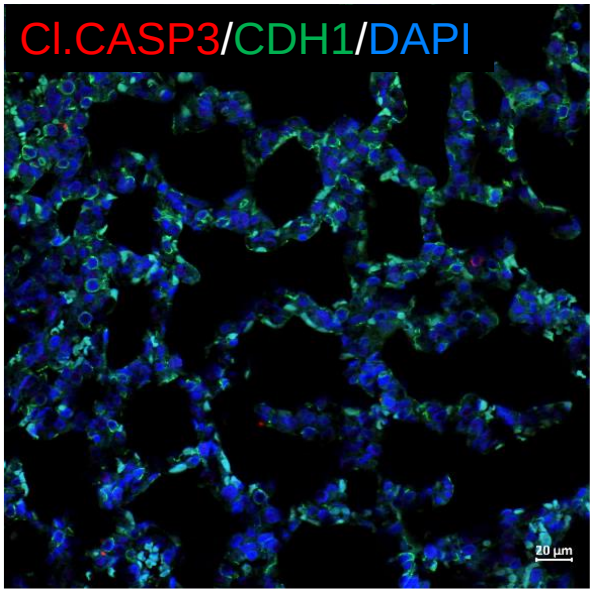

PND 7 Hyperoxia Vehicle

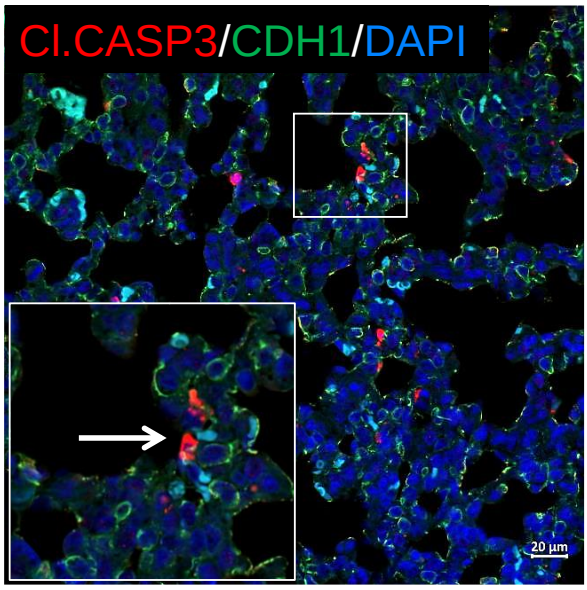

PND 7 Hyperoxia Desipramine

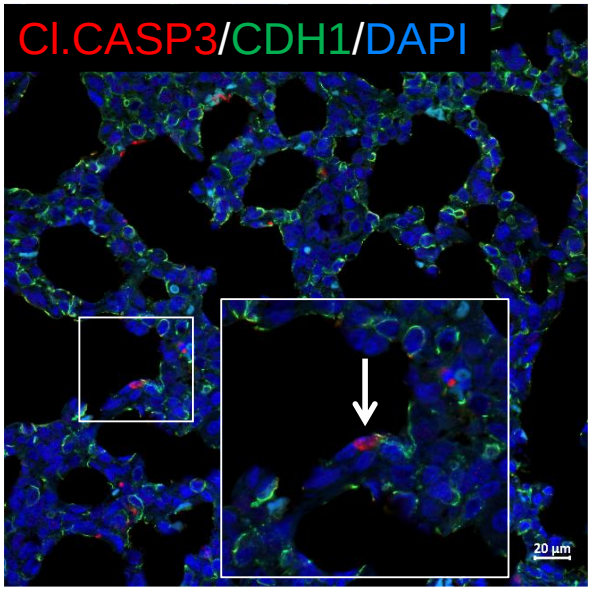

Figure 15: Co-IF staining of the apoptosis marker Cl.Casp 3 (red) and epithelial cell marker CDH1 (green) on PND 7 lung sections of newborn rat pups exposed to either room air vehicle or hyperoxia and treated with either vehicle or Desipramine. The figure highlights a higher immunoreactivity of Cl.Casp 3 due to hyperoxia exposure, with a noticeable reduction observed with Desipramine treatment. Additionally, colocalization of Cl.Casp 3 with CDH1 is evident in the alveolar epithelium of newborn rat lungs exposed to hyperoxia.

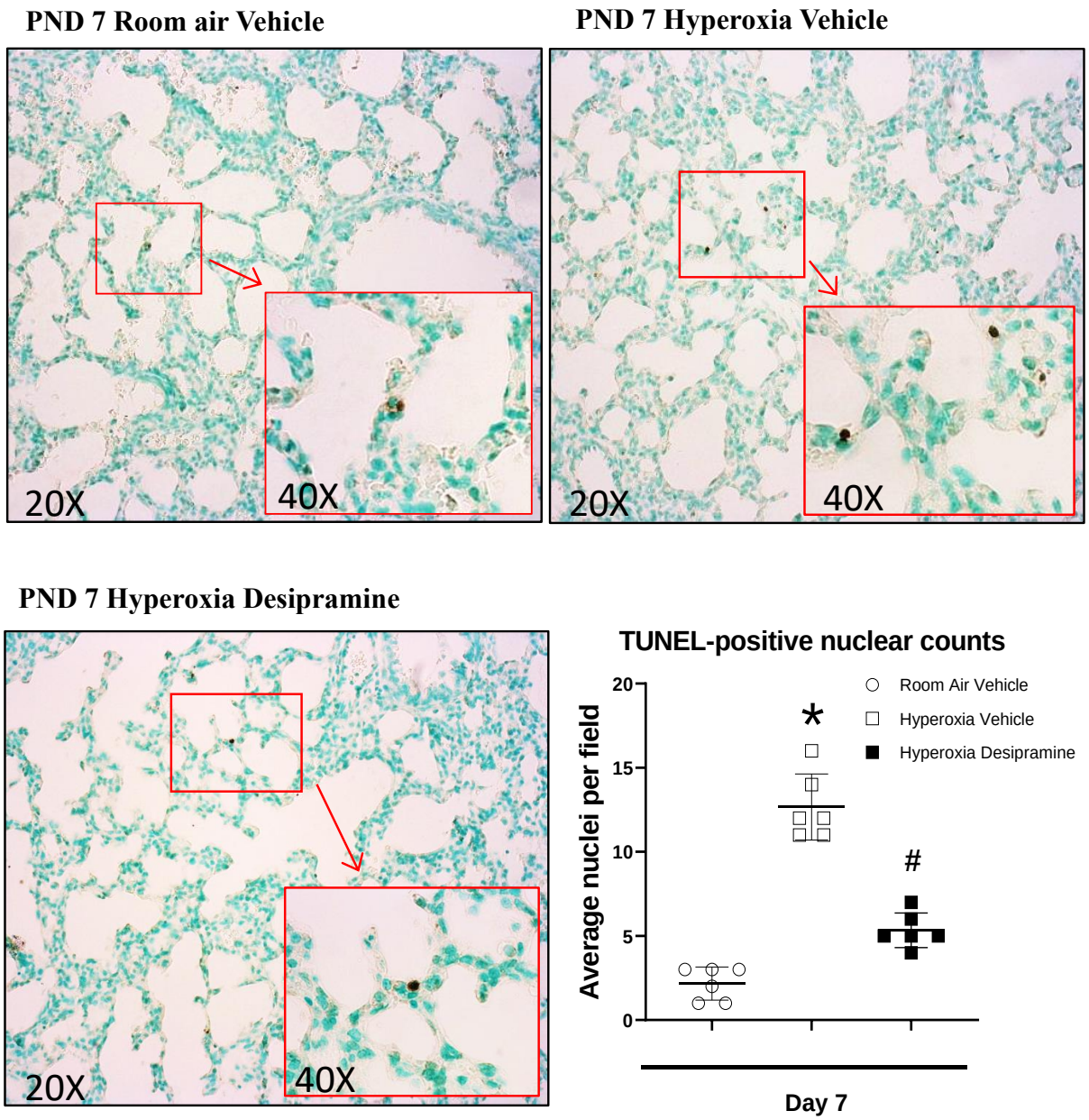

Figure 16: Detection and quantification of apoptosis by TUNEL assay. The images illustrate the detection of apoptotic cells (brown nuclei) in the PND 7 lung sections of rat pups using the TUNEL assay. Quantification of TUNEL-positive nuclei reveals a significant increase of apoptosis in the hyperoxia-exposed group compared to the control. Treatment with Desipramine resulted in a significant reduction of TUNEL-positive nuclei. The TUNEL assay reaffirms the findings from WB and co-IF staining results regarding increased hyperoxia-mediated apoptosis on PND 7. (* compared to Day-7 room air vehicle group, # compared to Day-7 hyperoxia vehicle group; $P < 0.05$, by one-way ANOVA, $n = 6$ samples per group)

3.2.3 Effects of Hyperoxia and Desipramine on Lung SMPD1:

Previous reports have demonstrated that MV in newborn rats is associated with an increase in SMPD1 activity, subsequently leading to ceramide upregulation [46]. In this study, it was observed that hyperoxia exposure results in a significant elevation of ceramides lung tissues, particularly on PND 1 with some species persisting to PND 7. To investigate further, I performed co-IF staining to examine SMPD1 content in PND 1 lung sections. The finding revealed a higher content of SMPD1 in the lungs of the hyperoxia-exposed newborn rats compared to the room air control, confirming the colocalization of SMPD1 with the epithelial cell marker CDH1 in the alveolar epithelium. Consistent with previous results, Desipramine treatment led to a noticeable reduction in SMPD1 immunoreactivity in the lung sections of hyperoxia-exposed animals compared to the vehicle-treated groups (Figure 17).

PND 1 Room air Vehicle

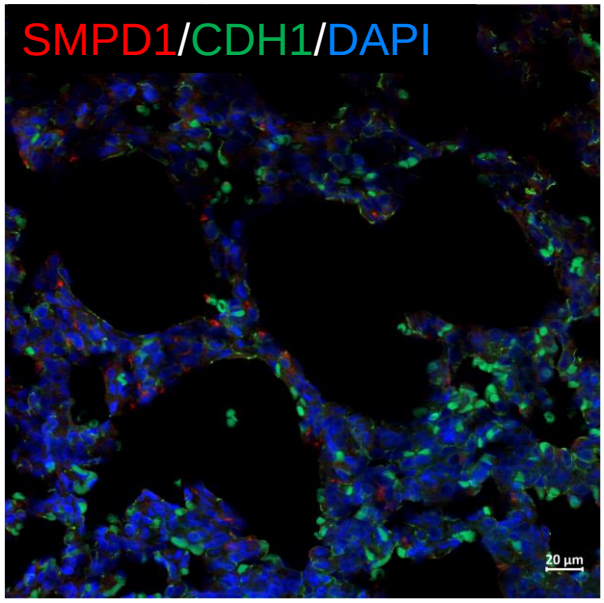

PND 1 Hyperoxia Vehicle

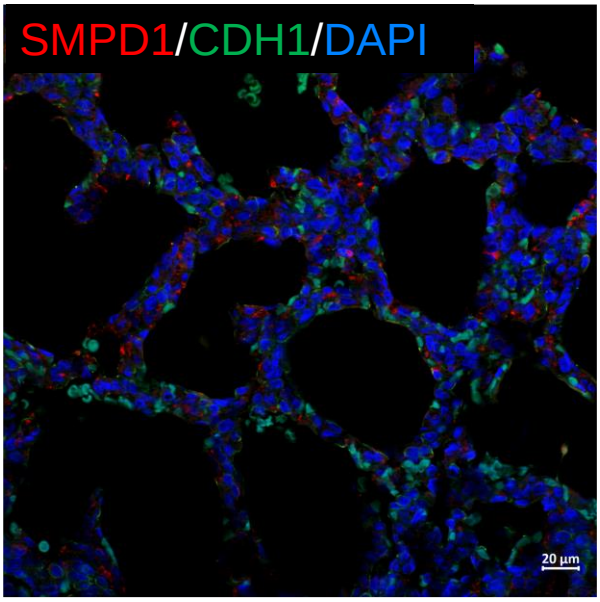

PND 1 Hyperoxia Desipramine

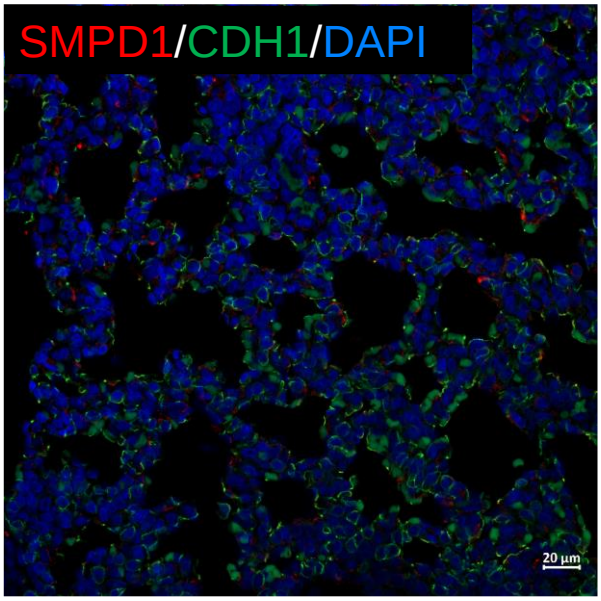

Figure 17: Co-IF staining of SMPD1 (red) and epithelial cell marker CDH1(green) on PND 1 lung sections of newborn rat pups exposed to either room air vehicle or hyperoxia and treated with either vehicle or Desipramine. The images illustrate a higher expression of SMPD1 due to hyperoxia exposure, with a noticeable reduction observed with Desipramine treatment. Additionally, co-localization of SMPD1 with CDH1 is evident in the alveolar epithelium of newborn rat lungs exposed to hyperoxia.

3.3 Objective Three: To assess the effectiveness of Desipramine in preventing experimental BPD-like lung injury in newborn rats.

Building upon insights gained from PND 1 and PND 7 studies, we conducted an extensive 21-day animal study involving a larger number of pups. The primary objective of this prolonged experiment was to induce a lung injury in newborn rats resembling BPD and to assess the therapeutic potential of Desipramine administration in preventing abnormal lung structure. On PND 21, ceramide levels in lung tissue were measured, and designed-based stereological analysis of the lung structure was employed to quantitatively assess morphological changes in the lung of rat pups. In addition to evaluating alveolar structure, the pups were assessed for another important comorbidity associated with BPD, namely chronic pulmonary hypertension (cPH).

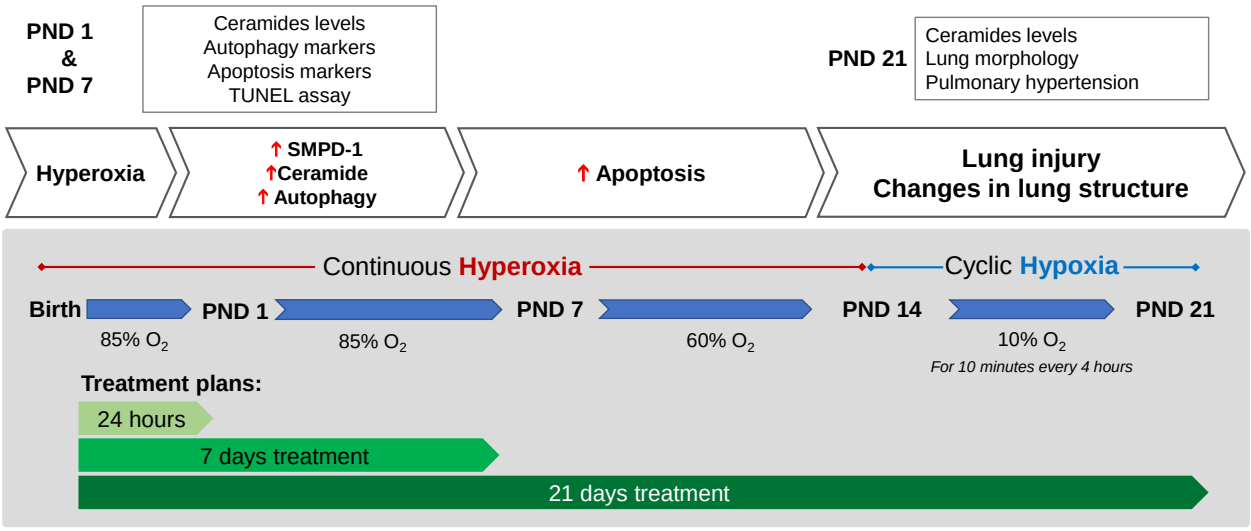

Figure 18: Illustration of the hyperoxia-intermittent hypoxia (HIH) rat model of BPD and an overview of the experimental approach. The animal study encompassed three distinct time points with varying O_2 exposures and end points. Based on the hypothesis, PND 1 and PND 7 were selected for examination of ceramide levels and cell death markers (autophagy and apoptosis) in lung tissue. To conduct a morphological evaluation of the lung structure, PND 21 was chosen as a key time point. During the study, the pups received a daily S.C injection of Desipramine (10mg/kg) and/or vehicle (Water for injection). At the end of each treatment period (PND 1, PND 7, PND 21), the lungs were harvested, and the right lobs were resected for fresh frozen storage at -80°C for biochemical analysis. Left lobes were prepared for histological and morphological investigations (formalin-fixed, paraffin-embedded).

3.3.1 Effects of HIH on Lung Ceramides:

Unlike findings on PND 1 and PND 7, there was no significant increase in ceramide levels on PND 21, in keeping with ceramide up-regulation being an early event in the evolution of lung injury (Figure 19).

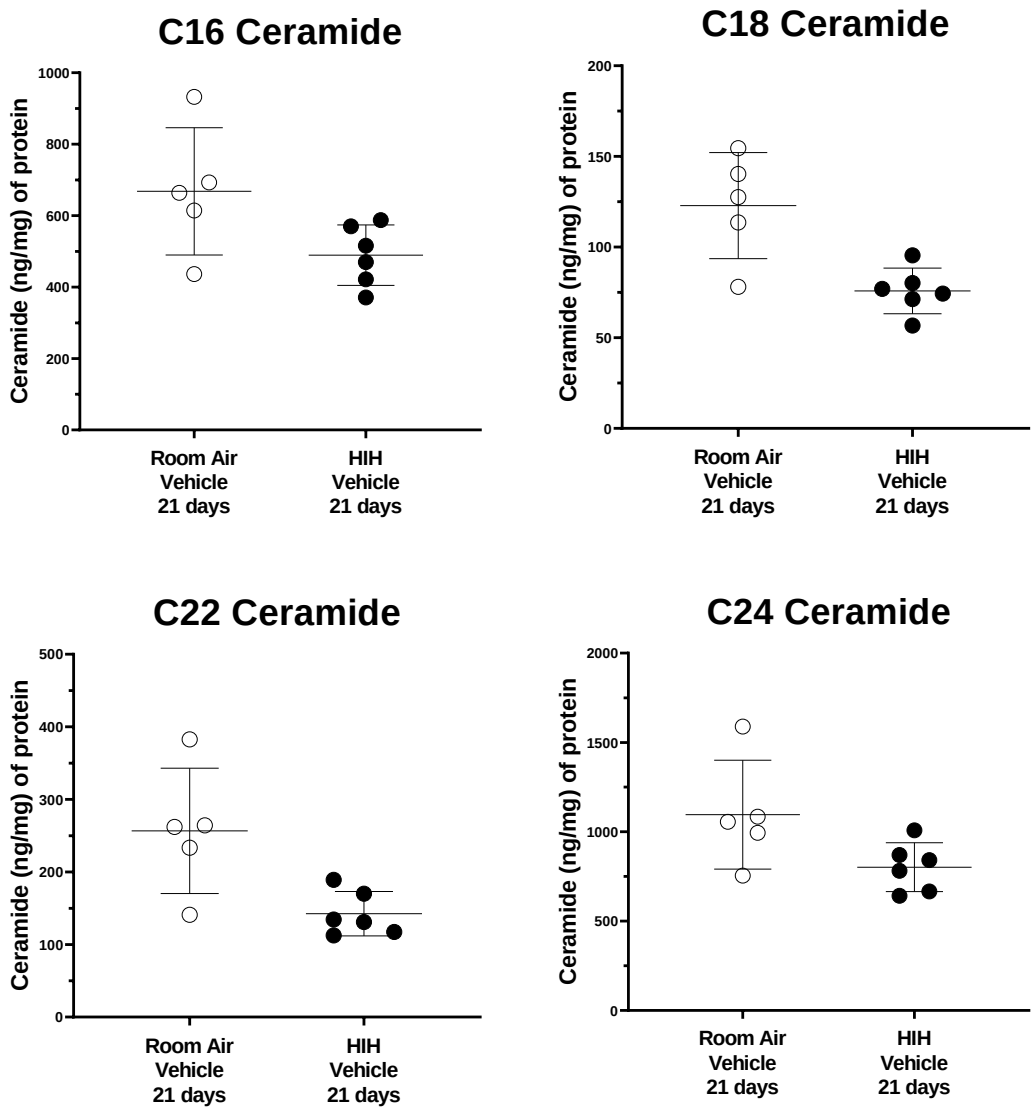

Figure 19: Ceramide levels after 21 days of exposure to either room air or HIH. No significant increase in ceramide levels was observed in the lungs of rats in the HIH group compared to the room air group. (HIH vehicle compared with room air control group; P = NS, by t test, n = 6-5 samples per group)

3.3.2 Effects of HIH and Desipramine on Lung Structure:

Design-based stereology was performed on left lung lobes to examine markers of alveologenesis and angiogenesis. Morphological analysis of lungs exposed to HIH revealed several significant differences compared to the air-exposed control group. HIH-exposed pups exhibited a significantly lower number of alveoli per unit lung volume (Total alveolar number; Figure 20), a larger average alveolar size (increased mean linear intercept [MLI], Figure 21), decreased alveolar surface density (surface area per unit volume; Figure 22), reduced total length of small blood vessels (20-60 μm external diameter; Figure 23), and an increased total number of interstitial CD68+ macrophages (Figure 24). Desipramine treatment of rat pups exposed to HIH partially improved abnormal alveolar morphology, as evidenced by a partial increase in alveolar surface density (Figure 22) and a decrease in MLI (Figure 21), with values no longer significantly differing from those observed in the room air control group. Furthermore, treatment with Desipramine significantly increased small vessel length (Figure 23) and decreased inflammation, as evidenced by decreased interstitial macrophage counts (Figure 24) when compared to the HIH animals treated with vehicle.

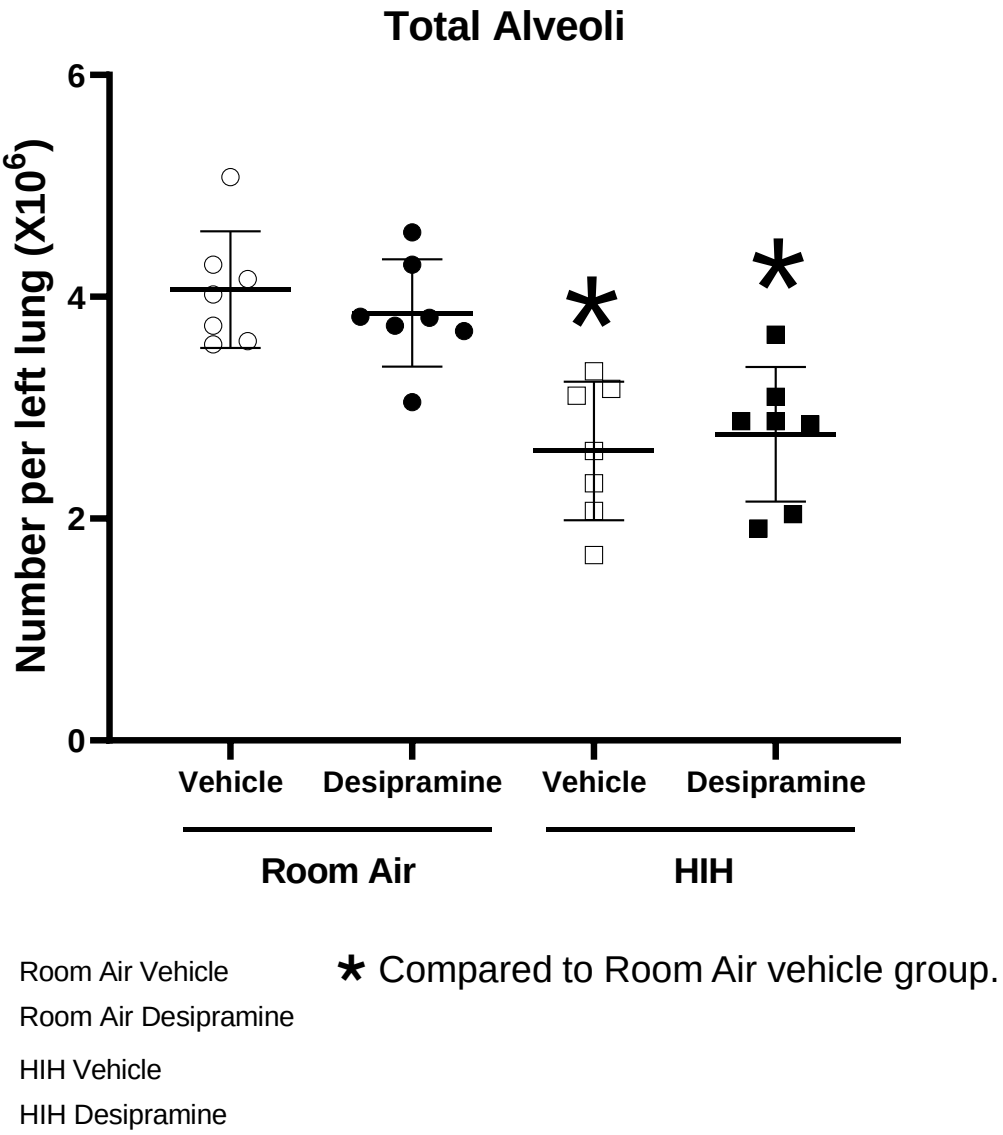

Figure 20: Measurement of total alveolar number. Exposure to HIH resulted in a significant decrease in alveolar number, indicative of alveolar hypoplasia, a pathognomonic feature of BPD. There was a significant difference between the room air vehicle and HIH vehicle groups. Treatment with Desipramine did affect total alveolar number. Specifically, there was no significant difference between HIH vehicle and HIH Desipramine group, with a significant difference observed between the room air vehicle and either HIH Desipramine or HIH vehicle group. (* compared to room air vehicle; $P < 0.05$, by one-way ANOVA, $n = 7$ samples per group)

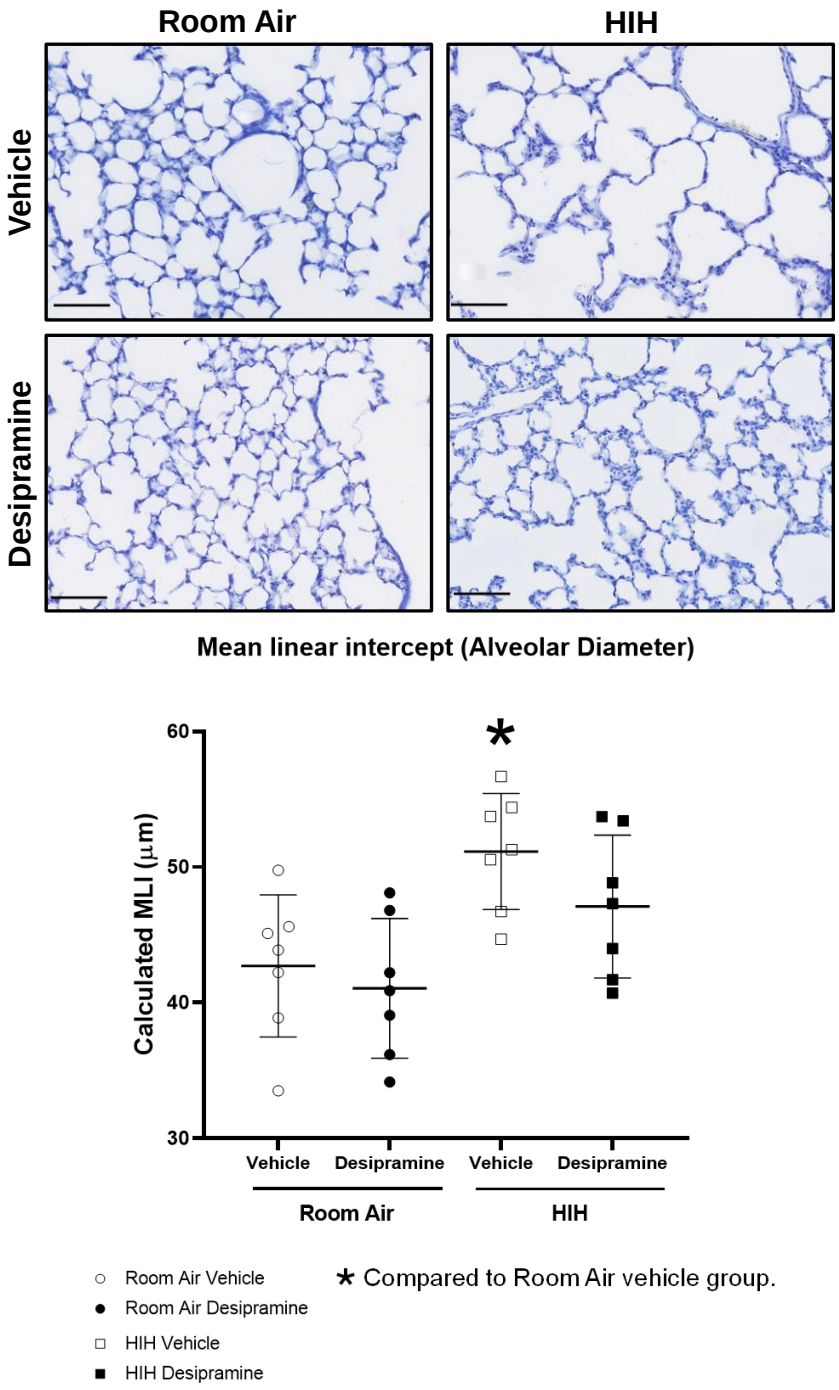

Figure 21: Measurement of MLI or average alveolar diameter. Representative photomicrographs of toluidine blue–stained lung sections of PND 21 rats are shown above the graph of measured MLI by stereology. Exposure to HIH had a negative impact on lung structure, resulting in an increased MLI, indicative of enlarged distal airspaces. A significant difference was observed between the room air vehicle and HIH vehicle groups. Treatment with Desipramine led to a partial improvement in lung structure; no significant difference was observed between the room air vehicle and HIH Desipramine groups. (Scale bars, 100 μm; * compared to room air vehicle; $P < 0.05$, by one-way ANOVA, $n = 7$ samples per group)

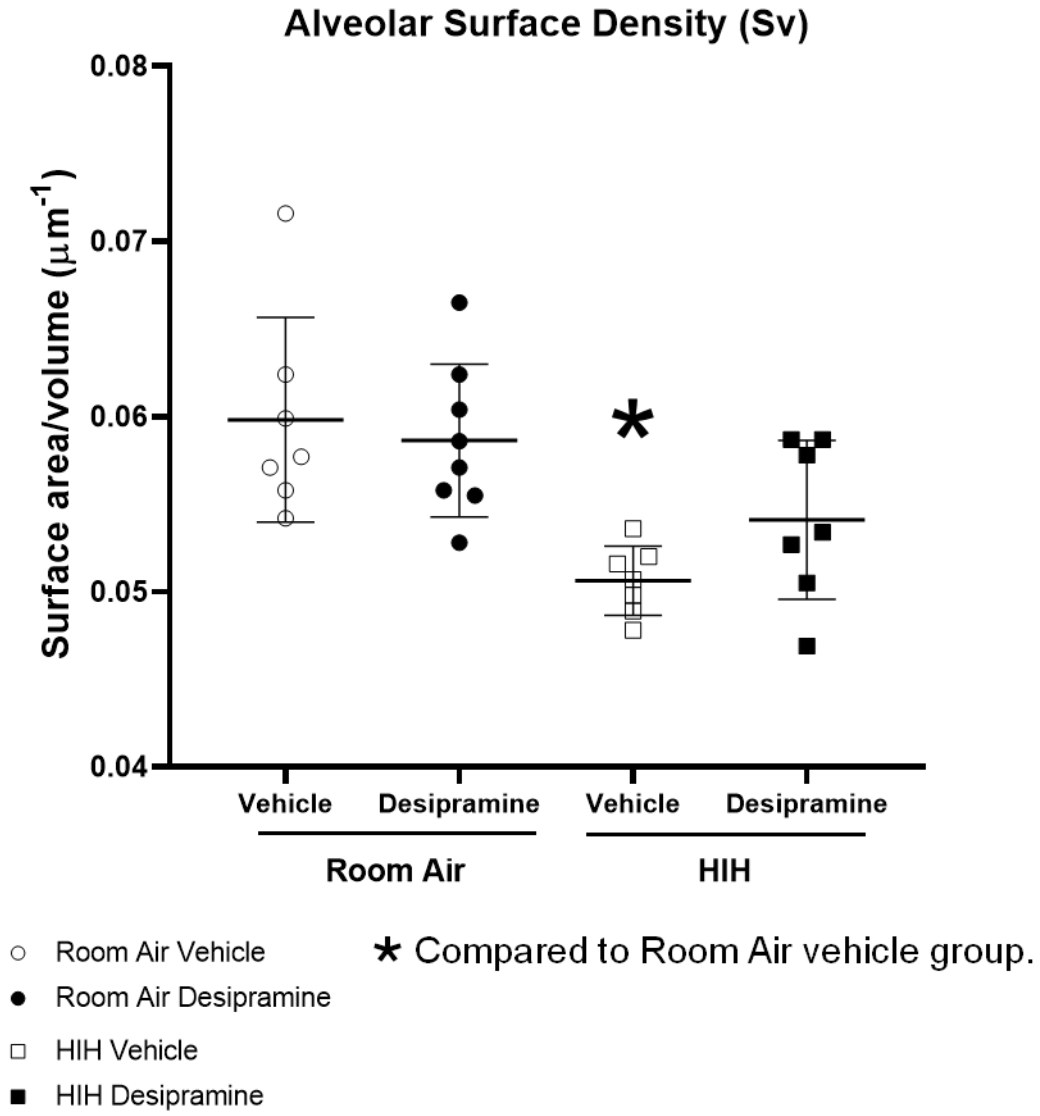

Figure 22: Measurement of alveolar surface density. Exposure to HIH significantly decreased lung alveolar surface density, as evidenced by a significant difference between the room air vehicle and HIH vehicle groups. Treatment with Desipramine resulted in a partial improvement, with no significant difference observed between the room air vehicle and HIH Desipramine groups. (* compared to room air vehicle; $P < 0.05$, by one-way ANOVA, n = 7-8 samples per group)

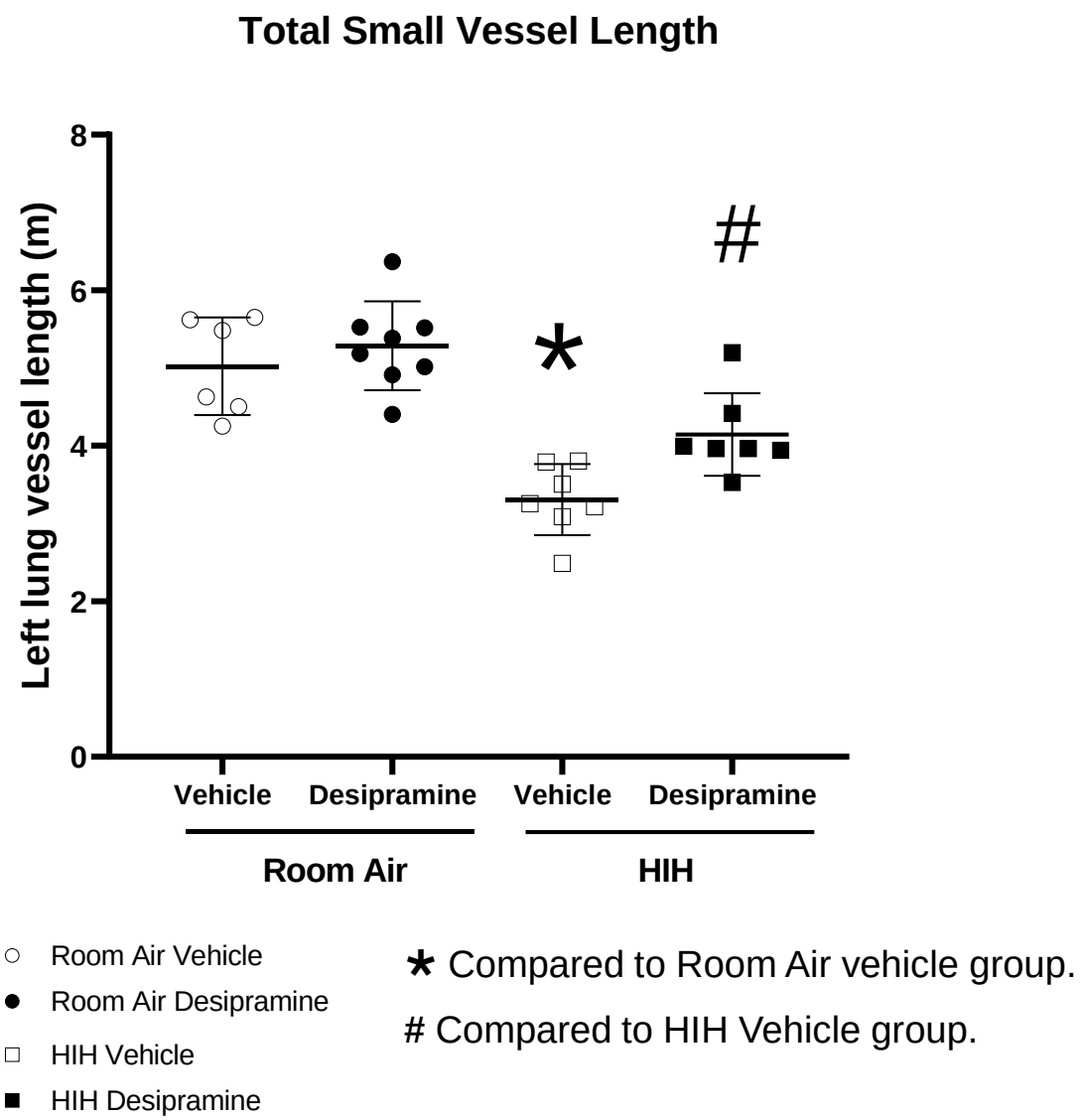

Figure 23: Measurement of total small vessel length (20-60 μm external diameter) as a marker of pulmonary vascularization. Exposure to HIH had a negative impact on lung vascular density. Treatment with Desipramine resulted increased total length of small vessels, as evidenced by a significant difference between HIH vehicle and HIH Desipramine groups. No significant difference was observed between room air vehicle and HIH Desipramine groups. (* compared to room air vehicle, # compared to HIH; vehicle; $P < 0.05$, by one-way ANOVA, $n = 6$-8 samples per group)

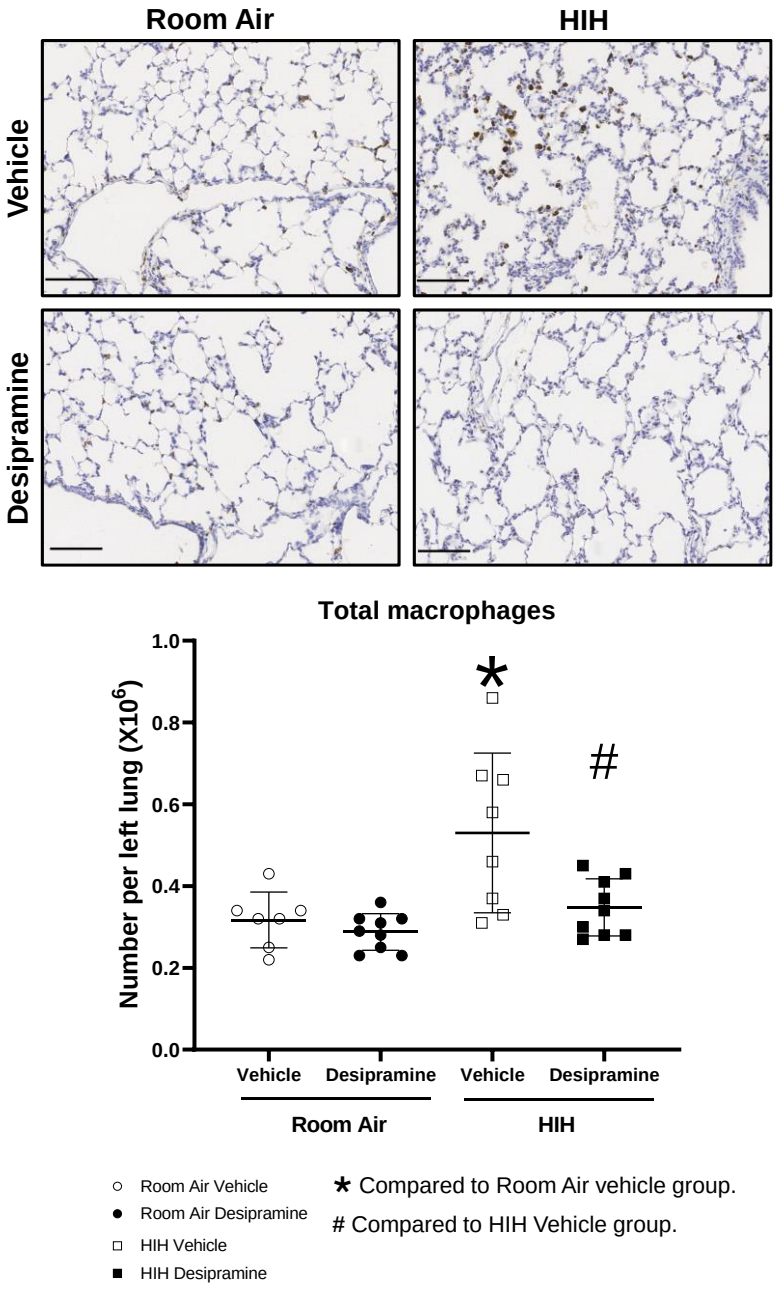

Figure 24: Measurement of total macrophages number on PND21 rat lung sections using CD68 IHC staining, a specific macrophage marker. Representative photomicrographs of CD68-positive macrophages in the lung sections of PND 21 rats are shown above the graph of total macrophage numbers measured by stereology. Exposure to HIH resulted in a significant increase in the number of macrophages in the lung tissues as indicated by a significant difference between the room air vehicle and HIH vehicle groups. Treatment with Desipramine led to a notable decrease in macrophage numbers, demonstrating a prominent impact. This decrease was statistically significant when comparing the HIH vehicle and HIH Desipramine groups. No significant difference was observed between the room air vehicle and HIH Desipramine groups, (Scale bars, 100 µm; * compared to room air vehicle, # compared to HIH vehicle, $P < 0.05$, by one-way ANOVA, n = 7-9 samples per group)

3.3.3 Effects of HIH and Desipramine on Markers of cPH:

cPH is a common comorbidity of BPD, characterized by increased pulmonary arterial pressure (PAP) and pulmonary vascular resistance (PVR) [25]. In BPD patients, vascular remodeling and thickening of pulmonary arteries contribute to elevated PAP and PVR [92]. In severe cases, this leads to RV hypertrophy, RV failure, and eventual mortality [93, 94]. In addition to evaluating alveolar structure, I examined markers of cPH, by quantifying RV hypertrophy (Fulton's index) and measuring pulmonary vascular remodeling (% arterial medial wall area). The Fulton's index (FI) is calculated as the weight ratio of the RV to the sum of the left ventricle (LV) and septum (S), [FI=RV/(LV+S)].

The acquired data revealed that exposure to HIH induced cPH in newborn rats. This was evident from the significant increase in the Fulton's index and MWA of pulmonary arteries when compared to the control group. Desipramine treatment demonstrated a robust and significant preventive effect on cPH, as evidenced by a reduction in the Fulton's index (Figure 25) and arterial MWA (Figure 26) when compared to HIH-exposed animals treated with the vehicle.

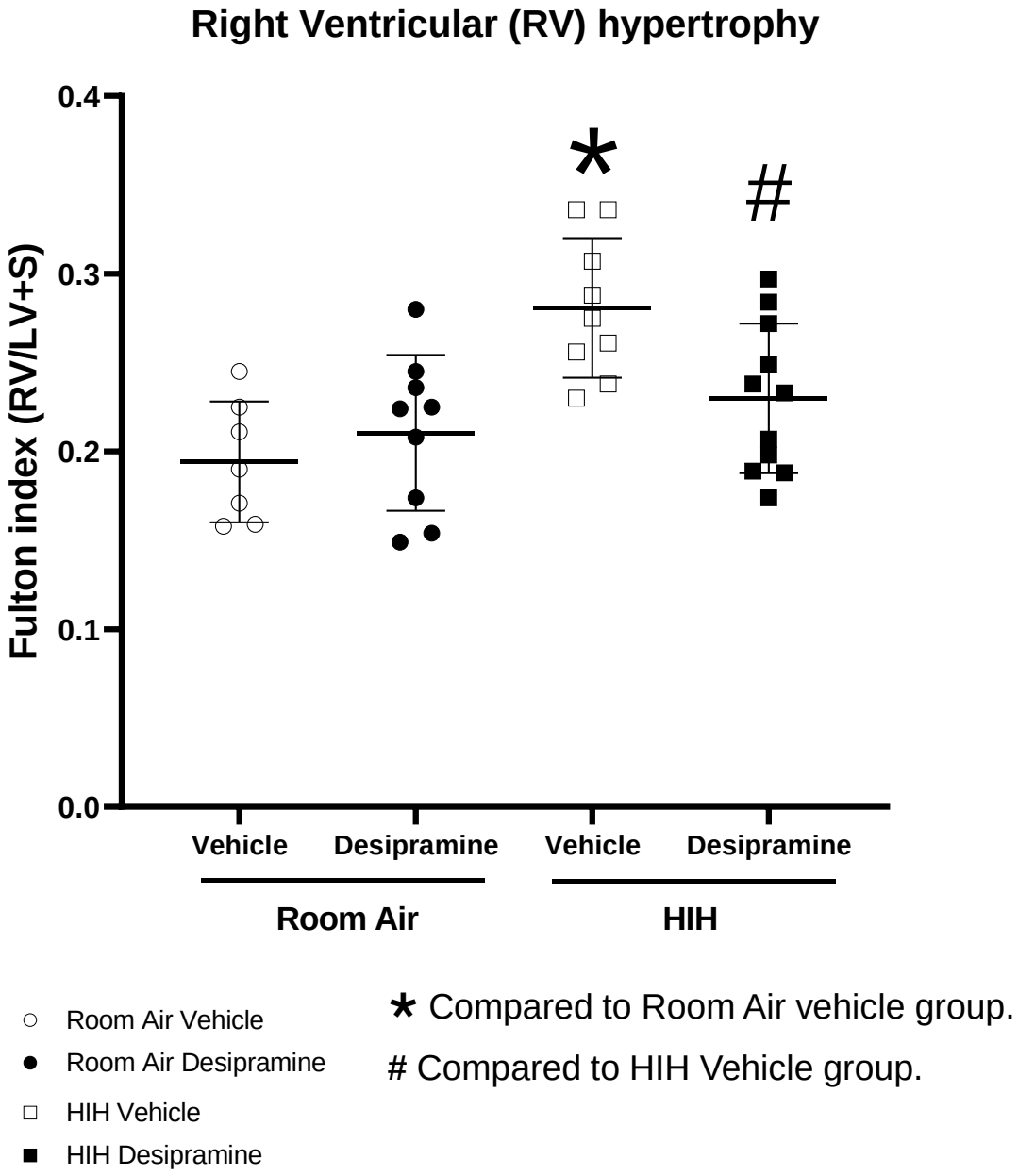

Figure 25: Measurement of RV hypertrophy (Fulton's index). Exposure to HIH significantly increased Fulton's index, indicating cPH, as evidenced by a significant difference between the room air vehicle and HIH vehicle groups. Treatment with Desipramine resulted in a significant decrease in Fulton's index, when comparing the HIH Vehicle to HIH Desipramine group. No significant difference was observed between the room air vehicle and HIH Desipramine groups. (* compared to room air vehicle, # compared to HIH vehicle; $P < 0.05$, by one-way ANOVA, n = 7-11 samples per group)

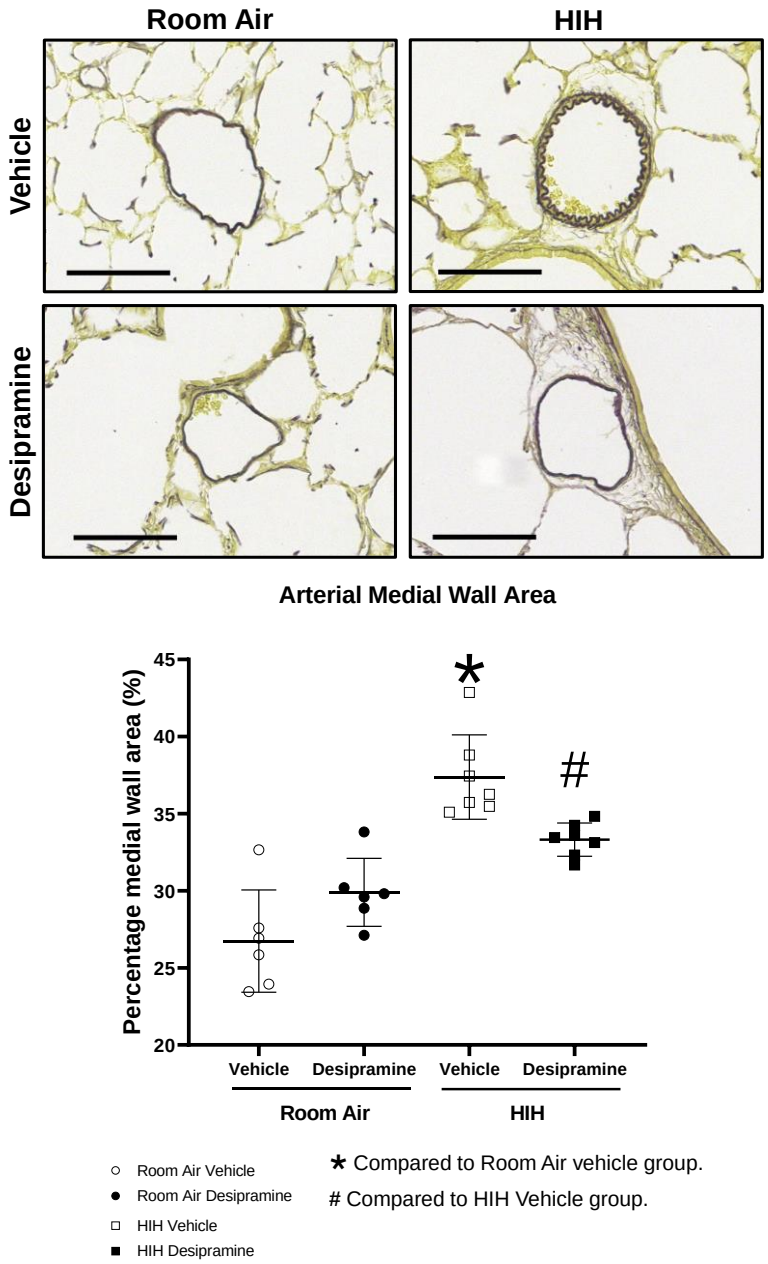

Figure 26: Measurement of arterial medial wall area. Representative photomicrographs of elastin-stained pulmonary arteries of PND 21 rats are shown above the graph of measured arterial medial wall area by stereology. This parameter is used to characterize the vascular remodeling in patients with cPH. Exposure to HIH was accompanied by a significant increase in arterial medial wall area. This was evident from the significant difference between the room air vehicle and HIH vehicle groups. In comparison to HIH-exposed vehicle-treated animals, Desipramine treatment significantly decreased arterial wall remodeling. as evidenced by a significant difference between HIH vehicle and HIH Desipramine groups. No significant difference was observed between the room air vehicle and HIH Desipramine groups. (Scale bars, 100 μm; * compared to room air vehicle, # compared to HIH vehicle; $P < 0.05$, by one-way ANOVA, n = 6-7 samples per group)

3.4 Objective Four: To examine key ceramide pathway proteins in lung tissue sections from extremely premature infants (autopsy specimens) who passed away, both with and without BPD.

The objective of this study, which involved human lung samples, was to quantitatively assess four key proteins within the ceramide pathway. Specifically, Sphingomyelin phosphodiesterase1 (SMPD1), Sphingomyelin synthase1 (SGMS1), Ceramide synthase1 (Lass1), and Ceramide synthase2 (CerS2).

Archived paraffin-embedded lung samples from matched lung lobes were obtained from autopsies conducted at Children's Hospital of Eastern Ontario (CHEO) between January 2000 and December 2017. Cases (<29 completed weeks' GA at birth and <1000 g birthweight without major congenital malformations) were identified by interrogation of the CHEO autopsy database followed by detailed review of the autopsy record and patient chart. 47 autopsies meeting the above criteria were identified and separated into two groups based on age at death: 1) 1-27 days (early/evolving lung disease [Control] group; n = 30) and 2) 28 days or more on positive pressure respiratory support and supplemental O_2 (FiO_2 > 0.3) at 28 days (if death occurred <36 completed weeks' GA) or a clinical diagnosis of severe BPD at 36 weeks' corrected GA using established criteria (32) (BPD group; n = 17). For each patient, IHC staining was employed to stain one lung section per ceramide pathway protein. As the inventory of BPD samples had become depleted, tissues were only available for 14 of 17 BPD cases, except for SMPD1 IHC where 16 samples were stained. Subsequently, the distribution and density of the IHC staining were semi-quantified using the H-score: 0 = no staining/minimal nonspecific staining (<10% of section); 1 = focal/patchy staining (10-50% of section); 2 = diffuse/intense staining (>50% of section). This assessment was conducted by an experienced perinatal pathologist (Dr. David Grynspan) who was blinded to group allocation.

The lung sections utilized in this study were previously validated in a recent publication by Dr. Jankov's laboratory [95]. This validation affirmed that the control group exhibited less lung injury (fibrosis, inflammation, nitroxidative stress) when compared to the BPD group. The results obtained from this study revealed significant increases in immunoreactivity of three out of the four ceramide pathway proteins assessed, (SMPD1, SGMS1, and Lass1) in BPD samples. These findings further support a potential pathogenic role for the ceramide pathway in the context of chronic neonatal lung injury.

3.4.1 SMPD1:

SMPD1, also known as acid sphingomyelinase, functions as a hydrolase within the lysosome and catalyzes the conversion of sphingomyelin to ceramide [46]. Compared to the control group, lung sections from individuals with BPD exhibited a significantly higher H-score for SMPD1 (Figure 27).

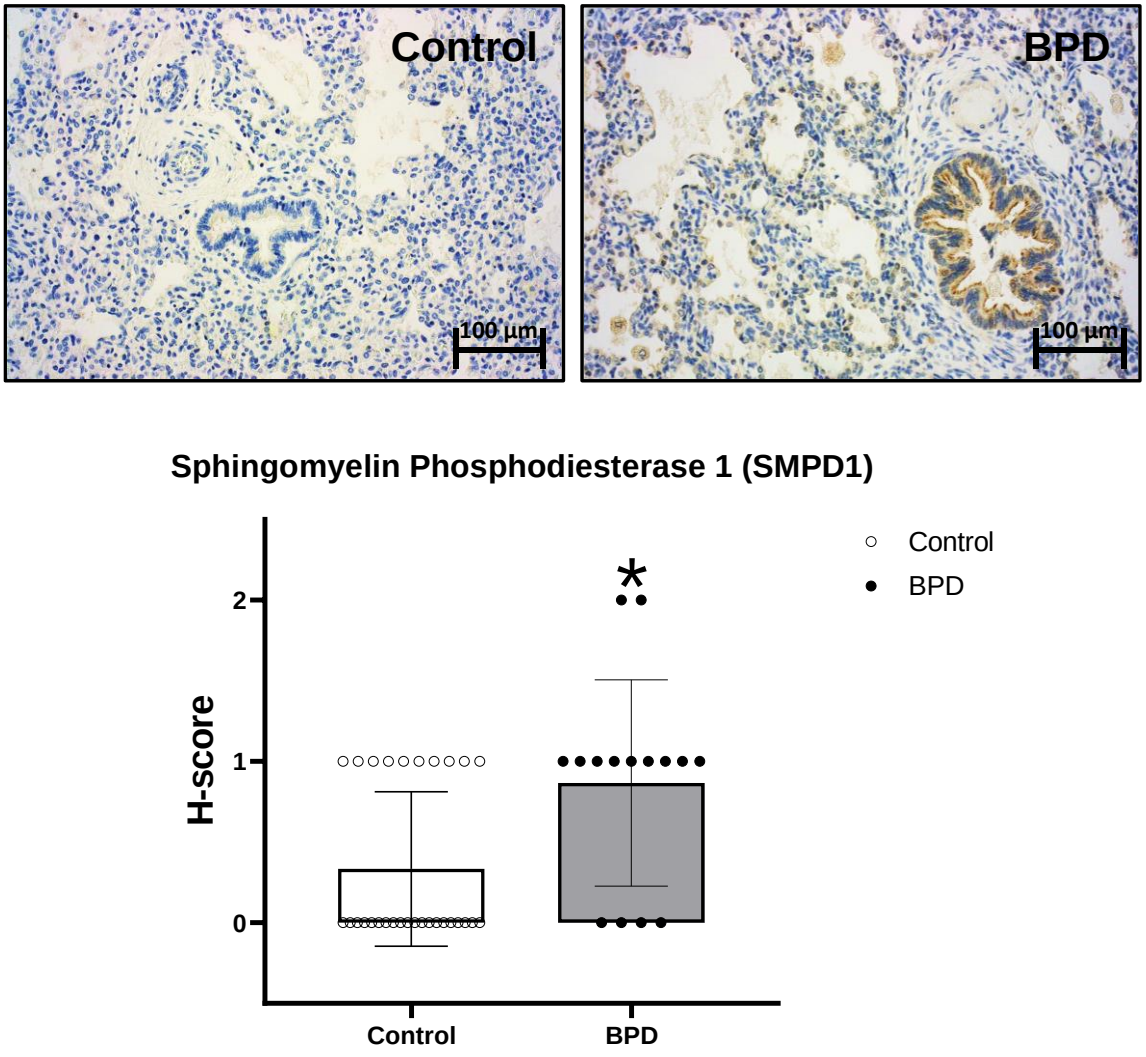

Figure 27: IHC staining and H-score for SMPD1. Representative photomicrographs of SMPD1 IHC staining (brown) are shown above the graph. The statistical analysis of the H-score indicates a significant increase in SMPD1 levels in the lungs of human infants with BPD compared to the control group. (* compared to control; $P < 0.05$, by Mann–Whitney U test, $n = 30$ and 16 samples per group, respectively)

3.4.2 SGMS1:

SGMS1 is an important enzyme within the ceramide pathway, catalyzing the synthesis of sphingomyelin and diacylglycerol from ceramide and phosphatidylcholine [96]. Compared to the control group, lung sections from individuals with BPD displayed a significantly greater H-score for SGMS1 (Figure 28).

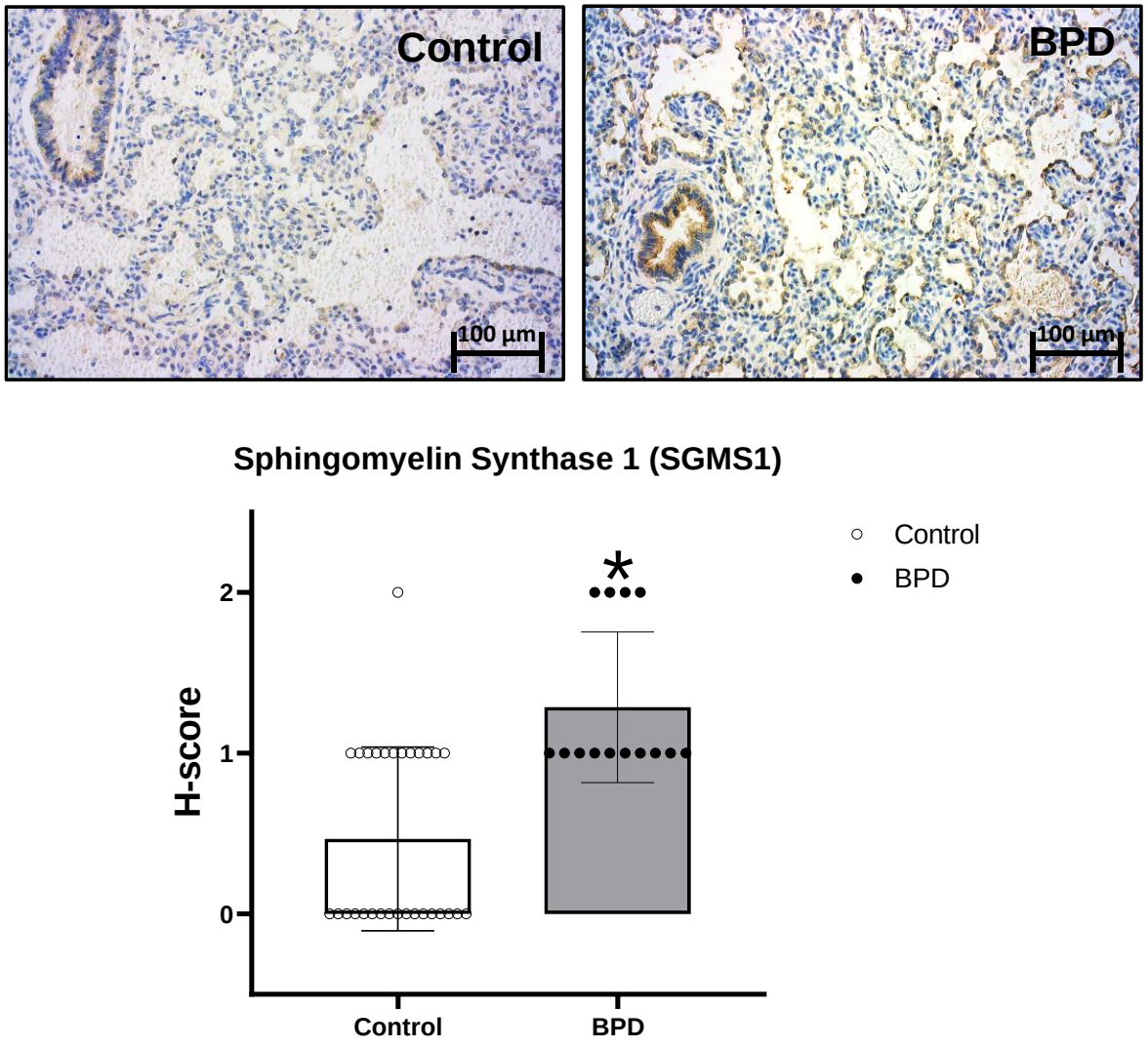

Figure 28: IHC staining and H-score for SGMS1. Representative photomicrographs of SGMS1 IHC staining (brown) are shown above the graph . The statistical analysis of the H-score indicates a significant increase in SGMS1 levels in the lungs of human infants with BPD compared to the control group. (* compared to control; $P < 0.05$, by Mann–Whitney U test, $n = 30$ and 14 samples per group, respectively)

3.4.3 Lass1:

The Ceramide synthase family comprises key enzymes involved in the *de novo* synthesis of ceramide. Lass1, within this family, facilitates the attachment of C18 fatty acyl CoA to the sphingoid base [97]. Compared to the control group, lung sections from individuals with BPD exhibited a significantly increased H-score for Lass1 (Figure 29).

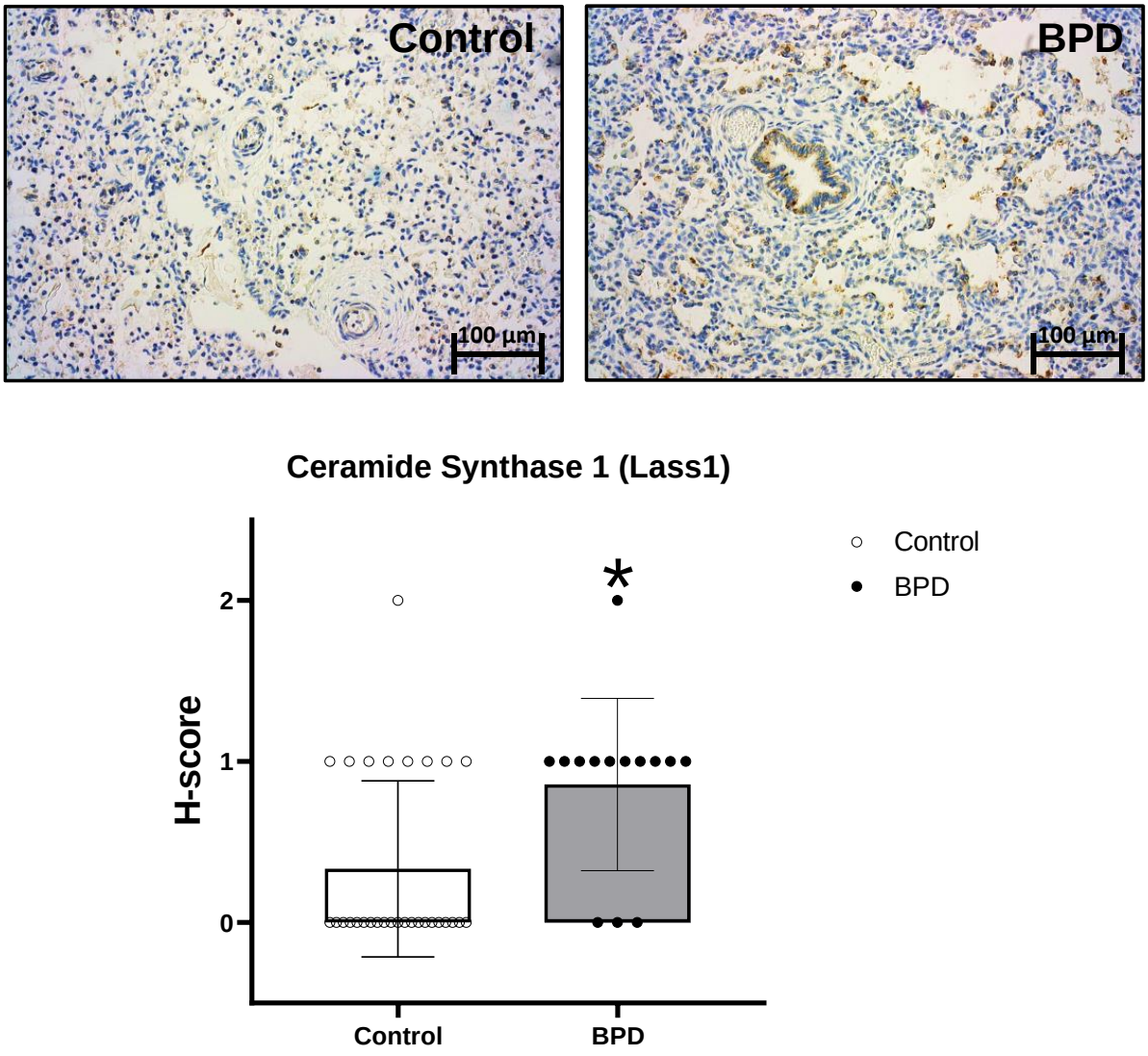

Figure 29: IHC staining and H-score for Lass1. Representative photomicrographs of Lass1 IHC staining (brown) are shown above the graph. The statistical analysis of the H-score indicates a significant increase in Lass1 levels in the lungs of human infants with BPD compared to the control group. (* compared to control; $P < 0.05$, by Mann–Whitney U test, $n = 30$ and 14 samples per group, respectively)

3.4.4 CerS2:

As previously highlighted, ceramide synthase constitutes a family of six isoforms enzymes (CS1 to CS6). The CerS2 is the primary synthase responsible for synthesizing very long-chain (C22-C24) ceramide through the *de novo* pathway [98]. IHC staining revealed overall very high immunoreactivity in both groups localized to proximal respiratory epithelium, with no significant difference in the H-score of CerS2 between cases of BPD and control (Figure 30).

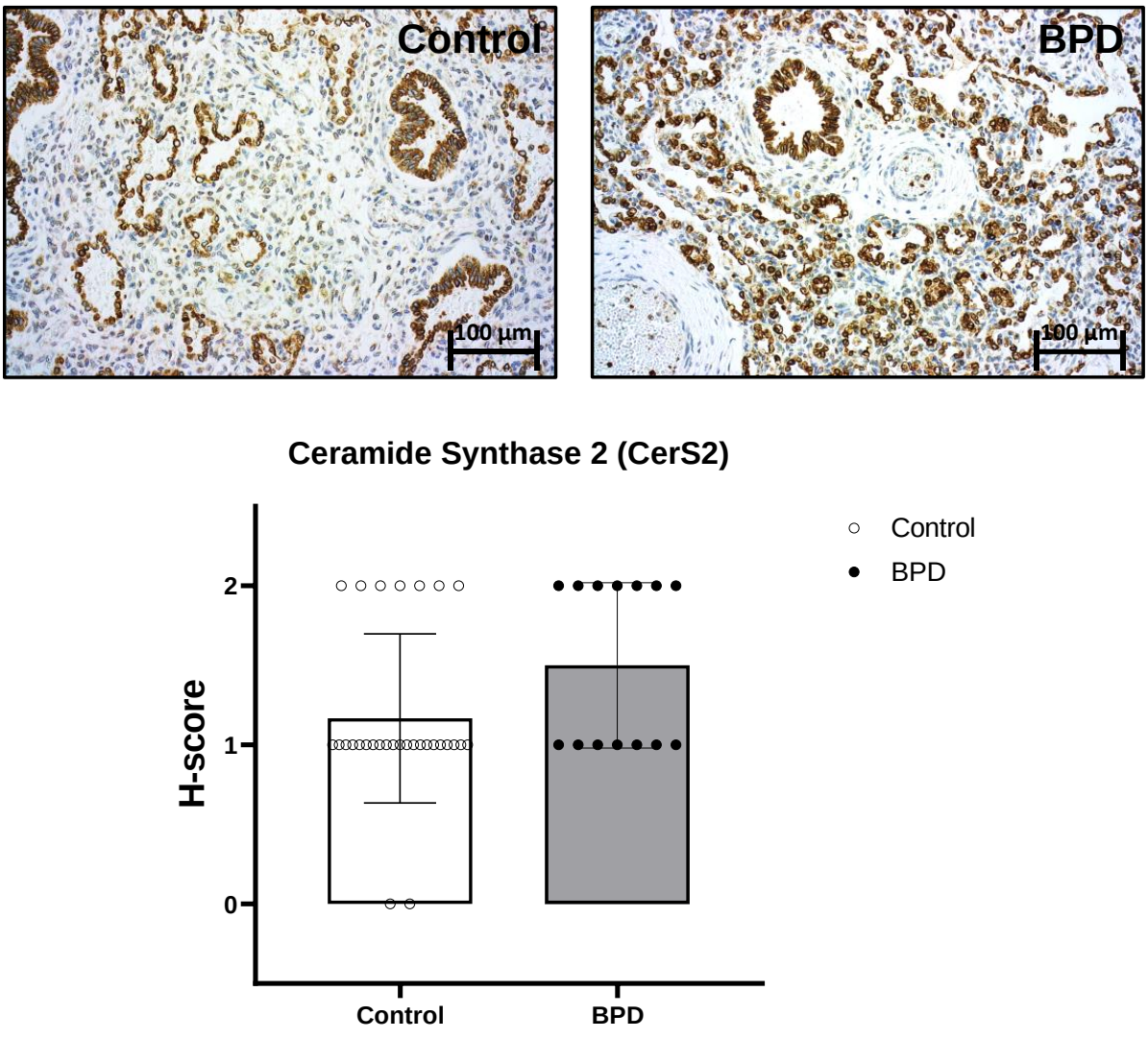

Figure 30: IHC staining and H-score for CerS2. Representative photomicrographs of CerS2 IHC staining (brown) are shown above the graph. The statistical analysis of the H-score indicates no significant difference observed for CerS2 between the BPD and control groups. n = 30 and 14 samples per group, respectively.

Chapter 4: Discussion

4.1 Hyperoxia, BPD and Ceramide:

Since its first description by Northway and colleagues in 1967 [99], there has been an extensive body of research conducted on BPD. BPD represents a disease of intricate pathogenesis with a multifactorial etiology [100]. The standard of care for respiratory distress syndrome (RDS) in preterm neonates includes MV and supplemental oxygen, both of which are major contributors to the development of BPD [30]. The development of non-invasive ventilation strategies has reduced volutrauma/barotrauma to the premature lung [101, 102], but has not reduced the overall incidence of BPD. Furthermore, various reports suggest that prolonged oxygen therapy plays a pivotal role in the pathogenesis of BPD by generating reactive oxygen species (ROS) in preterm lung tissue [31]. Reactive nitrogen species (RNS) are also produced when exogenous or endogenous nitric oxide (NO) interacts with ROS such as superoxide and hydrogen peroxide (H_2O_2) [103]. Previous research in the laboratory of Dr. Jankov has highlighted nitroxidative stress as a crucial factor in neonatal lung injury [9].

Previous work has revealed dysregulation in sphingolipid metabolism and altered ceramide level in the lung diseases, including asthma [70], cystic fibrosis [104], COPD [105], and emphysema [106]. Additionally, a few studies have implicated the upregulation of ceramide in MV-induced experimental neonatal lung injury and in tracheal aspirates from human preterm neonates [45, 46]. These findings have led to significant interest in the potential role of sphingolipids in the pathogenesis of BPD [69]. However, the precise connections between exposure to high levels of oxygen, lung damage, ceramide levels, and cell death remain incompletely elucidated.

In my thesis, I have demonstrated that after a 24-hour exposure to hyperoxia, pro-apoptotic ceramides were rapidly and significantly upregulated in the lungs of newborn rats, particularly the

well-known pro-apoptotic C16 and C18 ceramide species [107]. This finding aligns with a previous report on MV in rat lungs, where C16 ceramide was markedly increased in bronchoalveolar lavage fluid (BALF) [46]. Continuous hyperoxia exposure until PND 7 contributed to the persistent significant elevation of C18 and other known pro-apoptotic ceramide species, including C22 and C24. These findings are consistent with a prior investigation, which demonstrated the upregulation of ceramide in response to hyperoxia exposure in a time-dependent fashion [44, 45], being evident within 24 hours. Subsequently, some ceramide species remained upregulated on PND 7, with no further upregulation on PND 21.

The IF staining of PND 1 lung sections revealed a notable increase in SMPD1 content within epithelial cells. However, a reliable quantification of SMPD1 enzymatic activity in lung tissue posed challenges, stemming from the heterogeneous nature of the lung tissue, which encompasses a variety of cell populations, most of which do not express SMPD1. Therefore, we were unable to observe any increase in SMPD-1 enzymatic activity secondary to hyperoxia.

4.2 Autophagy, Hyperoxia and Ceramide Elevation in Lung:

Autophagy, a metabolic process integral to cellular survival and maintenance, orchestrates the degradation and recycling damaged or aged organelles, particularly in response to stress stimuli [56]. Dysregulation in autophagy pathway has been reported in various disease conditions, suggesting its close association with pathophysiologic mechanisms [108]. Notably, disruptions in autophagy have been strongly implicated in the development of diverse pulmonary diseases [109].

Supporting this, Kim et al. reported a similar finding, highlighting an increase of LC3BII due to smoke extract exposure was leading to the activation of caspases (-8, -9, -3) and resulting in apoptotic cell death after 12 hours [110]. A recent study by Yeganeh and colleagues

demonstrated that experimental MV-induced lung injury in newborn rats was associated with excessive autophagy activity, contributing to apoptosis and eventual alveolar epithelial cell death [46]. This study also revealed that autophagy preceded apoptosis and triggered the extrinsic apoptosis pathway via LC3B-FAS interaction [46].

In the context of my thesis work, a significant increase in autophagy markers (ATG5-12 and LC3BII) was observed in lung epithelial cells of newborn rat on PND 1, concurrent with increased ceramides, while assessment of autophagic activity on PND 7 did not reveal a marked elevation in autophagy markers. These findings align with previous observations, emphasizing that autophagy signaling serves as the primary response to both lung injurious stimulus (hyperoxia or MV), which subsequently leads to cell death [46, 111].

4.3 Apoptosis and Hyperoxia-induced Lung Injury Following Ceramide Elevation:

Apoptosis, a meticulously orchestrated program of cell death, plays a pivotal role in eliminating damaged cells and maintaining homeostasis while mitigating inflammation [112]. Its significance extends to organogenesis regulation, acting as a homeostatic mechanism to control cell populations during the development of various tissue organs, particularly in the lung structural maturation [113, 114]. Several studies have established that apoptotic cell death pathway is a downstream consequence of detrimental stimuli in acute lung injuries, including microbial infections [115, 116], MV [46], and hyperoxia exposure [83]. Notably, MV and hyperoxia are principal factors in the development of BPD in preterm neonates [30].

Several reports have emphasized the crucial role of apoptotic death in the lung epithelial cells of rat pups subjected to MV, contributing to hypo-alveolarization [117, 118]. Yeganeh and colleagues, in a mechanistic study, elucidated the relationship between ceramide elevation and the

activation of the apoptosis pathway in the lung epithelial cells during acute experimental MV in newborn rats [46]. In my study, I observed that ceramide upregulation due to hyperoxia exposure was concomitant with a significant increase in apoptosis activity. The WB analysis of apoptosis marker (Cl.PARP) on PND 7 indicated a substantial increase in the hyperoxia exposed newborn rats compared to the room air control. Complementing this, utilizing TUNEL assay to visualize apoptotic cells in lung sections of PND 7 rat pups confirmed the results obtained through WB analysis. Furthermore, co-IF staining using antibodies against apoptosis proteins (Cl.Casp 3 and Cl.PARP) along with the epithelial cell marker (CDH1) revealed an increased apoptosis activity in alveolar epithelial cells. These findings align with previous reports on hyperoxia exposure and apoptotic cell death in experimental animal models [119].

Tanaka and colleagues previously reported that prolonged hyperoxia exposure in adult mice (8 to 12 weeks of age) led to the activation of Casp 3 and apoptotic cell death in lung epithelial cells, which was further confirmed in an *in vitro* model, using pulmonary epithelial cells of human [119]. More recently, a study reported temporal activation of both autophagy and apoptosis pathways following hyperoxia exposure in adult rats [120]. Ren et al. demonstrated that hyperoxia-induced autophagy and apoptosis in the type 2 alveolar epithelial cell, and inhibiting autophagy activity resulted in reduced apoptosis and lung injury [120].

The findings of my study in newborn rats hold particular clinical relevance to hyperoxia injury in the BPD model of preterm neonates, initiated in the early days after birth when they are at the saccular stage of lung maturation. Despite the fact that most studies on hyperoxia-induced lung injury have been conducted on adult animals, whose mechanisms may differ fundamentally from those of newborn rats, my results indicate that hyperoxia causes significant lung damage in newborn rats. The marked increase in apoptosis activity during this critical period of lung

development may be a crucial factor contributing to impaired lung growth and maturation in the animals exposed to high oxygen concentrations.

4.4 The Effect of Desipramine on Ceramide, Autophagy, and Apoptosis:

In 1986, for the first time, it was discovered that sphingolipids, apart from simply serving as components of cell membranes, exhibit potent inhibitory effects on protein kinase C (PKC) [121]. Subsequently, in 1990, the role of ceramide as an intracellular mediators in cell proliferation and apoptosis was elucidated [122]. An accumulating body of evidence derived from studies on lung disease suggests that dysregulation in sphingolipid metabolism leads to altered ceramide levels, implicating ceramide in the pathogenesis of various respiratory disorders [45, 70-72]. As a result, pharmacologically targeted inhibition of ceramide synthesis has been embraced as a therapeutic strategy in numerous diseases associated with ceramide upregulation, aimed at mitigating the pathophysiological impacts [123]. In a study conducted by Petrache and colleagues, the use of myriocin (a potent inhibitor of serine palmitoyl transferase in the *de novo* pathway) in an emphysema model was accompanied by a reduction in alveolar cell death and oxidative stress injury [124]. In another study, a murine model of Cystic fibrosis (CF) was treated with SMPD1 inhibitors, resulting in improved lung function through the reduction of ceramide levels in bronchial epithelial cells and subsequently attenuated inflammation [71].

In a more recent investigation, Yeganeh et al. demonstrated an increased in SMPD1 activity in a rat model of MV, reporting that inhibition of SMPD1 by Desipramine or Fluoxetine ameliorated autophagy and prevented apoptosis cell death [46]. Consistent with these findings, I observed that Desipramine reduced lung ceramide content by inhibiting SMPD1 in hyperoxia-exposed rat pups on PND 1. Apparently, the decrease in ceramide levels was associated with reduced autophagy, as indicated by reduction in autophagy markers (ATG5-12) and (LC3BII) in

WB and IF staining, respectively on PND 1. Notably, Desipramine treatment during the first seven days of hyperoxia exposure resulted in a significant reduction in apoptotic cell death in the rat alveolar epithelial cells. This effect was consistently observed in WB, co-IF staining, and TUNEL assay results.

4.5 The Administration of Desipramine for Preventing Lung Structural Injury:

Several studies have elucidated a potentially deleterious aspect of respiratory support, including MV [117] and supplemental oxygen therapy [125], on lung tissue in animals. These interventions were associated with ceramide upregulation due to increased activity of SMPD1 [46], consequently leading to augmented autophagy-mediated apoptosis in alveolar epithelial cells [120]. This cascade of events is believed to play a pivotal role in the pathogenesis of BPD. While Desipramine, through the inhibition of SMPD1, prevented activation of apoptotic cell death, until now it remained unexplored whether Desipramine treatment also ameliorates experimental BPD-like lung injury.

This study also introduced a novel dimension by employing design-based stereology to quantitatively assess morphological changes in lung structure. Stereology, recognized as a gold standard morphometric method, mitigates bias through stringent sampling and adheres to well-established geometrical and statistical principles [86]. In the realm of lung research, microscopy-based stereology emerges as the most detailed, accurate, and statistically valid approach for elucidating alveolar number, size, surface area, septal thickness and cell count [88, 89].

Previous investigations utilizing stereological analysis in BPD models have contributed valuable insights. For instance, Madurga and colleagues, employed stereological analysis to examine the impact of hydrogen sulfide (H_2S) on postnatal alveolarization in a mouse BPD model

[126], assessing parameters such as MLI, alveolar septal wall thickness, total alveolar septal volume and surface area, and alveolar number [126]. Similarly, Mühlfeld et al. conducted design-based stereological analysis in the hyperoxia-based BPD model in preterm rabbit, revealing reductions in alveolar number and surface area, thickening of alveolar septa, and the accumulation of edema fluid and inflammatory cells at intra-alveolar space in hyperoxia exposed group [127]. More recently in a study published by Dr. Jankov and his colleagues, they have elucidated the pathogenic role of thrombospondin-1 (TSP-1) in activating transforming growth factor-β1 (TGF-β1) on a BPD rat model secondary to bleomycin exposure. Employing design-based stereological methods, they assessed lung structure and inflammation. The findings revealed that inhibition of TSP-1-induced TGF-β1 signaling led to an improvement in lung structure, characterized by an increase in alveolar surface density and alveolar numerical density, along with concomitant decrease in macrophage numbers [95].

In the current study, results of design-based stereology on PND 21 revealed marked structural abnormalities in rat lung exposed to HIH compared to the control group. Notable alterations included fewer alveolar per unit lung volume, larger average alveolar size, more simplified alveoli, reduced length of small blood vessels (20-60 μm external diameter), and an increased total number of lung macrophages. Alongside these findings on aberrant alveolar architecture, a significant increase in RV hypertrophy (Fulton's index) and pulmonary vascular remodeling, two main hallmarks of cPH, was evident in HIH-exposed animals.

Notably, the treatment of rat pups exposed to HIH conditions with Desipramine resulted in partial improvement in alveolarization parameters. This was evidenced by a partial increase in alveolar surface density and a decrease in MLI, with no significant difference observed compared to the control group. Nevertheless, Desipramine exerted significant impact on attenuating vascular

hypoplasia in BPD, as evidenced by an increase in small vessel length, and it effectively prevented the infiltration of lung inflammatory cells, specifically reducing macrophage infiltration into alveolar air spaces. Additionally, Desipramine treatment in the HIH-exposed group was accompanied by a remarkable improvement in pulmonary hypertension parameters, as manifested by a reduction in Fulton's index and arterial medial wall area.

Previous reports have indicated that the MV and hyperoxia exposure can lead to apoptotic cell death, contributing to reduced alveolar formation and simplified alveoli [117, 128]. Roper et al. demonstrated that *in vivo* hyperoxia exposure induces injury in alveolar type 2 cell in mice, altering their function as progenitor cells in alveolar epithelium [129]. In the present study, a notable increase in apoptosis cell death in experimental-BPD lungs was observed after hyperoxia exposure in alveolar epithelial cells, suggesting a pivotal role in altered lung development. Considering the protective effect of Desipramine on lung alveolar and vascular structure, an enticing hypothesis is that Desipramine treatment significantly reduces apoptosis of lung epithelial cells exposed to hyperoxia, thus preventing BPD-like lung injury.

Postnatal growth restriction poses a potential confounding factor in neonatal animal studies, as it can have adverse effects on lung development even in the absence of other inciting injuries [80]. In the present study, a notable disparity in average weight was observed between Desipramine- and vehicle-treated animals on PND 21, in both room air and HIH-exposed groups. This weight reduction was particularly evident in the room air-exposed rat pups, raising concerns about potential side effects of Desipramine on postnatal growth. Indeed, Nobrega and colleagues reported in rats that Desipramine treatment resulted in a reduction in food intake and weight loss [130]. To address this concern, we conducted an additional animal study, with the objective of minimizing such effects. This was achieved by modifying the duration of Desipramine treatment

to just one week (PND 1-7), during the period when hyperoxia-mediated ceramide up-regulation peaks. Importantly, analysis of weight records on PND 7 in the initial study revealed no significant difference in the average weight between Desipramine- and vehicle-treated groups at that time point. This finding reassured us that adverse effects by Desipramine on somatic growth occurred after this period. In accord, we observed no differences on body weight between vehicle- and Desipramine-treated groups on PND 21 when Desipramine was administered only for the first 7 days (Figure 31). We are currently undertaking stereological analysis to examine effects of the modified Desipramine administration protocol on markers of alveolarization. However, the results were not yet available at the time of writing.

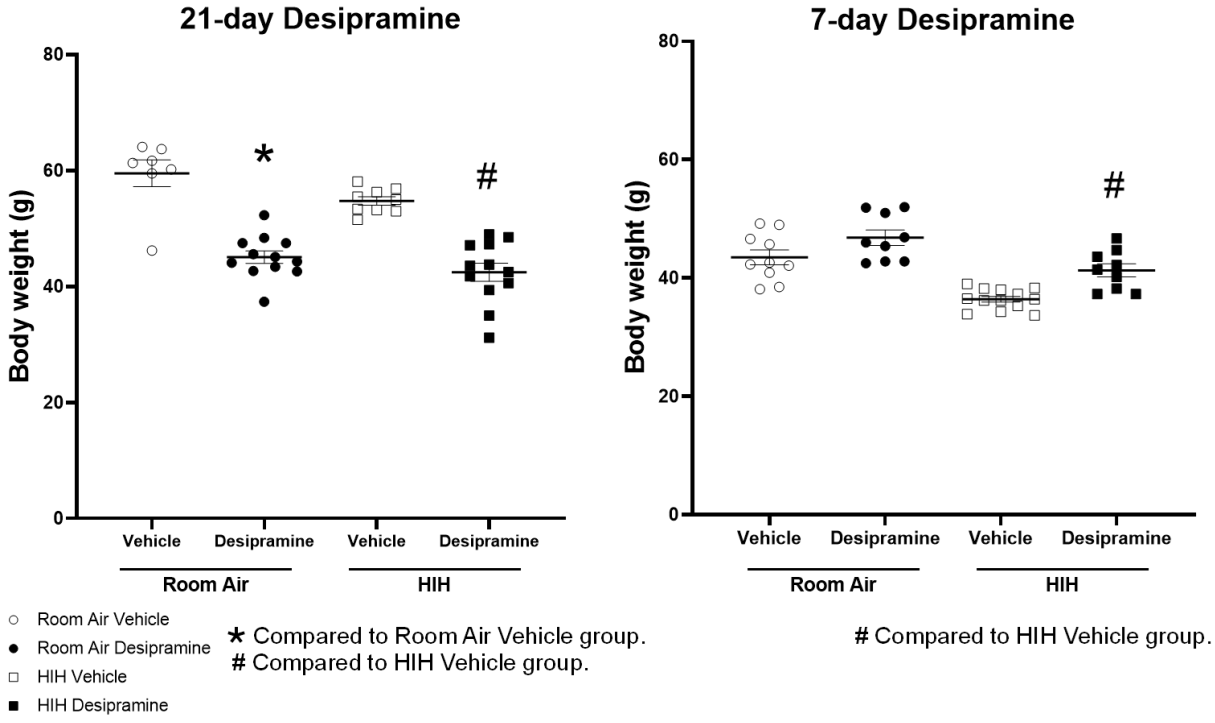

Figure 31: Measurement of the body weight of rat pups on PND 21. In the left-hand graph, a significantly lower body weight is shown in 21-day Desipramine treatment regimen, both in room air and HIH cases. On the right graph, the new 7-day treatment plan is associated with notable improvement in body weight of Desipramine-treated animals. In room air rat pups, there was no longer a significant difference from the vehicle group. In the HIH condition, Desipramine-treated pups exhibited a higher average body weight than HIH vehicle subjects. (* compared to room air vehicle, # compared to HIH vehicle; $P < 0.05$, by one-way ANOVA, n = 7-11 samples per group)

4.6 The Key Ceramide Metabolizing Proteins in Lung Tissue Sections from Extremely Premature Infants:

Ceramides have emerged as pivotal second messenger lipids implicated in the pathogenesis of various lung diseases [45, 70-72]. Importantly, these insights are primarily derived from animal models, as studies on human BPD infant tissue are incredibly rare. In BPD, proteomics and metabolomics studies on human tissues could provide deeper insights into disease pathophysiology. However, obtaining lung samples from infants presents considerable ethical and safety challenges [131]. Tracheal aspirates are one way to circumvent these issues, but require that a patient be endotracheally intubated [132]. In a study on human infant utilizing tracheal aspirates, van Mastrigt and colleagues demonstrated a significant increase in ceramide concentration, both long chain and very long chain, in 122 mechanically ventilated preterm Dutch newborns during the first 7 days of life [45]. The paucity of lung tissue from early-stage of BPD patients and the survivors represents a significant limitation in understanding the pathophysiology of this disease and developing an effective therapeutic approach. It is therefore notable that our laboratory has gained access to the FFPE lung tissue from extremely preterm infants at CHEO. From this archive, 47 cases have been collected, including 17 BPD cases and 30 controls [95]. We utilized these same samples to gain insights into altered contents of ceramide pathway enzymes, namely SMPD1, SGMS1, Lass1, and CerS2.

The results revealed significant differences in three ceramide pathway proteins, including SMPD1, SGMS1, and Lass1, in the BPD cases compared to control groups. Lass 1, (or CerS1) is a key enzyme in *de novo* pathway of ceramide synthesis by attaching C18 fatty acyl CoA to the sphingoid base [97]. A study conducted by Choi and colleagues highlighted the significant role of sphingolipid metabolism in the development of obese asthma, reporting increased expression of

CerS1 and CerS6 in the lung tissues of obese mice. Results of this study suggested that alteration in ceramide accumulation, particularly C18 ceramides, may contribute to the development of obese asthma [133]. Considering mechanistic reports linking increased SMPD1 activity and subsequent ceramide upregulation with the pathology of lung disease [46, 71], coupled with my results from experimental-BPD rat model, the higher expression of SMPD1 in the lung the of BPD infants reaffirms the potential of SMPD1 as a novel therapeutic target for the treatment of chronic lung injury in newborn infants. These findings underscore a potential pathogenic role for the ceramide pathway, particularly SMPD1, in the context of BPD in human neonates.

4.7 Conclusions:

In this study, I employed an experimental rat model of BPD to investigate hyperoxia-induced lung injury through the mechanism of ceramide upregulation. The findings of my study indicated a significant increase in ceramide levels in newborn rat lungs exposed to hyperoxia, leading to the activation of the autophagy and apoptosis, ultimately resulting in epithelial cell death. Moreover, Desipramine treatment effectively prevented hyperoxia-mediated ceramide generation. This in turn attenuated hyperoxia-induced autophagy and subsequent apoptotic cell death. My results suggest that the elevated ceramide levels and apoptotic cell death contributed to vascular hypoplasia, cPH and, possible inhibited alveolarization. Coupled with earlier studies, these findings further support a potential pathological role for the ceramide pathway in chronic neonatal lung injury.

4.8 Limitations:

It is important to acknowledge and address potential limitations that may impact the interpretation and generalizability of my findings. Firstly, this study lacked sufficient statistical

power to discern potential sex interactions in disease severity or response to treatment. Clinical observations have suggested that male premature neonates not only exhibit an increased susceptibility to respiratory complications and development of BPD compared to females [134, 135], but they are also more likely to succumb to the complications of BPD [136].

Another limitation of this study was the number of biological replicates in WB analysis, with four biological replicates (n = 4 animals) selected per exposure and treatment group. Moreover, the room air Desipramine-treated samples were not included in the WB analysis on PND 1 and PND 7, although in our preliminary experiments we did not observe any differences between these two samples. Studies are ongoing to address these deficiencies.

Regarding hyperoxia-induced autophagy, while results from WB analysis and IF staining confirmed a significant increase in autophagy markers in the lungs of newborn rat pups after 24 hours of exposure to hyperoxia, autophagy activity has been reported to peak at varying intervals from the onset of hyperoxia, ranging from 12 hours to 48 hours or even 7 days [40, 61, 119, 120]. To address this inconsistency, I conducted an additional animal study under hyperoxia exposure, incorporating two extra time points (12 and 48 hours) to determine when autophagic activity peaked.

Several studies have emphasized the presence of highly specific lipid profiles in different cells, tissues, and organs [137, 138]. However, a comprehensive understanding of lipidomic variations in physiological or pathological conditions across different organs and intra- or extra-cellular fluids is lacking. In this study, the limitation was the sphingolipidome of rat pups, particularly the ceramide profile in the lungs of neonates. Despite existing studies exploring the role of ceramides in various diseases, a specific profile of ceramide species in rat neonates has not been established. Furthermore, despite reports of increased of SMPD1 activity in ceramide

upregulations due to lung injurious stimuli [46, 71], this study did not successfully demonstrate differences in the SMPD1 activity after hyperoxia exposure in lung tissue homogenate. The likely explanation is that SMPD1 activity appears largely restricted to distal alveolar epithelium, which represents a minority of cells in the lung, thus diluting measurements when utilizing whole lung.

Based on the results of this study, SMPD1 inhibition emerges as a potential therapeutic strategy to prevent hyperoxia-induced lung injury in BPD patients. However, it is crucial to note that Desipramine, used as a SMPD1 inhibitor in my study, is a drug indicated to be used for adults or children, and direct safety evaluations of Desipramine in neonates remain lacking.

In this study, I investigated the presence of key ceramide pathway proteins in autopsy lung sections obtained from extremely premature infants. Autolysis is the process of self-digestion that normally occurs after death and may lead to degradation of cellular structures and proteins, potentially influencing the accuracy of protein detection in the autopsy tissue. Therefore, it is important to note that the presence of autolysis in these samples could potentially impact protein integrity and influence IHC staining outcomes. Furthermore, obtaining age-matched lung sections from healthy neonates to serve as controls posed a significant challenge. This difficulty arises because a substantial proportion of preterm infants typically exhibit some degree of lung injury. Additionally, instances of death in preterm infants without significant associated lung injury are rare. As a result, the availability of well-matched control samples free from lung injury is impossible, complicating the establishment of an ideal control group for comparative analyses. Despite these challenges, this study aimed to extract meaningful insights into the expression of ceramide pathway proteins in the context of premature infant lung tissue, acknowledging the inherent limitations associated with containing human samples.

4.9 Future Directions:

In vitro studies to assess SMPD1 activity in primary lung cells exposed to hyperoxia, with a specific focus on distal epithelial alveolar cells, would provide valuable mechanistic insights into the relationships between hyperoxia, ceramides, autophagy, and cell death.

In the current study, Desipramine was administered subcutaneously due to its favorable characteristics such as high bioavailability and rapid onset of action. However, the invasive nature of needle injecting may result in localized side effects at the injection site, including redness, itching, swelling, pain, and bruising [139]. Therefore, it is advisable to explore alternative drug delivery methods, specifically focusing on pulmonary delivery for respiratory diseases. Inhalation drug delivery not only offers a non-invasive administration route, but also enables targeted drug delivery to the disease site in pulmonary disorders. This approach can lead to more efficient therapeutic outcomes while minimizes systemic adverse effect [71, 140]. Developing pulmonary Desipramine delivery strategies can enhance the overall safety and efficacy of treatments, making it a promising avenue for future investigations.

Given that BPD-induced lung impairment persists in adult survivors, follow-up studies are warranted to address the long-term outcomes of Desipramine treatment in our HIH BPD-like lung injury model, which should include assessments of lung structural and functional parameters [141], exercise tolerance [142], and neurocognitive performance [143].

References

1. Liu, L., et al., *Global, regional, and national causes of child mortality in 2000-13, with projections to inform post-2015 priorities: an updated systematic analysis.* Lancet, 2015. **385**(9966): p. 430-40.
2. Cisneros-Franco, J.M., et al., *Critical periods of brain development.* Handb Clin Neurol, 2020. **173**: p. 75-88.
3. Warburton, D., *Overview of Lung Development in the Newborn Human.* Neonatology, 2017. **111**(4): p. 398-401.
4. Giancotti, A., et al., *Functions and the Emerging Role of the Foetal Liver into Regenerative Medicine.* Cells, 2019. **8**(8).
5. Anderson, P.J. and L.W. Doyle, *Neurodevelopmental outcome of bronchopulmonary dysplasia.* Semin Perinatol, 2006. **30**(4): p. 227-32.
6. Blencowe, H., et al., *National, regional, and worldwide estimates of preterm birth rates in the year 2010 with time trends since 1990 for selected countries: a systematic analysis and implications.* Lancet, 2012. **379**(9832): p. 2162-72.
7. Morgan, A.S., et al., *Management and outcomes of extreme preterm birth.* BMJ, 2022. **376**: p. e055924.
8. Rolnitsky, A., et al., *The price of neonatal intensive care outcomes - in-hospital costs of morbidities related to preterm birth.* Front Pediatr, 2023. **11**: p. 1068367.
9. Jankov, R., & Tanswell, A., *Chronic Neonatal Lung Injury and Care Strategies to Decrease Injury*, in *Fetal and Neonatal Lung Development: Clinical Correlates and Technologies for the Future*, J.W. A. Jobe, & S. Abman, Editor. 2016, Cambridge University Press. p. 205-222.
10. Thebaud, B., et al., *Bronchopulmonary dysplasia.* Nat Rev Dis Primers, 2019. **5**(1): p. 78.
11. Whitsett, J.A., S.E. Wert, and B.C. Trapnell, *Genetic disorders influencing lung formation and function at birth.* Hum Mol Genet, 2004. **13 Spec No 2**: p. R207-15.
12. Davidson, L.M. and S.K. Berkelhamer, *Bronchopulmonary Dysplasia: Chronic Lung Disease of Infancy and Long-Term Pulmonary Outcomes.* J Clin Med, 2017. **6**(1).
13. Baker, C.D. and C.M. Alvira, *Disrupted lung development and bronchopulmonary dysplasia: opportunities for lung repair and regeneration.* Curr Opin Pediatr, 2014. **26**(3): p. 306-14.
14. Ehrenkranz, R.A., et al., *Validation of the National Institutes of Health consensus definition of bronchopulmonary dysplasia.* Pediatrics, 2005. **116**(6): p. 1353-60.
15. Baraldi, E. and M. Filippone, *Chronic lung disease after premature birth.* N Engl J Med, 2007. **357**(19): p. 1946-55.
16. Coalson, J.J., *Pathology of new bronchopulmonary dysplasia.* Seminars in neonatology SN, 2003. **8**(1): p. 73–81.
17. Pierce, M.R. and E. Bancalari, *The role of inflammation in the pathogenesis of bronchopulmonary dysplasia.* Pediatr Pulmonol, 1995. **19**(6): p. 371-8.
18. Popova, A.P., *Mechanisms of bronchopulmonary dysplasia.* J Cell Commun Signal, 2013. **7**(2): p. 119-27.
19. Abman, S.H., E. Bancalari, and A. Jobe, *The Evolution of Bronchopulmonary Dysplasia after 50 Years.* Am J Respir Crit Care Med, 2017. **195**(4): p. 421-424.
20. Stoll, B.J., et al., *Trends in Care Practices, Morbidity, and Mortality of Extremely Preterm Neonates, 1993-2012.* JAMA, 2015. **314**(10): p. 1039-51.
21. Shah, P.S., et al., *Outcomes of preterm infants <29 weeks gestation over 10-year period in Canada: a cause for concern?* J Perinatol, 2012. **32**(2): p. 132-8.

22. Landry, J.S., et al., *Long-term impact of bronchopulmonary dysplasia on pulmonary function.* Can Respir J, 2011. **18**(5): p. 265-70.
23. O'Reilly, M., F. Sozo, and R. Harding, *Impact of preterm birth and bronchopulmonary dysplasia on the developing lung: long-term consequences for respiratory health.* Clin Exp Pharmacol Physiol, 2013. **40**(11): p. 765-73.
24. Greenough, A., *Long term respiratory outcomes of very premature birth (<32 weeks).* Semin Fetal Neonatal Med, 2012. **17**(2): p. 73-6.
25. Hansmann, G., et al., *Pulmonary hypertension in bronchopulmonary dysplasia.* Pediatr Res, 2021. **89**(3): p. 446-455.
26. Gough, A., et al., *Impaired lung function and health status in adult survivors of bronchopulmonary dysplasia.* Eur Respir J, 2014. **43**(3): p. 808-16.
27. Islam, J.Y., et al., *Understanding the Short- and Long-Term Respiratory Outcomes of Prematurity and Bronchopulmonary Dysplasia.* Am J Respir Crit Care Med, 2015. **192**(2): p. 134-56.
28. Gunville, C.F., et al., *Scope and impact of early and late preterm infants admitted to the PICU with respiratory illness.* J Pediatr, 2010. **157**(2): p. 209-214 e1.
29. Offringa, M., et al., *Applying Regulatory Science to Develop Safe and Effective Medicines for Neonates: Report of the US Food and Drug Administration First Annual Neonatal Scientific Workshop, October 28-29, 2014.* Ther Innov Regul Sci, 2015. **49**(5): p. 623-631.
30. Jobe, A.H., *The new bronchopulmonary dysplasia.* Curr Opin Pediatr, 2011. **23**(2): p. 167-72.
31. Wang, J. and W. Dong, *Oxidative stress and bronchopulmonary dysplasia.* Gene, 2018. **678**: p. 177-183.
32. Kilic, M., et al., *Nitric oxide levels and antioxidant enzyme activities in jaundices of premature infants.* Cell Biochem Funct, 2004. **22**(5): p. 339-42.
33. Jensen, E.A. and B. Schmidt, *Epidemiology of bronchopulmonary dysplasia.* Birth Defects Res A Clin Mol Teratol, 2014. **100**(3): p. 145-57.
34. Lavoie, P.M., C. Pham, and K.L. Jang, *Heritability of bronchopulmonary dysplasia, defined according to the consensus statement of the national institutes of health.* Pediatrics, 2008. **122**(3): p. 479-85.
35. Parad, R.B., et al., *Role of Genetic Susceptibility in the Development of Bronchopulmonary Dysplasia.* J Pediatr, 2018. **203**: p. 234-241 e2.
36. Hartling, L., Y. Liang, and T. Lacaze-Masmonteil, *Chorioamnionitis as a risk factor for bronchopulmonary dysplasia: a systematic review and meta-analysis.* Arch Dis Child Fetal Neonatal Ed, 2012. **97**(1): p. F8-F17.
37. Stoll, B.J., et al., *Late-onset sepsis in very low birth weight neonates: the experience of the NICHD Neonatal Research Network.* Pediatrics, 2002. **110**(2 Pt 1): p. 285-91.
38. Gien, J. and J.P. Kinsella, *Pathogenesis and treatment of bronchopulmonary dysplasia.* Curr Opin Pediatr, 2011. **23**(3): p. 305-13.
39. Mankouski, A., et al., *Intermittent hypoxia during recovery from neonatal hyperoxic lung injury causes long-term impairment of alveolar development: A new rat model of BPD.* Am J Physiol Lung Cell Mol Physiol, 2017. **312**(2): p. L208-L216.
40. Sureshbabu, A., et al., *Inhibition of Regulatory-Associated Protein of Mechanistic Target of Rapamycin Prevents Hyperoxia-Induced Lung Injury by Enhancing Autophagy and Reducing Apoptosis in Neonatal Mice.* Am J Respir Cell Mol Biol, 2016. **55**(5): p. 722-735.
41. Fuchs, Y. and H. Steller, *Programmed cell death in animal development and disease.* Cell, 2011. **147**(4): p. 742-58.
42. Hargitai, B., et al., *Apoptosis in various organs of preterm infants: histopathologic study of lung, kidney, liver, and brain of ventilated infants.* Pediatr Res, 2001. **50**(1): p. 110-4.
43. Attaye, I., et al., *The effects of hyperoxia on microvascular endothelial cell proliferation and production of vaso-active substances.* Intensive Care Med Exp, 2017. **5**(1): p. 22.

44. Husari, A.W., et al., *Apoptosis and the activity of ceramide, Bax and Bcl-2 in the lungs of neonatal rats exposed to limited and prolonged hyperoxia.* Respir Res, 2006. **7**: p. 100.
45. van Mastrigt, E., et al., *Ceramides in tracheal aspirates of preterm infants: Marker for bronchopulmonary dysplasia.* PLoS One, 2018. **13**(1): p. e0185969.
46. Yeganeh, B., et al., *Acid Sphingomyelinase Inhibition Attenuates Cell Death in Mechanically Ventilated Newborn Rat Lung.* Am J Respir Crit Care Med, 2019. **199**(6): p. 760-772.
47. Kerr, J.F., A.H. Wyllie, and A.R. Currie, *Apoptosis: a basic biological phenomenon with wide-ranging implications in tissue kinetics.* Br J Cancer, 1972. **26**(4): p. 239-57.
48. Elmore, S., *Apoptosis: a review of programmed cell death.* Toxicol Pathol, 2007. **35**(4): p. 495-516.
49. Shi, Y., *Caspase activation, inhibition, and reactivation: a mechanistic view.* Protein Sci, 2004. **13**(8): p. 1979-87.
50. Kumar, S., *Caspase function in programmed cell death.* Cell Death Differ, 2007. **14**(1): p. 32-43.
51. Yanumula, A. and J.K. Cusick, *Biochemistry, Extrinsic Pathway of Apoptosis*, in *StatPearls*. 2023: Treasure Island (FL) ineligible companies. Disclosure: John Cusick declares no relevant financial relationships with ineligible companies.
52. Glick, D., S. Barth, and K.F. Macleod, *Autophagy: cellular and molecular mechanisms.* J Pathol, 2010. **221**(1): p. 3-12.
53. He, C. and D.J. Klionsky, *Regulation mechanisms and signaling pathways of autophagy.* Annu Rev Genet, 2009. **43**: p. 67-93.
54. Yu, L., Y. Chen, and S.A. Tooze, *Autophagy pathway: Cellular and molecular mechanisms.* Autophagy, 2018. **14**(2): p. 207-215.
55. Yamamoto, H., S. Zhang, and N. Mizushima, *Autophagy genes in biology and disease.* Nat Rev Genet, 2023. **24**(6): p. 382-400.
56. Yeganeh, B., et al., *Autophagy is required for lung development and morphogenesis.* J Clin Invest, 2019. **129**(7): p. 2904-2919.
57. Pattingre, S., et al., *Bcl-2 antiapoptotic proteins inhibit Beclin 1-dependent autophagy.* Cell, 2005. **122**(6): p. 927-39.
58. Yeganeh, B., et al., *Autophagy activation is required for influenza A virus-induced apoptosis and replication.* Biochim Biophys Acta Mol Cell Res, 2018. **1865**(2): p. 364-378.
59. Gump, J.M. and A. Thorburn, *Autophagy and apoptosis: what is the connection?* Trends Cell Biol, 2011. **21**(7): p. 387-92.
60. Codogno, P. and A.J. Meijer, *Autophagy and signaling: their role in cell survival and cell death.* Cell Death Differ, 2005. **12 Suppl 2**: p. 1509-18.
61. Zhang, D., et al., *Autophagy inducers restore impaired autophagy, reduce apoptosis, and attenuate blunted alveolarization in hyperoxia-exposed newborn rats.* Pediatric Pulmonology, 2018. **53**(8): p. 1053-1066.
62. Lee, J., et al., *Sphingolipids as cell fate regulators in lung development and disease.* Apoptosis, 2015. **20**(5): p. 740-57.
63. Quinville, B.M., et al., *A Comprehensive Review: Sphingolipid Metabolism and Implications of Disruption in Sphingolipid Homeostasis.* Int J Mol Sci, 2021. **22**(11).
64. Hannun, Y.A. and L.M. Obeid, *Sphingolipids and their metabolism in physiology and disease.* Nat Rev Mol Cell Biol, 2018. **19**(3): p. 175-191.
65. Sandhoff, R., *Very long chain sphingolipids: Tissue expression, function and synthesis.* FEBS Letters, 2010. **584**(9): p. 1907-1913.
66. Choi, R.H., et al., *Ceramides and other sphingolipids as drivers of cardiovascular disease.* Nat Rev Cardiol, 2021. **18**(10): p. 701-711.

67. Koybasi, S., et al., *Defects in cell growth regulation by C18:0-ceramide and longevity assurance gene 1 in human head and neck squamous cell carcinomas.* J Biol Chem, 2004. **279**(43): p. 44311-9.
68. Hartmann, D., et al., *Long chain ceramides and very long chain ceramides have opposite effects on human breast and colon cancer cell growth.* Int J Biochem Cell Biol, 2012. **44**(4): p. 620-8.
69. Thomas, J.M., et al., *The Role of Sphingolipid Signaling in Oxidative Lung Injury and Pathogenesis of Bronchopulmonary Dysplasia.* Int J Mol Sci, 2022. **23**(3).
70. Ono, J.G., T.S. Worgall, and S. Worgall, *Airway reactivity and sphingolipids-implications for childhood asthma.* Mol Cell Pediatr, 2015. **2**(1): p. 13.
71. Becker, K.A., et al., *Acid sphingomyelinase inhibitors normalize pulmonary ceramide and inflammation in cystic fibrosis.* Am J Respir Cell Mol Biol, 2010. **42**(6): p. 716-24.
72. Levy, M., et al., *Neutral sphingomyelinase 2 is activated by cigarette smoke to augment ceramide-induced apoptosis in lung cell death.* Am J Physiol Lung Cell Mol Physiol, 2009. **297**(1): p. L125-33.
73. Kornhuber, J., et al., *Functional Inhibitors of Acid Sphingomyelinase (FIASMAs): a novel pharmacological group of drugs with broad clinical applications.* Cell Physiol Biochem, 2010. **26**(1): p. 9-20.
74. Uguz, F., *A New Safety Scoring System for the Use of Psychotropic Drugs During Lactation.* Am J Ther, 2021. **28**(1): p. e118-e126.
75. Nguyen, H.Q., E. Callegari, and R.S. Obach, *The Use of In Vitro Data and Physiologically-Based Pharmacokinetic Modeling to Predict Drug Metabolite Exposure: Desipramine Exposure in Cytochrome P4502D6 Extensive and Poor Metabolizers Following Administration of Imipramine.* Drug Metab Dispos, 2016. **44**(10): p. 1569-78.
76. Daniel, W.A. and J. Wojcikowski, *Contribution of lysosomal trapping to the total tissue uptake of psychotropic drugs.* Pharmacol Toxicol, 1997. **80**(2): p. 62-8.
77. Gulbins, E., et al., *Acid sphingomyelinase-ceramide system mediates effects of antidepressant drugs.* Nat Med, 2013. **19**(7): p. 934-8.
78. Yoder, B.A. and J.J. Coalson, *Animal models of bronchopulmonary dysplasia. The preterm baboon models.* Am J Physiol Lung Cell Mol Physiol, 2014. **307**(12): p. L970-7.
79. Burri, P.H., *The postnatal growth of the rat lung. 3. Morphology.* Anat Rec, 1974. **180**(1): p. 77-98.
80. O'Reilly, M. and B. Thebaud, *Animal models of bronchopulmonary dysplasia. The term rat models.* Am J Physiol Lung Cell Mol Physiol, 2014. **307**(12): p. L948-58.
81. Rabinovitch, M., et al., *Age and sex influence on pulmonary hypertension of chronic hypoxia and on recovery.* Am J Physiol, 1981. **240**(1): p. H62-72.
82. Chen, Y.F., et al., *Dominant negative mutation of the TGF-beta receptor blocks hypoxia-induced pulmonary vascular remodeling.* J Appl Physiol (1985), 2006. **100**(2): p. 564-71.
83. Tibboel, J., et al., *Amelioration of hyperoxia-induced lung injury using a sphingolipid-based intervention.* Eur Respir J, 2013. **42**(3): p. 776-84.
84. Hsia, C.C., et al., *An official research policy statement of the American Thoracic Society/European Respiratory Society: standards for quantitative assessment of lung structure.* Am J Respir Crit Care Med, 2010. **181**(4): p. 394-418.
85. Ochs, M. and J. Schipke, *A short primer on lung stereology.* Respir Res, 2021. **22**(1): p. 305.
86. Schneider, J.P. and M. Ochs, *Stereology of the lung.* Methods Cell Biol, 2013. **113**: p. 257-94.
87. Weibel, E.R., C.C. Hsia, and M. Ochs, *How much is there really? Why stereology is essential in lung morphometry.* J Appl Physiol (1985), 2007. **102**(1): p. 459-67.
88. Ochs, M. and C. Muhlfeld, *Quantitative microscopy of the lung: a problem-based approach. Part 1: basic principles of lung stereology.* Am J Physiol Lung Cell Mol Physiol, 2013. **305**(1): p. L15-22.

89. Muhlfeld, C. and M. Ochs, *Quantitative microscopy of the lung: a problem-based approach. Part 2: stereological parameters and study designs in various diseases of the respiratory tract.* Am J Physiol Lung Cell Mol Physiol, 2013. **305**(3): p. L205-21.
90. Ochs, M., et al., *The number of alveoli in the human lung.* Am J Respir Crit Care Med, 2004. **169**(1): p. 120-4.
91. Chung, H.Y., et al., *Acid Sphingomyelinase Inhibition Prevents Development of Sepsis Sequelae in the Murine Liver.* Sci Rep, 2017. **7**(1): p. 12348.
92. Wong, M.J., et al., *Simvastatin prevents and reverses chronic pulmonary hypertension in newborn rats via pleiotropic inhibition of RhoA signaling.* Am J Physiol Lung Cell Mol Physiol, 2016. **311**(5): p. L985-L999.
93. Bogaard, H.J., et al., *The right ventricle under pressure: cellular and molecular mechanisms of right-heart failure in pulmonary hypertension.* Chest, 2009. **135**(3): p. 794-804.
94. Bronicki, R.A. and H.P. Baden, *Pathophysiology of right ventricular failure in pulmonary hypertension.* Pediatr Crit Care Med, 2010. **11**(2 Suppl): p. S15-22.
95. Ruschkowski, B.A., et al., *Thrombospondin-1 Plays a Major Pathogenic Role in Experimental and Human Bronchopulmonary Dysplasia.* Am J Respir Crit Care Med, 2022. **205**(6): p. 685-699.
96. Voelker, D.R. and E.P. Kennedy, *Cellular and enzymic synthesis of sphingomyelin.* Biochemistry, 1982. **21**(11): p. 2753-9.
97. Park, W.J. and J.W. Park, *The effect of altered sphingolipid acyl chain length on various disease models.* Biol Chem, 2015. **396**(6-7): p. 693-705.
98. Raichur, S., *Ceramide Synthases Are Attractive Drug Targets for Treating Metabolic Diseases.* Front Endocrinol (Lausanne), 2020. **11**: p. 483.
99. Northway, W.H., Jr., R.C. Rosan, and D.Y. Porter, *Pulmonary disease following respirator therapy of hyaline-membrane disease. Bronchopulmonary dysplasia.* N Engl J Med, 1967. **276**(7): p. 357-68.
100. Kalikkot Thekkeveedu, R., M.C. Guaman, and B. Shivanna, *Bronchopulmonary dysplasia: A review of pathogenesis and pathophysiology.* Respir Med, 2017. **132**: p. 170-177.
101. Schmolzer, G.M., et al., *Non-invasive versus invasive respiratory support in preterm infants at birth: systematic review and meta-analysis.* BMJ, 2013. **347**: p. f5980.
102. Isayama, T., C. Chai-Adisaksopha, and S.D. McDonald, *Noninvasive Ventilation With vs Without Early Surfactant to Prevent Chronic Lung Disease in Preterm Infants: A Systematic Review and Meta-analysis.* JAMA Pediatr, 2015. **169**(8): p. 731-9.
103. Auger, C., et al., *The metabolic reprogramming evoked by nitrosative stress triggers the anaerobic utilization of citrate in Pseudomonas fluorescens.* PLoS One, 2011. **6**(12): p. e28469.
104. Teichgraber, V., et al., *Ceramide accumulation mediates inflammation, cell death and infection susceptibility in cystic fibrosis.* Nat Med, 2008. **14**(4): p. 382-91.
105. Scarpa, M.C., et al., *Ceramide expression and cell homeostasis in chronic obstructive pulmonary disease.* Respiration, 2013. **85**(4): p. 342-9.
106. Tibboel, J., et al., *Ceramides: a potential therapeutic target in pulmonary emphysema.* Respir Res, 2013. **14**(1): p. 96.
107. Wang, Z., et al., *Overexpression of ceramide synthase 1 increases C18-ceramide and leads to lethal autophagy in human glioma.* Oncotarget, 2017. **8**(61): p. 104022-104036.
108. Yang, N. and H.M. Shen, *Targeting the Endocytic Pathway and Autophagy Process as a Novel Therapeutic Strategy in COVID-19.* Int J Biol Sci, 2020. **16**(10): p. 1724-1731.
109. Zhang, Y., J. Zhang, and Z. Fu, *Role of autophagy in lung diseases and ageing.* Eur Respir Rev, 2022. **31**(166).
110. Kim, H.P., et al., *Autophagic proteins regulate cigarette smoke-induced apoptosis: protective role of heme oxygenase-1.* Autophagy, 2008. **4**(7): p. 887-95.

111. Nakahira, K., et al., *Autophagy: a crucial moderator of redox balance, inflammation, and apoptosis in lung disease.* Antioxid Redox Signal, 2014. **20**(3): p. 474-94.
112. Renehan, A.G., C. Booth, and C.S. Potten, *What is apoptosis, and why is it important?* BMJ, 2001. **322**(7301): p. 1536-8.
113. Haanen, C. and I. Vermes, *Apoptosis: programmed cell death in fetal development.* Eur J Obstet Gynecol Reprod Biol, 1996. **64**(1): p. 129-33.
114. Del Riccio, V., M. van Tuyl, and M. Post, *Apoptosis in lung development and neonatal lung injury.* Pediatr Res, 2004. **55**(2): p. 183-9.
115. Kotelkin, A., et al., *Respiratory syncytial virus infection sensitizes cells to apoptosis mediated by tumor necrosis factor-related apoptosis-inducing ligand.* J Virol, 2003. **77**(17): p. 9156-72.
116. FitzGerald, E.S., N.F. Luz, and A.M. Jamieson, *Competitive Cell Death Interactions in Pulmonary Infection: Host Modulation Versus Pathogen Manipulation.* Front Immunol, 2020. **11**: p. 814.
117. Kroon, A.A., et al., *Prolonged mechanical ventilation induces cell cycle arrest in newborn rat lung.* PLoS One, 2011. **6**(2): p. e16910.
118. Kroon, A.A., et al., *Mechanical ventilation-induced apoptosis in newborn rat lung is mediated via FasL/Fas pathway.* Am J Physiol Lung Cell Mol Physiol, 2013. **305**(11): p. L795-804.
119. Tanaka, A., et al., *Hyperoxia-induced LC3B interacts with the Fas apoptotic pathway in epithelial cell death.* Am J Respir Cell Mol Biol, 2012. **46**(4): p. 507-14.
120. Ren, Y., et al., *Hyperoxia can Induce Lung Injury by Upregulating AECII Autophagy and Apoptosis Via the mTOR Pathway.* Mol Biotechnol, 2023.
121. Hannun, Y.A., et al., *Sphingosine inhibition of protein kinase C activity and of phorbol dibutyrate binding in vitro and in human platelets.* J Biol Chem, 1986. **261**(27): p. 12604-9.
122. Okazaki, T., et al., *Role of ceramide as a lipid mediator of 1 alpha,25-dihydroxyvitamin D3-induced HL-60 cell differentiation.* J Biol Chem, 1990. **265**(26): p. 15823-31.
123. Beckmann, N., et al., *Inhibition of acid sphingomyelinase by tricyclic antidepressants and analogons.* Front Physiol, 2014. **5**: p. 331.
124. Petrache, I., et al., *Superoxide dismutase protects against apoptosis and alveolar enlargement induced by ceramide.* Am J Physiol Lung Cell Mol Physiol, 2008. **295**(1): p. L44-53.
125. McGrath-Morrow, S.A. and J. Stahl, *Apoptosis in neonatal murine lung exposed to hyperoxia.* Am J Respir Cell Mol Biol, 2001. **25**(2): p. 150-5.
126. Madurga, A., et al., *Systemic hydrogen sulfide administration partially restores normal alveolarization in an experimental animal model of bronchopulmonary dysplasia.* Am J Physiol Lung Cell Mol Physiol, 2014. **306**(7): p. L684-97.
127. Muhlfeld, C., et al., *Design-Based Stereology of the Lung in the Hyperoxic Preterm Rabbit Model of Bronchopulmonary Dysplasia.* Oxid Med Cell Longev, 2021. **2021**: p. 4293279.
128. Allison, B.J., et al., *Ventilation of the very immature lung in utero induces injury and BPD-like changes in lung structure in fetal sheep.* Pediatr Res, 2008. **64**(4): p. 387-92.
129. Roper, J.M., et al., *In vivo exposure to hyperoxia induces DNA damage in a population of alveolar type II epithelial cells.* Am J Physiol Lung Cell Mol Physiol, 2004. **286**(5): p. L1045-54.
130. Nobrega, J.N. and D.V. Coscina, *Effects of chronic amitriptyline and desipramine on food intake and body weight in rats.* Pharmacol Biochem Behav, 1987. **27**(1): p. 105-112.
131. Alvarez-Fuente, M., et al., *Preventing bronchopulmonary dysplasia: new tools for an old challenge.* Pediatr Res, 2019. **85**(4): p. 432-441.
132. Kimble, A., M.E. Robbins, and M. Perez, *Pathogenesis of Bronchopulmonary Dysplasia: Role of Oxidative Stress from 'Omics' Studies.* Antioxidants (Basel), 2022. **11**(12).
133. Choi, Y., et al., *Metabolic shift favoring C18:0 ceramide accumulation in obese asthma.* Allergy, 2020. **75**(11): p. 2858-2866.

134. Trembath, A. and M.M. Laughon, *Predictors of bronchopulmonary dysplasia.* Clin Perinatol, 2012. **39**(3): p. 585-601.
135. Binet, M.E., et al., *Role of gender in morbidity and mortality of extremely premature neonates.* Am J Perinatol, 2012. **29**(3): p. 159-66.
136. Laughon, M.M., et al., *Prediction of bronchopulmonary dysplasia by postnatal age in extremely premature infants.* Am J Respir Crit Care Med, 2011. **183**(12): p. 1715-22.
137. Pradas, I., et al., *Lipidomics Reveals a Tissue-Specific Fingerprint.* Front Physiol, 2018. **9**: p. 1165.
138. Symons, J.L., et al., *Lipidomic atlas of mammalian cell membranes reveals hierarchical variation induced by culture conditions, subcellular membranes, and cell lineages.* Soft Matter, 2021. **17**(2): p. 288-297.
139. Engmann, L., et al., *Local side effects of subcutaneous and intramuscular urinary gonadotropins for ovarian stimulation in in vitro fertilization: a prospective, randomized study.* Fertil Steril, 1998. **69**(5): p. 836-40.
140. Labiris, N.R. and M.B. Dolovich, *Pulmonary drug delivery. Part I: physiological factors affecting therapeutic effectiveness of aerosolized medications.* Br J Clin Pharmacol, 2003. **56**(6): p. 588-99.
141. Caskey, S., et al., *Structural and Functional Lung Impairment in Adult Survivors of Bronchopulmonary Dysplasia.* Ann Am Thorac Soc, 2016. **13**(8): p. 1262-70.
142. Lovering, A.T., et al., *Ventilatory and sensory responses in adult survivors of preterm birth and bronchopulmonary dysplasia with reduced exercise capacity.* Ann Am Thorac Soc, 2014. **11**(10): p. 1528-37.
143. Sriram, S., et al., *Cognitive Development and Quality of Life Associated With BPD in 10-Year-Olds Born Preterm.* Pediatrics, 2018. **141**(6).